

AD-A038 239

AIR FORCE GEOPHYSICS LAB HANSCOM AFB MASS
LWIR (7-24 MICROMETER) MEASUREMENTS FROM THE LAUNCH OF A ROCKET--ETC(U)
NOV 76 J W ROGERS, A T STAIR, N B WHEELER

F/G 4/1

UNCLASSIFIED

AFGL-TR-76-0274

DNA-HAES-51

NL

1 of 2
AD
A038239



AD A 038239

AFGL-TR-76-0274

ENVIRONMENTAL RESEARCH PAPERS, NO. 583
HAES REPORT NO. 51



LWIR (7-24 μ m) Measurements From the Launch of a Rocketborne Spectrometer Into an Aurora (1973)

JAMES W. ROGERS
A.T. STAIR, Jr.
NED B. WHEELER
CLAIR L. WYATT
DORAN J. BAKER

15 November 1976



Approved for public release; distribution unlimited.

This research was sponsored by the Defense Nuclear Agency under Subtask
K11BAXHX534, Work Unit 18, entitled "Infrared Auroral Measurements."

OPTICAL PHYSICS DIVISION PROJECT 2310

AIR FORCE GEOPHYSICS LABORATORY

HANSCOM AFB, MASSACHUSETTS 01731

AIR FORCE SYSTEMS COMMAND, USAF

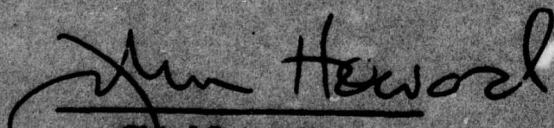


ADJ NO. _____
DDC FILE COPY

This report has been reviewed by the ESD Information Office (OI) and is releasable to the National Technical Information Service (NTIS).

This technical report has been reviewed and is approved for publication.

FOR THE COMMANDER


Chief Scientist

Qualified requestors may obtain additional copies from the Defense Documentation Center. All others should apply to the National Technical Information Service.

Unclassified

micrometer

SECURITY CLASSIFICATION OF THIS PAGE (When Data Entered)

REPORT DOCUMENTATION PAGE		READ INSTRUCTIONS BEFORE COMPLETING FORM
1. REPORT NUMBER	2. GOVT ACCESSION NO.	3. RECIPIENT'S CATALOG NUMBER
14 AFGL-TR-76-0274	AFGL-ERP-583	
4. TITLE (and Subtitle)		5. TYPE OF REPORT & PERIOD COVERED
6 LWIR (7-24 micrometer) MEASUREMENTS FROM THE LAUNCH OF A ROCKETBORNE SPECTROMETER INTO AN AURORA (1973).		Scientific. Interim. # (HAES Report No. 51)
7. AUTHOR(s)		6. PERFORMING ORG. REPORT NUMBER
10 James W./Rogers, Clair L./Wyatt* A.T./Stair, Jr., Doran J./Baker* Ned B./Wheeler.		ERP, No. 583
9. PERFORMING ORGANIZATION NAME AND ADDRESS		8. CONTRACT OR GRANT NUMBER(s)
Air Force Geophysics Laboratory (OPR) Hanscom AFB, Massachusetts 01731		18 DNA 19 HAES-51
11. CONTROLLING OFFICE NAME AND ADDRESS		10. PROGRAM ELEMENT, PROJECT, TASK AREA & WORK UNIT NUMBERS
Air Force Geophysics Laboratory (OPR) Hanscom AFB, Massachusetts 01731		16 2310/G404 17 G4 61102F
14. MONITORING AGENCY NAME & ADDRESS (if different from Controlling Office)		12. REPORT DATE
12 127 p.		11 15 Nov 1976
		13. NUMBER OF PAGES
		128
		15. SECURITY CLASS. (of this report)
		Unclassified
		15a. DECLASSIFICATION/DOWNGRADING SCHEDULE
16. DISTRIBUTION STATEMENT (of this Report)		
Approved for public release; distribution unlimited.		
9 Interim rept.		
17. DISTRIBUTION STATEMENT (of the abstract entered in Block 20, if different from Report)		
18. SUPPLEMENTARY NOTES		
This research was sponsored by the Defense Nuclear Agency under Subtask K11BAXHX584, Work Unit 18, entitled "Infrared Auroral Measurements." *Utah State University, Electrodynamics Laboratory, Logan, Utah 84321		
19. KEY WORDS (Continue on reverse side if necessary and identify by block number)		
Long-wavelength infrared Rocketborne spectrometer CO ₂ emission O ₃ emission		
20. ABSTRACT (Continue on reverse side if necessary and identify by block number)		
A liquid-helium-cooled, long-wavelength infrared (LWIR) spectrometer was successfully launched by the Air Force Geophysics Laboratory onboard a Black Brant VC rocket (A18.006-2) on 22 Mar 1973 from the University of Alaska's Poker Flat Research Range at Chatanika, Alaska. This flight was part of the Defense Nuclear Agency ICECAP 73 Program. The spectrometer, which employs a circular-variable filter (CVF), was developed by AFGL and Utah State University and has provided the first measurements of the altitude		

DDC
APR 14 1977
RECEIVED

next page

Unclassified

SECURITY CLASSIFICATION OF THIS PAGE(When Data Entered)

20. (Cont)

cont → profile of the infrared spectrum of the upper-atmospheric emissions between 7 and 24 μm (micrometer)

micrometer → During an IBC II aurora, data were obtained on the 15- μm carbon dioxide (μm) emission from 65 to 150 km and on the 9.6- μm ozone (μm) emission between 45 and 100 km. In addition, emission data on the long-wavelength wing of the 6.3- μm water band between 6.7 and 7.6 μm were also obtained between 50 and 75 km. Above 100 km, significant unidentified emission was observed at 9.3 μm with weaker features at 6.9, 7.3, 8.0, 11.1, and 12.3 μm .

↑
This report documents in detail the data obtained along with the rocket and payload performance, the auroral conditions at launch and a comparison with theoretical models.

Unclassified

2 SECURITY CLASSIFICATION OF THIS PAGE(When Data Entered)

ACCESSION for	
NTIS	WHL Section <input checked="" type="checkbox"/>
DCC	DRI Section <input type="checkbox"/>
UNANNOUNCED	
JUSTIFICATION	
BY	
DISTRIBUTION/AVAIL	FILE CODES
Dist.	AVAIL. SP. DIST.
A	

Preface

The High Altitude Effects Simulation (HAES) Program sponsored by the Defense Nuclear Agency since the early 1970 time period, comprises several groupings of separate, but interrelated technical activities, for example, ICECAP (Infrared Chemistry Experiments - Coordinated Auroral Program). Each of the latter has the common objective of providing information, ascertained as essential for the development and validation of predictive computer codes designed for use with high priority DoD radar, communications, and optical defensive systems.

Since the inception of the HAES Program, significant achievements and results have been described in reports published by DNA, participating service laboratories, and supportive organizations. In order to provide greater visibility for such information and enhance its timely applications, significant reports published since early calendar 1974 have been identified with an assigned HAES serial number and the appropriate activity acronym (for example, ICECAP) as part of the report title. A complete and current bibliography of all HAES reports issued prior to and subsequent to HAES Report No. 1, dated 5 February 1974 entitled "Rocket Launch of an SWIR Spectrometer into an Aurora (ICECAP 72)", AFCRL Environmental Research Paper No. 466, is maintained and available on request from DASIAC, DoD Nuclear Information and Analysis Center, 816 State Street, Santa Barbara, California 93102, Telephone (805) 965-0551.

This report, the fifty-first in the HAES series, presents the data obtained from the launch of a liquid-helium-cooled, long-wavelength infrared spectrometer into an aurora. While preliminary data have been presented previously (see references 1 and 24), this report documents in detail the data obtained along with the rocket and

payload performance, the auroral conditions at launch and a comparison with theoretical models.

The authors wish to thank the personnel from various organizations who made significant contributions to the success of this experiment including: Dr. H.C. Fitz, Jr. and Mr. Herb Mitchell* of DNA; Neil Brown of The University of Alaska; Tom Condon, Ed McKenna, Ray Wilton and Floyd Cook of AFGL; Gary Frodsham and Val King of Utah State University; Ed Allen of Space Data Corporation; Ed Butterfield of White Sands Missile Range and Larry O'Connor and Dick Morin of Northeastern University.

***Presently with R&D Associates**

Contents

1. INTRODUCTION	5
2. PAYLOAD CONFIGURATION	8
2.1 LWIR CVF Spectrometer Description	8
2.2 Photometer Description	11
3. ROCKET AND PAYLOAD PERFORMANCE	11
4. LAUNCH CONDITIONS	12
5. EXPERIMENTAL RESULTS	15
5.1 N_2^+ (1N) Altitude Profile	15
5.2 LWIR CVF Infrared Spectra	16
5.3 O_3 and CO_2 Zenith Radiance Profiles	18
5.4 H_2O Zenith Radiance Profile	22
5.5 Unidentified Emissions	23
6. CONCLUSIONS	29
REFERENCES	31
APPENDIX A: Spectral Data Scans Obtained During the Flight	35
APPENDIX B: List of HAES Reports	113
APPENDIX C: Distribution List	121

Illustrations

1. Cutaway View of the Liquid-Helium Cooled CVF Spectrometer Used for IR Atmospheric Emissions	10
2. Final Flight Calibration of the CVF Spectrometer	11
3. Spectrometer Detector and Baffle Temperatures During Flight	13
4. The Altitude Profile of Overhead Radiance at 3914 Å as Measured Onboard the Rocket	15
5. Spectral Radiance Values for Scan 477 at 185 km	16
6. Spectral Radiance Values for Scan 755 at 94 km	16
7. Spectral Radiance Values at Apogee Obtained by Averaging Over 34 Scans	17
8. Altitude Dependence of the Spectral Radiance During Ascent from 100 to 185 km	17
9. Altitude Dependence of the Spectral Radiance During Descent from 185 to 100 km	18
10. Altitude Dependence of the Spectral Radiance During Descent from 100 to 50 km	18
11. Zenith Radiance Altitude Profile at 9.6 μm Measured With the LWIR Spectrometer	19
12. Zenith Radiance Altitude Profile at 15 μm Measured With the LWIR Spectrometer	19
13. Zenith Radiance Altitude Profile at 9.6 μm Measured With the LWIR Spectrometer Compared With Theoretical Model	20
14. Zenith Radiance Altitude Profile at 15 μm Measured With the LWIR Spectrometer Compared With Theoretical Models	21
15. Zenith Radiance Altitude Profile of the Emission from 6.7 to 7.6 μm Measured With the LWIR Spectrometer Compared With the Theoretical H_2O Calculations of Degges	22
16. Zenith Radiance Altitude Profile of the Strong Unidentified Emission at 9.3 μm	24
17. Zenith Radiance of the Unidentified Emission Feature at 9.3 μm as a Function of Time After Launch	24
18. Zenith Radiance Values of Weaker Unidentified Emissions as Functions of Time After Launch	

Tables

1. Poker Flat Temperatures ($^{\circ}\text{C}$) From Rocket Sounding Data (1973)	14
2. Summary of Selected Ionospheric Parameters at the Time of the 22 March 1973 Black Brant (A18.006-2) Launch	14

LWIR (7-24 μm) Measurements From the Launch of a Rocketborne Spectrometer Into an Aurora (1973)

1. INTRODUCTION

A liquid-helium-cooled, long-wavelength infrared (LWIR) spectrometer was successfully launched by the Air Force Geophysics Laboratory (AFGL)* onboard a Black Brant VC rocket (A18.006-2) on 22 March 1973 from the University of Alaska's Poker Flat Research Range at Chatanika, Alaska. This flight was part of the Defense Nuclear Agency (DNA) ICECAP 73 Program. The spectrometer, which employs a circular-variable filter (CVF), was developed by AFGL and Utah State University (USU) and has provided the first measurements of the altitude profile of the infrared spectrum of the upper-atmospheric emissions between 7 and 24 μm .

During an IBC II aurora, data were obtained on the 15- μm carbon dioxide (ν_2) emission from 65 to 150 km and on the 9.6- μm ozone (ν_3) emission between 45 and 100 km as reported by Stair, et al.¹ Emission data on the long-wavelength wing of the 6.3- μm water band between 6.7 and 7.6 μm were also obtained between 50 and 75 km. Above 100 km, significant unidentified emission was observed at 9.3 μm with weaker features at 6.9, 7.3, 8.0, 11.1, and 12.3 μm .

(Received for publication 12 November 1976)

* Formerly the Air Force Cambridge Research Laboratories.

1. Stair, A. T., Jr., Ulwick, J. C., Baker, K. D. and Baker, D. J. (1975) Rocketborne observations of atmospheric infrared emissions in the auroral region, *Atmospheres of Earth and Planets*, edited by B. M. McCormac (D. Reidel, Dordrecht-Holland), pp 335-346.

The calibration particulars and an analysis of the spectrometer performance along with the methods of processing the data have been presented in separate reports by Condrón² and Rogers.³ This report documents in detail the data obtained along with the rocket and payload performance, the auroral conditions at launch and a comparison with theoretical models.

2. PAYLOAD CONFIGURATION

In addition to the liquid-helium-cooled LWIR CVF spectrometer, the rocket payload was instrumented with diagnostic sensors to provide information on local auroral conditions plus rocket and payload performance. These included a 3914 Å photometer, a light-scattering dust detector, mechanical vibration spectrometers, an aspect gyro, and a spin magnetometer.

The rocket was assembled with a "clamshell" split-nosecone which could be opened during ascent at a predetermined altitude above which the LWIR sensor would not seriously cryo-pump. The clamshell could then be reclosed during descent. The payload was outfitted with a recovery system employing a parachute and beacon. A dust detector was provided to indicate the presence of local particulate matter which might pass through the field of view of the spectrometer. To minimize possible dust contamination problems, all portions of the payload were sealed, and both the sensor and the payload were assembled in a clean room. The final payload was then enclosed in a large plastic bag until launch.

A summary of the field requirements, along with the specifications of the Black Brant VC rocket can be found in a field requirements report by Space Data Corporation.⁴

2.1 LWIR CVF Spectrometer Description

The spectrometer flown was Model HS-1B-1B developed by USU and is described as follows. The spectral region from 7 to 24 μm is scanned at a rate of two scans per second with a full-angle field of view of 2 deg (9.6×10^{-4} sr). The entire optical subsection is cooled to liquid-helium temperature, including an arsenic-doped silicon

2. Condrón, T. P. (1973) Calibration of a Liquid Helium Cooled CVF Radiometer in a Warm Environment, AFCRL Instrumentation Papers, No. 199, AFCRL-TR-73-0480.
3. Rogers, J. W. (1975) Instrumentation Analysis and Data Processing for Rocket-borne LWIR Spectrometers (With Application to Rocket A18.006-2 of 22 March 1973), Environmental Research Papers, No. 539, AFCRL-TR-75-0535, HAES Rpt. No. 23.
4. ICECAP '73 Field Requirements and Procedures (1973) SDC TM-620, Revision D, Space Data Corporation, Phoenix, Arizona, 6 March 1973.

detector which is thereby operated with an effective zero radiation background. A key element of the spectrometer is the Optical Coating Laboratory, Inc. (OCLI) rotating variable interference filter. The spectral resolution of the filter was measured at AFGL by Condon² and the best estimate of the half-bandwidth for the flight- configured spectrometer was 2.63 percent for the short-wavelength filter half and 2.92 percent for the long-wavelength filter half. This circular variable filter element has led to this class of instruments being referred to as CVF spectrometers. A dynamic range of 3×10^4 is achieved by providing four data channels with different gains. The output data from the spectrometer along with the diagnostic information were transmitted to a ground telemetry site during the flight.

Many technical breakthroughs had to be achieved in order to assure satisfactory measurements. Most of these problems dealt with the cryogenics and the stringent requirements placed on the electronics and optics to perform remotely in a severe environment. A cutaway view of the spectrometer is shown in Figure 1. Only general information on the spectrometer will be given in this report while more specific details can be found in reports by Wyatt⁵⁻⁷ and Stair, et al.⁸

The CVF used is composed of two 180-deg wedge filter segments mounted together to form a disc. The short-wavelength half (rotational angles 0 to 180 deg) covers wavelengths from 6.5 to 13 μm . The long-wavelength half (angles from 180 to 360 deg) covers the range from 12.5 to 25 μm . Small portions of these spectral regions are not usable because opaque metal joining strips are placed over the interfaces between the two filter halves at 0 deg and at 180 deg. Each time the metal strip at 0 deg passes in front of the detector, a feedback circuit cancels the residual voltage caused by any amplifier dc drift. The voltage pulse which triggers this dc reset is monitored and outputted on the calibration reference channel of the spectrometer.

The rotational position of the CVF is monitored during each scan by a coded chopper that is attached to the same shaft as the CVF. This encoder is located at a distance of twenty centimeters behind the filter. The chopper periodically interrupts radiation from an incandescent source that is incident upon a silicon detector.

5. Wyatt, C.L. (1971) Infrared Helium-Cooled Circular-Variable Spectrometer Model HS-1, Final Report, AFCRL-71-0340, Contract No. F19628-67-C-0340, Utah State University, Logan, Utah, September 1971.
6. Wyatt, C.L. and Baker, D.J. (1975) Development of a Liquid-Helium Cooled Rocketborne Spectrometer, Scientific Report No. 2, AFCRL-TR-75-0164, Contract No. F19628-73-C-0048, Utah State University, Logan, Utah, February 1975.
7. Wyatt, C.L. (1975) Infrared Spectrometer; Liquid-helium-cooled rocketborne circular-variable filter, Applied Optics, 14, No. 12:3086-3091.
8. Stair, A.T., Jr., Wheeler, N.B., Baker, D.J., and Wyatt, C.L. (1973) Cryogenic IR spectrometer for rocketborne measurements, NEREM 73 Record, IEEE Catalog No. 73, CHO-841-7 NEREM, pp 80-89.

The end result is a series of 10 coded pulses produced during each filter rotation which are then outputted on the position reference channel. In principle, the rotational angle of the filter at each instant, and, therefore, the wavelength of peak transmission at that time, can be uniquely ascertained by the train of pulses produced by the chopper.

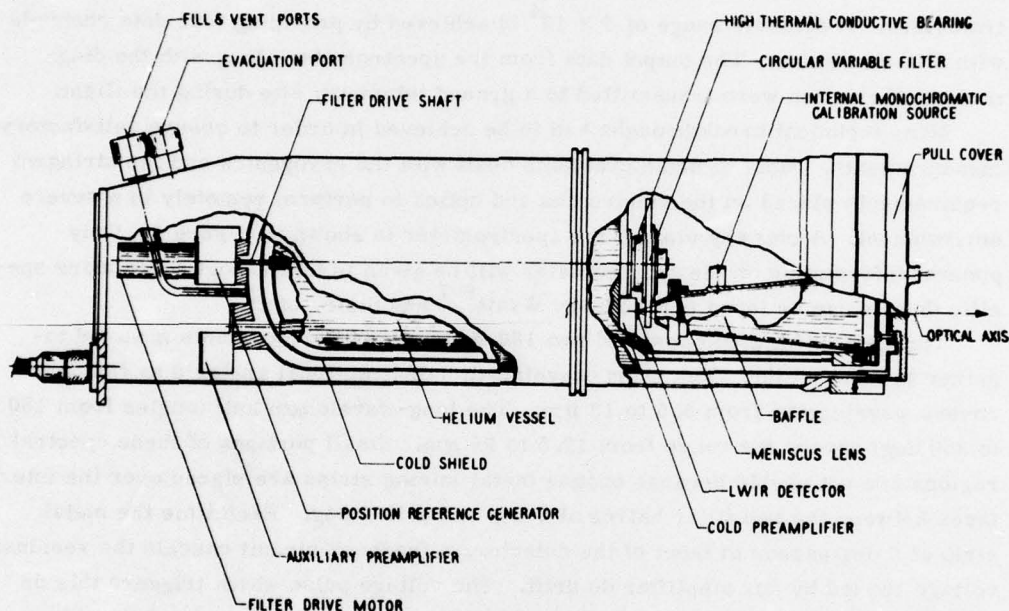


Figure 1. Cutaway View of the Liquid-Helium Cooled CVF Spectrometer Used for IR Atmospheric Emissions

The spectrometer also contains an internal calibration source which is activated every tenth scan. This source consists of a gallium-arsenide emitter which scatters unfiltered light onto the detector. Due to its temperature sensitivity, the internal source is insufficiently stable to provide an absolute inflight calibration of the spectrometer; however, the emitter can be used as a measure of the spectrometer performance. The internal calibration pulse voltage is monitored on the calibration reference channel output.

The final flight calibration of the spectrometer's absolute spectral response was performed at AFGL and is contained in a report by Condron.² The spectral response in $\text{W cm}^{-2} \text{sr}^{-1} \mu\text{m}^{-1} / \text{V}$ of the highest gain channel is shown in Figure 2 for both halves of the filter and is accurate to within a factor of two.

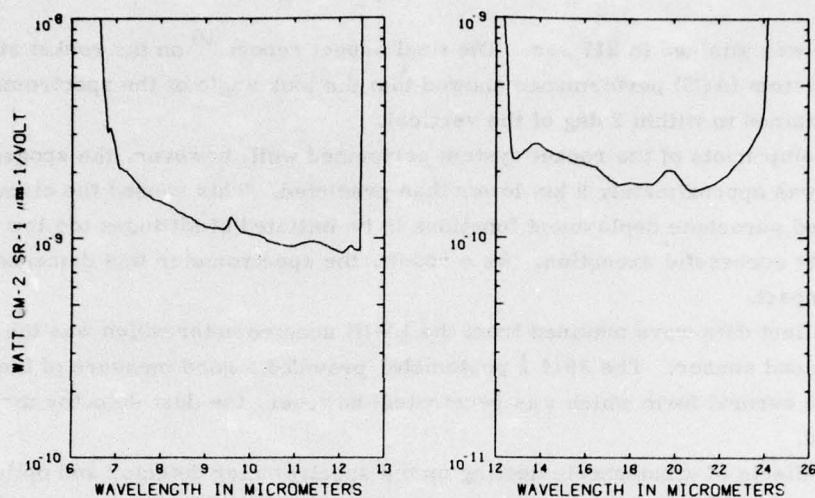


Figure 2. Final Flight Calibration of the CVF Spectrometer

2.2 Photometer Description

A 3914 Å photometer was included in the payload to provide a measure of the auroral energy deposition. The photometer field of view was coaligned with the LWIR spectrometer and had a value of 10.3 deg full angle (0.0254 sr). The transmittance of the interference filter peaked at 3907 Å with a spectral bandwidth of 17 Å. The unattenuated dynamic response of the photometer ranged from 0.2 to 500 Rayleigh/Å.

The photometer operated directly coupled in an analog mode with a dual-range linear channel. A "dogleg" gain change of 10 was used to extend the dynamic range over the single linear telemetry channel that was available.

3. ROCKET AND PAYLOAD PERFORMANCE

The Black Brant VC rocket (A18.006-2) with the LWIR CVF spectrometer payload was launched at 1212:57 hours UT on 22 March 1973. The payload was integrated at AFGL under the direction of E. McKenna with R. Wilton of AFGL responsible for telemetry and tracking. Trajectory data are contained in a report prepared by the Analysis and Simulation Branch of the AFGL Computation Center.⁹ The altitudes reported are accurate to within 0.5 km and indicate that an apogee of

9. Trajectory Report, Rocket No. A18-006-2 (1973) Analysis and Simulation Branch, AFCRL Computation Center.

185.4 km was attained in 217 sec. The final aspect report ¹⁰ on the rocket attitude control system (ACS) performance showed that the look angle of the spectrometer was maintained to within 2 deg of the vertical.

All components of the rocket system performed well; however, the apogee obtained was approximately 9 km lower than predicted. This caused the clamshell closing and parachute deployment functions to be initiated at altitudes too low for completely successful execution. As a result, the spectrometer was damaged upon ground impact.

Excellent data were obtained from the LWIR spectrometer which was the primary payload sensor. The 3914 Å photometer provided a good measure of the intensity of the auroral form which was penetrated; however, the dust detector malfunctioned.

The effects of atmospheric heating on the spectrometer detector and optical baffle can be seen in Figure 3. The detector temperature rose to approximately 18° K immediately after the clamshell was opened at 70.5 sec (86 km), but returned to the temperature of liquid helium by 97 sec (119 km). During payload descent, the temperature started to rise at 375 sec (69 km) and was 35° K during the last usable data scan at 390 sec (45 km). The baffle temperature also rose after the clamshell opened and peaked at 50° K around 120 sec (142 km). This was well below the upper limit that would have affected the spectrometer performance. The baffle cooled off throughout the flight until around 365 sec (83.5 km). This cooling is attributable to the radiation of the heat energy which had built up during the clamshell opening shock. During the last usable data scan, the baffle was at 45° K.

4. LAUNCH CONDITIONS

A post-breakup auroral glow had persisted at the IBC Class II level for nearly 10 min prior to the penetration of the rocket into the region. At the time and location of penetration, the zenith radiance was 16.5 kR for the 5577 Å auroral green line as measured by The University of Alaska from Fort Yukon. The attitude of the optical axis of the spectrometer was inclined at an angle of 12.8 deg north relative to the magnetic field lines above Poker Flat. The aurora remained relatively stable during the rocket flight, but small scale changes occurred over the whole sky. The phenomenological situation appeared to be that the rocket was launched during an intense auroral substorm shortly after the poleward expansion had occurred.

10. Aspect Report, Rocket No. A18-006-2 (1974) Aspect Report Number 4531-9, Analysis and Simulation Branch, AFCRL Computation Center.

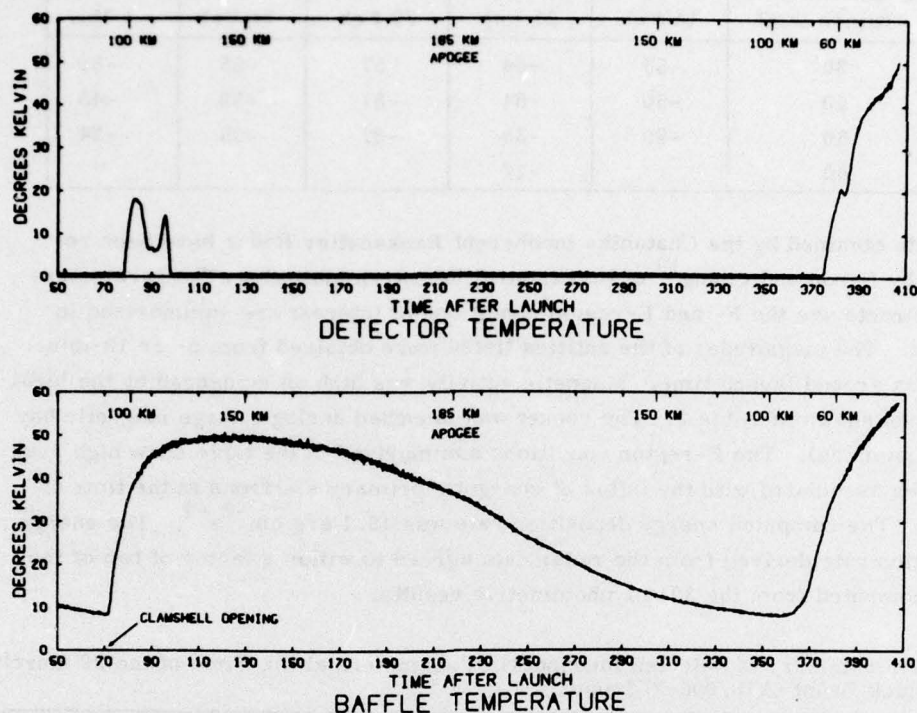


Figure 3. Spectrometer Detector and Baffle Temperatures During Flight

Additional aeronomic information pertinent to this experiment, including atmospheric meteorological data, ground station magnetometer, all-sky camera and photometric measurements can be found in the report from the Geophysical Institute of The University of Alaska by Romick.¹¹ The reported temperature profiles obtained from sounding rocket data are shown in Table 1. These temperatures help describe the atmospheric environment and are very important in analyzing the flight data. The characterization of the aurora during the flight has also been reported by Kofsky, et al¹² of Photometrics, Inc.

11. Romick, G. J. (1975) Report of the Geophysical Description and Available Data Associated with Rocket PF-BB-53, Scientific Rpt No. 2, AFCRL-TR-75-0040, Contract No. F19628-74-C-0188, Geophysical Institute, University of Alaska, January 1975.
12. Kofsky, I. L., Meriwether, J. W., Schroeder, J. W., and Sluder, R. B. (1974) Data Reduction and Auroral Characterizations of ICECAP, HAES Report No. 4, Final Report, DNA 3511F, Contract No. DNA001-73-C-0027, Photometrics, Inc., Lexington, Mass., September 1974.

Table 1. Poker Flat Temperatures ($^{\circ}\text{C}$) From Rocket Sounding Data (1973)

Altitude (km)	14 Feb	21 Feb	22 Feb	24 Feb	1 Mar
30	-55	-54	-57	-55	-59
40	-50	-51	-51	-52	-45
50	-39	-33	-37	-35	-24
60		-17			

Data obtained by the Chatanika Incoherent Backscatter Radar have been reported by Baron and Chang¹³ of the Stanford Research Institute. The parameters that characterize the F- and E-region conditions of interest are summarized in Table 2. The magnitudes of the entities listed were obtained from 5- or 10-min averages around launch time. Magnetic activity was high as evidenced by the local K-indices shown in Table 2. The rocket was launched during a large magnetic bay (~ 1500 gammas). The E-region conditions summarized in the table show high peak densities associated with the influx of energetic primary electrons at the time of launch. The computed energy deposition rate was $16.1 \text{ erg cm}^{-2} \text{ s}^{-1}$. The energy deposition rate derived from the radar data agreed to within a factor of two of the value computed from the 3914 \AA photometric results.

Table 2. Summary of Selected Ionospheric Parameters at the Time of the 22 March 1973 Black Brant (A18, 006-2) Launch

Local 3-hr K-index		8
F region		
N_e (300 km)	6×10^4	el/cm^3
T_e (230 km)	1350	$^{\circ}\text{K}$
T_i (230 km)	900	$^{\circ}\text{K}$
E region		
N_e (max)	6.6×10^5	el/cm^3
h_e (max)	90	km
Particle energy	50	keV
Number flux, Φ	2×10^8	$\text{cm}^{-2} \text{ s}^{-1}$
Electric fields:		
GM North	-16	mV/m
GM East	-9	mV/m
Joule heating	11	$\text{ergs/cm}^{-2} \text{ s}^{-1}$
Particle energy flux:		
Radar	16.1	$\text{ergs/cm}^{-2} \text{ s}^{-1}$
Optics	16.4	$\text{ergs/cm}^{-2} \text{ s}^{-1}$
Joule heating/particle energy flux	0.67	

13. Baron, M. and Chang, N.J. (1975) ICECAP '73A - Chatanika Radar Results. HAES Report No. 15, Topical Report, DNA 3531T, Contract No. DNA 001-74-C-0167, Stanford Research Institute, Menlo Park, California, April 1975.

5. EXPERIMENTAL RESULTS

The processing of the LWIR spectrometer data proceeded in a step-by-step manner to provide accurate final data complete with error limits. This also made it possible to assay the system performance. An analysis, with the determination of which data scans were actually usable, has been presented in a separate report by Rogers.³ After the payload clamshell was opened at 86.4 km, 680 scans (revolutions of the CVF) were obtained of which a total of 488 were considered usable. Scans were discarded when all channels were saturated, during internal calibration, when gamma ray disturbances occurred, and during the time of passage of an unidentified object through the spectrometer's field of view.

5.1 N_2^+ (1N) Altitude Profile

The measured altitude profile of the overhead radiance at 3914 Å due to the first negative band ($B^2 \Sigma_u^+ \rightarrow X^2 \Sigma_g^+$) of N_2^+ (0,0) in the near ultraviolet is given in Figure 4 as a function of rocket altitude. The half-power bandwidth of the photometer filter was 17 Å with a field of view of 10.3 deg full angle. On ascent, the overhead photon radiance decreased from about 5 kR at 100 km to 0.8 kR at 170 km as the rocket passed through the auroral form. Overhead at 185 km, the 3914 Å radiance was less than 140 R. During descent, the intensity below 140 km was consistently lower than on the upleg trajectory.

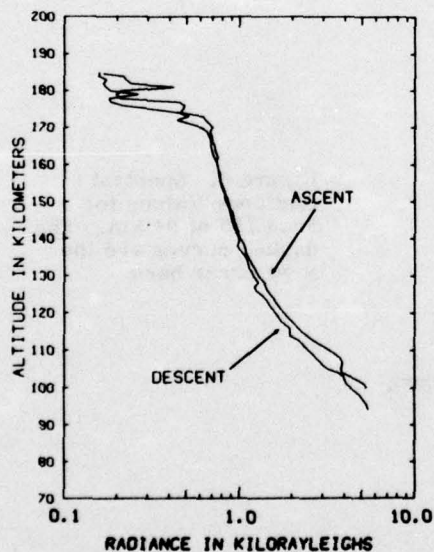


Figure 4. The Altitude Profile of Overhead Radiance at 3914 Å as Measured Onboard the Rocket

BEST AVAILABLE COPY

5.2 LWIR CVF Infrared Spectra

Figures 5 and 6 show typical examples of individual scans obtained with the dashed lines representing the $\pm 3\sigma$ error limits. Scan 477 (Figure 5) was taken 219.4 sec after launch near apogee at 185 km and scan 755 (Figure 6) was at 357.1 sec (94 km) during the downleg portion of the trajectory. At the higher altitudes, where the signals are weak and varying slowly, the data scans can be averaged to reduce the random noise at each wavelength. The resulting gain in signal-to-noise from this process is shown at apogee in Figure 7 where the spectral radiance values have been averaged over 34 scans. Appendix A contains data scans obtained throughout the entire flight. Averaging has been performed as indicated in the figure captions.

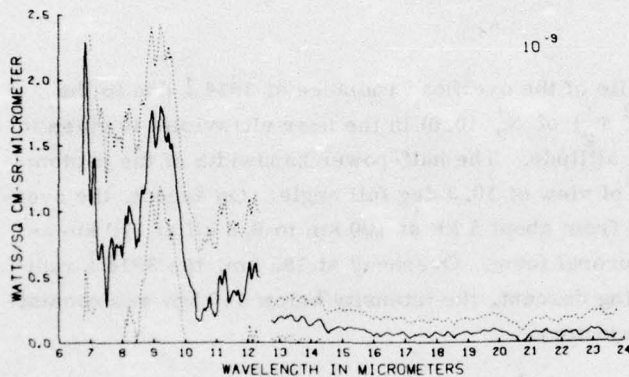


Figure 5. Spectral Radiance Values for Scan 477 at 185 km. The dashed curves are the $\pm 3\sigma$ error bars

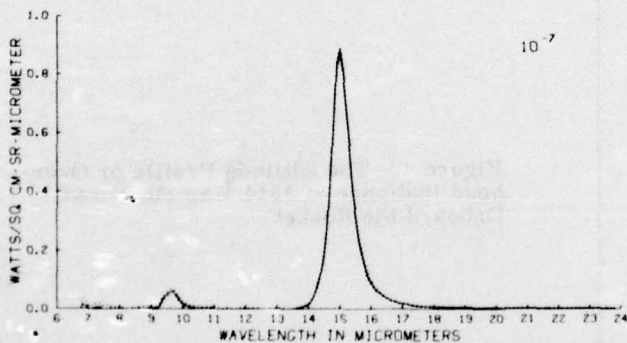


Figure 6. Spectral Radiance Values for Scan 755 at 94 km. The dashed curves are the $\pm 3\sigma$ error bars

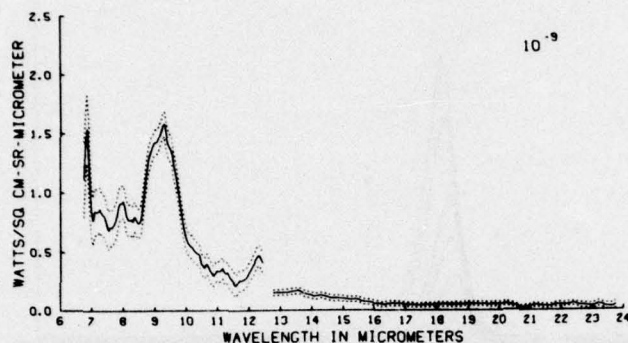


Figure 7. Spectral Radiance Values at Apogee Obtained by Averaging Over 34 Scans. The dashed curves are the $\pm 3\sigma$ error bars

Graphic portrayals of the spectral intensities measured during this experiment are given by three-dimensional presentations as shown in Figures 8, 9, and 10. Due to the dynamic range of the spectrometer some of the noise baseline features are lost in these plots. Figure 8 shows a portion of the ascent data between 100 and 185 km where the scans have been averaged over 2.5-km increments. The decay of the 15- μm CO_2 emission is clearly seen while the 9.6- μm O_3 emission is only shown near 100 km. At the higher altitudes, the unidentified emissions are evident at the shorter wavelengths. Figure 9 presents a similar view of the descent data from 185 to 100 km. Every scan from 100 to 50 km during descent is shown in Figure 10. The clipping of the 15- μm CO_2 at the lower altitudes is caused by amplifier saturation.

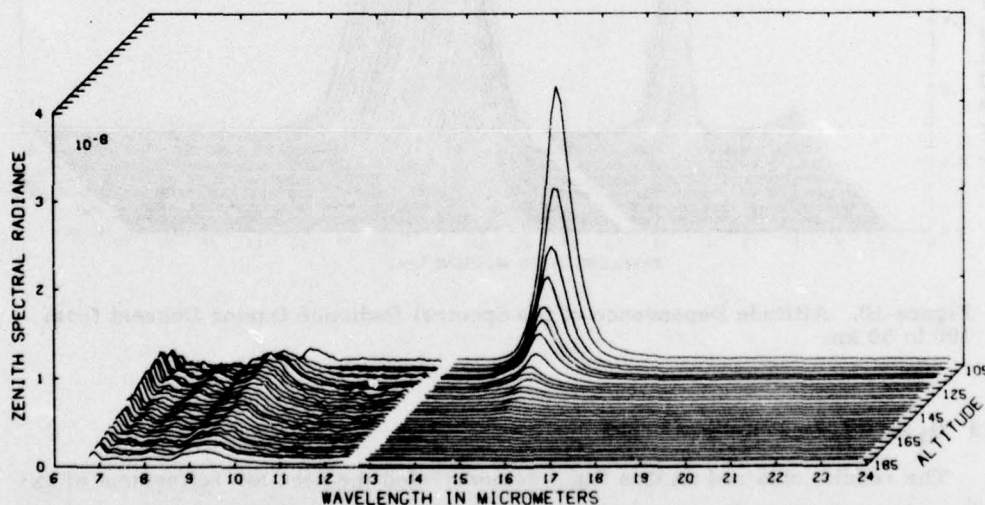


Figure 8. Altitude Dependence of the Spectral Radiance During Ascent from 100 to 185 km. Spectral scans are averages over 2.5 km increments

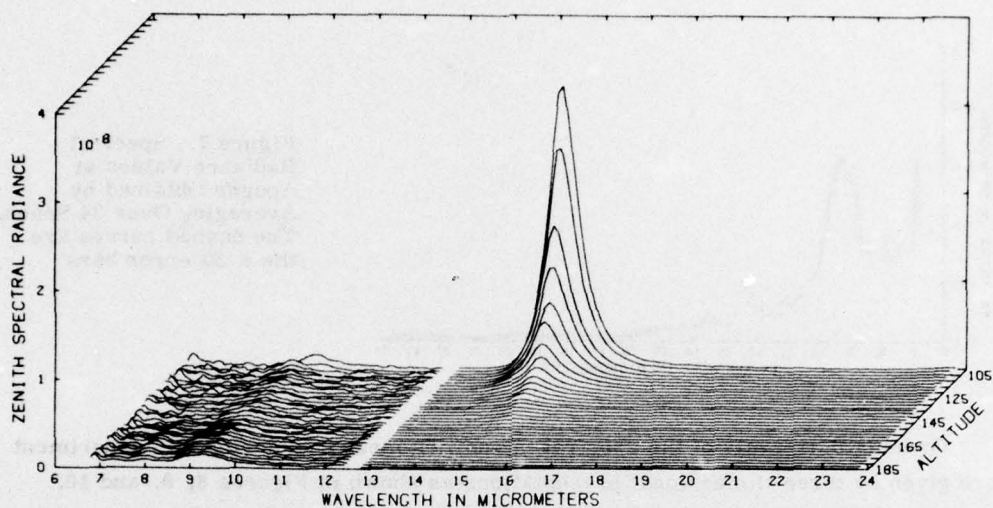


Figure 9. Altitude Dependence of the Spectral Radiance During Descent from 185 to 100 km. Spectral scans are averages over 2.5 km increments

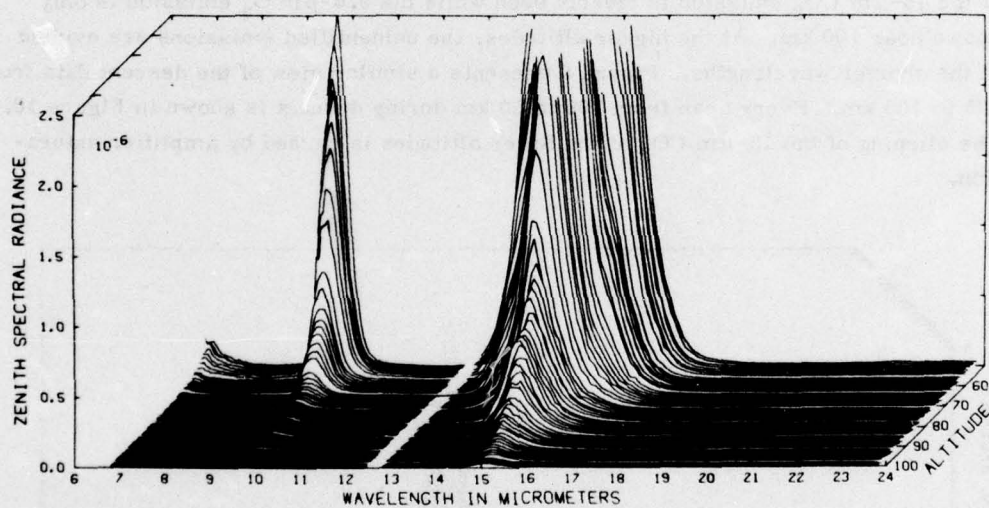


Figure 10. Altitude Dependence of the Spectral Radiance During Descent from 100 to 50 km

5.3 O₃ and CO₂ Zenith Radiance Profiles

The results obtained on this flight demonstrated the need for refinement of existing atmospheric radiance models. The zenith radiance altitude profile is shown in Figure 11 for the 9.6- μm O₃ and in Figure 12 for the 15- μm CO₂. The dashed

lines represent the $\pm 3\sigma$ error bars of the spectrometer data. Additional errors in the altitude profiles are introduced in altitude determination (0.5 km) and spectrometer calibration (a factor of 2). The larger spread between the data and the error bars at the higher altitudes indicates that the spectrometer's lower sensitivity level is being reached. At altitudes below 75 km, the measured ozone

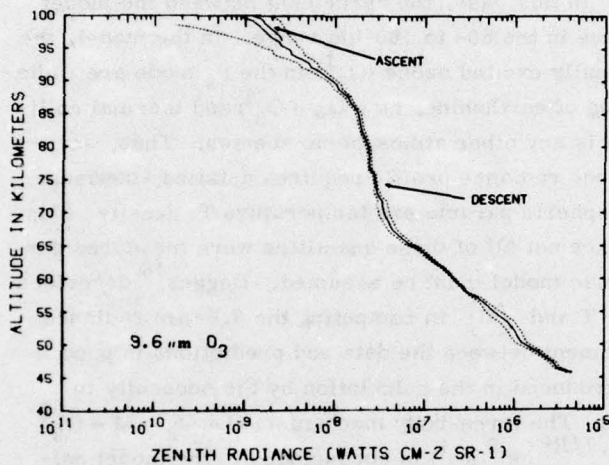


Figure 11. Zenith Radiance Altitude Profile at 9.6 μm Measured With the LWIR Spectrometer. The dashed curves are the $\pm 3\sigma$ error bars

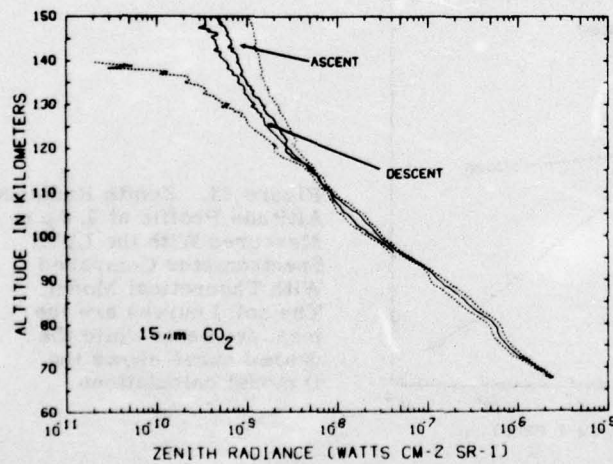


Figure 12. Zenith Radiance Altitude Profile at 15 μm Measured With the LWIR Spectrometer. The dashed curves are the $\pm 3\sigma$ error bars

emission values are in reasonable agreement with the most accurate models at the time of the flight (Corbin et al.¹⁴ and Degges¹⁵), but are two orders of magnitude larger at higher altitudes. The measured CO₂ emission data also agrees with the models of Corbin et al.¹⁴ and Degges¹⁵ only at the lower altitudes. The disagreement is a factor of 10 at 85 km and 2 orders of magnitude at 150 km.

Comparison between the measurements and a more recently calculated radiance profile by Degges¹⁶ using the ozone profile of Roble and Hays¹⁷ gives a much better agreement as shown in Figure 13. In this case, the agreement between the model and the data is within a factor of five in the 60- to 100-km range. In the model, the principal mechanisms for vibrationally excited ozone (O_3^{\dagger}) in the ν_3 mode are radiation transport; resonance scattering of earthshine, $h\nu + O_3 \rightarrow O_3^{\dagger}$; and thermal collisions, $O_3 + M \rightarrow O_3^{\dagger} + M$, where M is any other atmospheric species. Thus, accurate modelling of the 9.6- μm altitude radiance profile requires detailed knowledge of the altitude profiles of the atmospheric parameters temperature T; density $\{M\}$ and ozone concentration $\{O_3\}$. Since not all of these quantities were measured during this rocket flight, an atmospheric model must be assumed. Degges¹⁶ describes the atmospheric model he used for T and $\{M\}$ in computing the 9.6- μm radiance profile shown in Figure 13. Agreement between the data and predictions is good if one considers the uncertainties introduced in the calculation by the necessity to model the atmospheric parameters. The three-body mechanism $O + O_2 + M \rightarrow O_3^{\dagger} + M$ (with a rate of $3.2 \times 10^{-35} e^{1.7/Rt} \text{ cm}^6 \text{ s}^{-1}$) is not included in the model calculations shown in Figure 13, but is too slow to contribute significantly to the

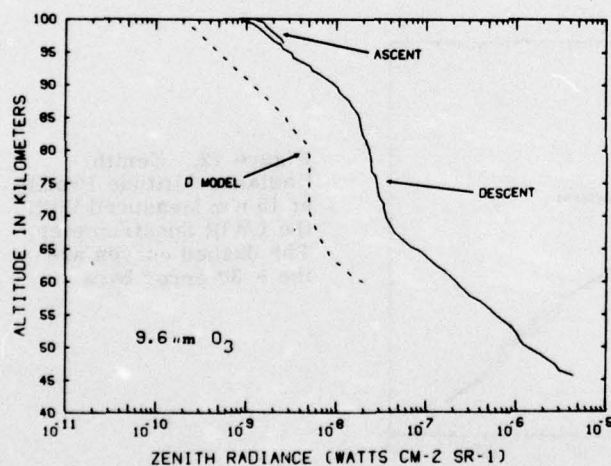


Figure 13. Zenith Radiance Altitude Profile at 9.6 μm Measured With the LWIR Spectrometer Compared With Theoretical Model. The solid curves are the measurements while the dashed curve shows the D model calculations

The references cited on the next several pages are too numerous to list here; see References on page 31.

emission above 80 km. However, it does become important below 80 km and its inclusion would place the theoretical model and experimental measurement in closer agreement in this altitude region.

Two new model calculations for the $15\text{ }\mu\text{m}$ CO_2 radiance profiles are compared with the measured results in Figure 14. These are the Degges¹⁶ model (D) and the results (KJ) of an independent calculation by James and Kumer¹⁸ and Kumer¹⁹. In these models, the principal mechanisms for producing CO_2 in the vibrationally excited ν_2 state (CO_2^\dagger) are radiation transport $h\nu + \text{CO}_2 \rightarrow \text{CO}_2^\dagger$ and thermal collisions $\text{CO}_2 + \text{M} \rightarrow \text{CO}_2^\dagger + \text{M}$. Again, accurate modelling requires a knowledge of the altitude profile of the atmospheric parameters, T , $\{\text{M}\}$, and $\{\text{CO}_2\}$. These were modelled in the two cases as described by Degges¹⁶ and Kumer.¹⁹ Differences in the D and KJ calculations largely reflect the differences in the atmospheric models employed. Also, the CO_2 mixing ratio in the D model remains constant at essentially 3.1×10^{-4} above 100 km whereas the KJ model utilizes the smaller CO_2 mixing ratio above 100 km which was introduced by James and Kumer.²⁰ Neither model accounts for the enhanced scattering of earthshine in the region above 100 km which should result from the CO_2 band and line broadening due to the increased temperature in the thermosphere. These models are in excellent agreement at the lower altitudes with the measurements, but exhibit discrepancies increasing with altitude.

Indirect evidence supports the claim that the experimental measurements are accurate to within a factor of two. First of all, upon extrapolation, the rocket data joins smoothly with the balloon measurements of Murcray et al.²¹ (Stair et al.²⁴). Secondly, satellite measurements tend to support the low altitude data (Conrath

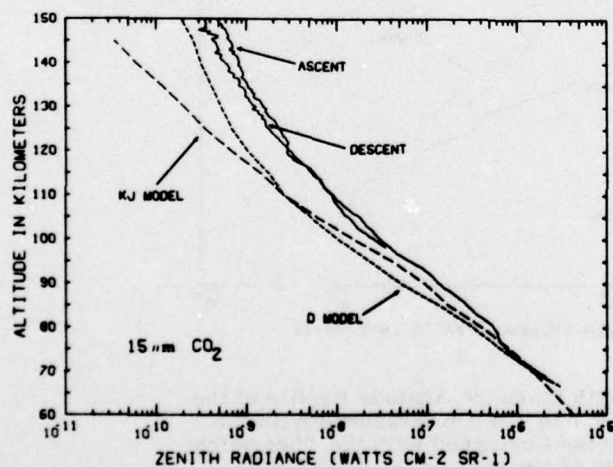


Figure 14. Zenith Radiance Altitude Profile at $15\text{ }\mu\text{m}$ Measured With the LWIR Spectrometer Compared With Theoretical Models. The solid curves are the measurements while the dashed curves show the model calculations of Kumer and James (KJ) and Degges (D)

et al.²²; Barnett et al.²³ Finally, preliminary analysis of the 1974 LWIR CVF rocket measurements under ambient conditions gives approximately the same intensity as under auroral conditions (Stair et al.²⁴). This was expected since neither band is predicted to be enhanced by aurora to any significant extent (Bishop et al.²⁵).

5.4 H₂O Zenith Radiance Profile

Apparent high altitude emission from the long-wavelength wing of the 6.3- μ m water band is evident in Figure 10. The resulting zenith radiance altitude profile obtained by integrating the data from 6.7 to 7.6 μ m is shown in Figure 15. Also shown by the dashed curve is a theoretical calculation for the water radiance profile in this wavelength region using the model of Degges¹⁶ and the fact that 20 percent of the 6.3- μ m water band emits between 6.7 and 7.6 μ m. The calculation used a standard arctic atmosphere with 5 ppm H₂O and temperatures from Table 1. The primary excitation processes for H₂O at these altitudes are earthshine $h\nu + \text{H}_2\text{O} \rightarrow \text{H}_2\text{O}^\dagger$, and the transfer of vibrational energy through thermal collision $\text{H}_2\text{O} + \text{M} \rightarrow \text{H}_2\text{O}^\dagger + \text{M}$. De-excitation of vibrationally excited H₂O is by radiation and collisional deactivation. Collisional excitation and de-excitation is mainly due to collisions with molecular oxygen and to a lesser degree with molecular nitrogen. The resulting agreement between the calculated and measured data supports the contention that the emission is indeed from the 6.3- μ m water band.

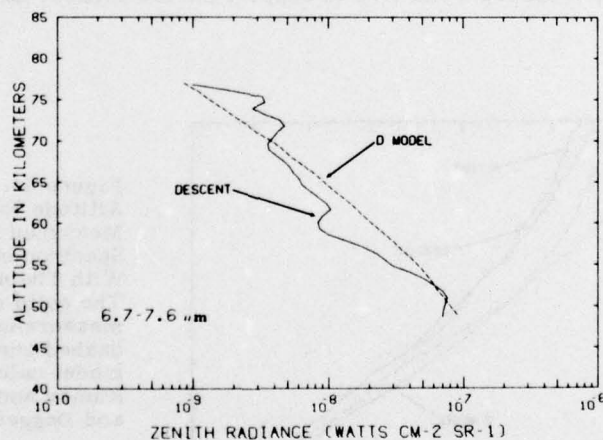


Figure 15. Zenith Radiance Altitude Profile of the Emission from 6.7 to 7.6 μ m Measured With the LWIR Spectrometer Compared With the Theoretical H₂O Calculations of Degges

5.5 Unidentified Emissions

Above 100 km, significant unidentified emission was observed at $9.3\text{ }\mu\text{m}$ with weaker features at 6.9 , 7.3 , 8.0 , 11.1 , and $12.3\text{ }\mu\text{m}$. All these emission bands can be seen in Figure 6 with the feature at $9.3\text{ }\mu\text{m}$ being a particularly strong emitter. Figure 16 is the zenith altitude profile of the $9.3\text{ }\mu\text{m}$ feature which shows a marked asymmetry between ascent and descent. The observed radiance values are plotted vs time in Figure 17 where it becomes obvious that, after an initial rise, the intensity decreases throughout the remainder of the flight. Figure 18 shows the time variations of the weaker unidentified emissions which were observed above 100 km. It is seen that all these features have a similar time dependence as the larger feature at $9.3\text{ }\mu\text{m}$. The horizontal velocity component of the payload is about 0.55 km/sec and during the time shown in these plots, the horizontal range from the launch point increases approximately 150 km.

Further examination of Figure 6 and the scans above 100 km in Appendix A, shows that in addition to the spectral features mentioned there is a background continuum which increases towards the shorter wavelengths. The decrease in the intensities of the emissions shown in Figures 17 and 18 is caused by both the unidentified bands and continuum background. For the zenith radiance profile between 8.5 and $10.9\text{ }\mu\text{m}$ shown in Figure 18, the continuum accounts for approximately 43 percent of the total emission up to 300 sec when it drops off to less than 20 percent.

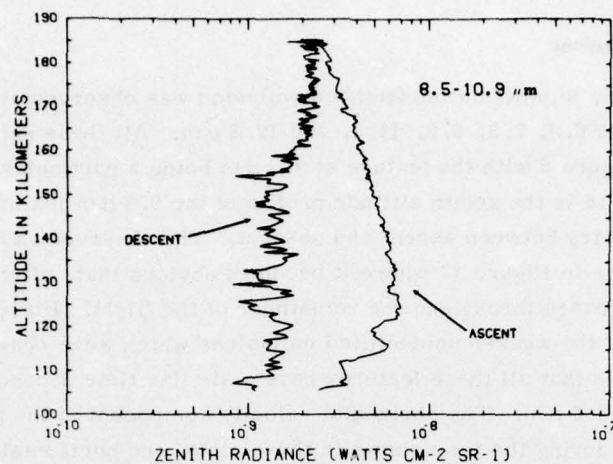


Figure 16. Zenith Radiance Altitude Profile of the Strong Unidentified Emission at $9.3 \mu\text{m}$

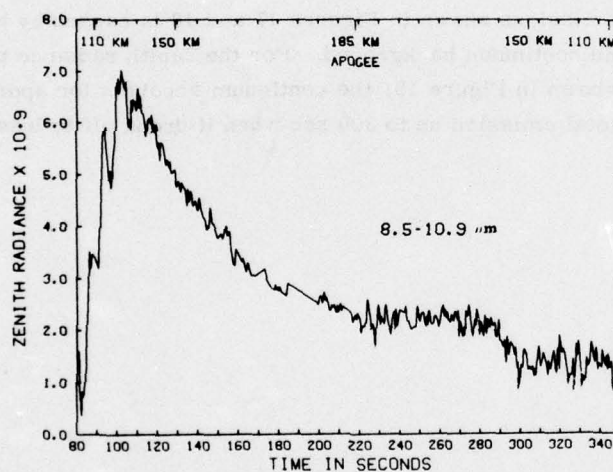


Figure 17. Zenith Radiance of the Unidentified Emission Feature at $9.3 \mu\text{m}$ as a Function of Time After Launch

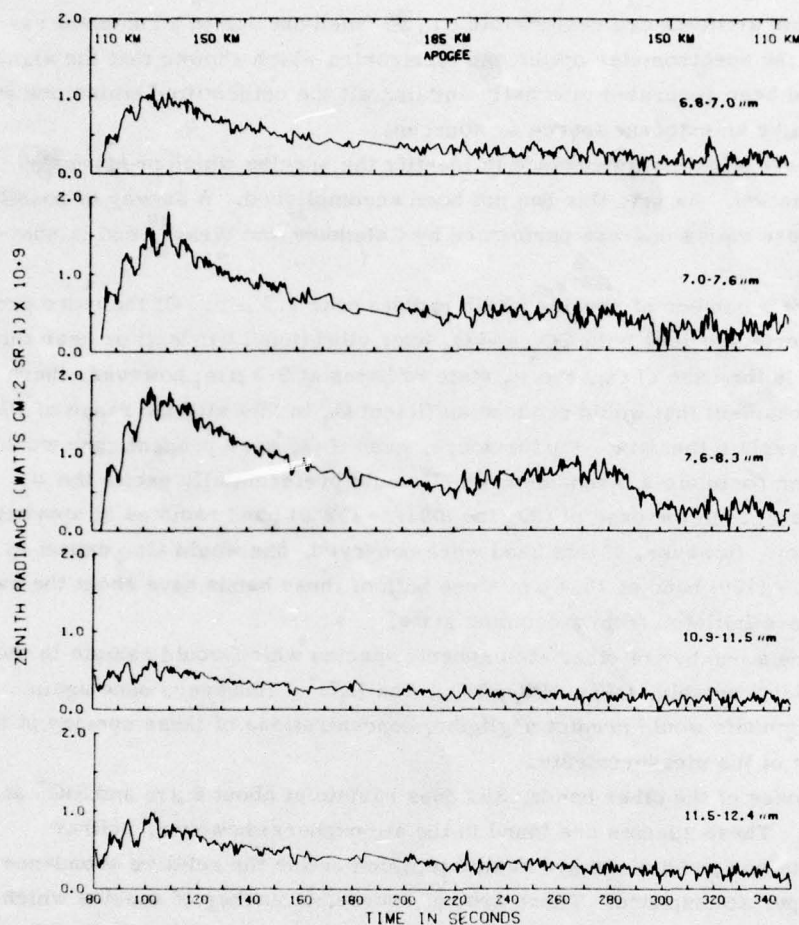


Figure 18. Zenith Radiance Values of Weaker Unidentified Emissions as Functions of Time After Launch

There are a number of possible explanations regarding these emissions. The first is that a yet unidentified atmospheric radiation was in the instruments's field-of-view during ascent, but due to its temporal and/or spatial behavior moved out of the field-of-view during descent. Auroral related emissions, for example, could have such profiles. Secondly, it is possible that these spectral features are due to exo-atmospheric sources such as dust clouds, stars, galaxies, and so forth. A third possibility is that the emissions are due to contaminants introduced by the measuring system or from the rocket exhaust which were carried along during the payload ascent and diffused at the higher altitudes. Finally, the possibility that

instrumentation artifacts are responsible can be ruled out due to a complete re-evaluation of the spectrometer optics and electronics which showed that the signals could not have been generated internally and that all the unidentified emissions were indeed caused by an external source or sources.

It is clearly of prime importance to identify the species which produce the observed radiation. As yet, this has not been accomplished. A survey of possible sources of these emissions was performed by Caledonia and Wray²⁶ and is summarized here.

There are a number of species which radiate near $9.3 \mu\text{m}$. Of the more prominent atmospheric species, both CO_2 and O_3 have vibrational bands at or near this wavelength. In the case of O_3 , the ν_1 state radiates at $9.3 \mu\text{m}$; however, there is no known mechanism that would produce sufficient O_3 in this altitude range of 100 to 185 km to explain the data. Furthermore, even if O_3 were present, one would have to further postulate a mechanism which would preferentially excite the ν_1 state over the ν_3 . In the case of CO_2 the $(001) \rightarrow (02^*0)$ band radiates at approximately $9.4 \mu\text{m}$. However, if this band were observed, one would also expect to see the $(001) \rightarrow (100)$ band at $10.4 \mu\text{m}$ since both of these bands have about the same lifetime and are initiated from a common state.

There are a number of other atmospheric species which would radiate in the region of $9.3 \mu\text{m}$ notably, CHO , HNO , HO_2 , and H_3O^+ . However, once again atmospheric models would predict negligible concentrations of these species at the high altitudes of the measurements.

For the case of the other bands, SiO does radiate at about $8 \mu\text{m}$ and SiO^+ at about $12 \mu\text{m}$. These species are found in the atmosphere; however, neither measurements nor predictions are available which define the relative abundance of SiO in the upper atmosphere. There are, of course, a number of species which would radiate at the designated wavelengths, for instance PO , AlN , B_2O , CH_2 , COS , FeO , WO , PO_2 , and so forth. Such species are not found in the natural atmosphere but might arise through instrumentation contamination.

A column density of the radiating species can be estimated from the data at $9.3 \mu\text{m}$. For a band radiance of $3 \times 10^{-9} \text{ W cm}^{-2} \text{ sr}^{-1}$ and a radiative lifetime of 10^{-2} sec , the required excited state column density would be $1.5 \times 10^{10} \text{ part-cm}^{-2}$.

The total species column density cannot be specified unless the excitation source is defined. For earthshine excitations and radiative decay as the only loss mechanism, a column density of $10^{13} \text{ part-cm}^{-2}$ would be required at a base altitude of 185 km. For comparative purposes, the column density of N_2 between 180 to 300 km

26. Caledonia, G. E. and Wray, K. L. (1974) Investigation of Auroral Phenomena and Light Scattering Models, Final Report, PSI-TR-5, Subcontract No. 129234B to Utah State University, Contract No. F19628-73-C-0048, Physical Sciences, Inc., Waverfield, Mass.

is approximately 2×10^{16} part-cm⁻². Based upon these numbers, it would appear that earthshine would be an unlikely excitation source for the observed radiation.

It is also possible to consider that the unknown radiation was collisionally excited. Assuming again that radiative decay is the only loss mechanism, a collisional rate constant of 10^{-10} cm³ sec⁻¹ and a collision partner number density of 10^{10} part-cm⁻³ (approximate atmospheric number density at 185 km) a lower bound requirement for the column density of 1.5×10^{12} part-cm⁻² is obtained. This bound is very crude and if collisions were the excitation source, most probably the column density of radiating species required to produce the observed radiation would be much larger.

With regard to the estimated excited state column density, it should be mentioned that if the observed radiation were due to instrument contamination, the molecular impurity levels would have to be relatively large. For example, for a radiative lifetime of 10^{-2} sec and a contamination length of one meter, the contaminant density would have to be larger than 1.5×10^8 part-cm⁻³ and this should be a strong lower bound.

There are a number of other possible radiation sources which cannot be ruled out. It is conceivable, for instance, that the observed bands could arise from electronic transitions of atmospheric species. For example, little is known about the high lying Rydberg states of N₂. High level Rydberg state transitions might well occur in the 10-μm region and highly nonequilibrium electronic state populations could be generated during an auroral event.

Another possibility would be particulate emission where the emissivity of the particulate material was highly structured so as to give the appearance of band radiation. For purposes of example, consider spherical particles at a temperature of 200°K and unity emissivity. For a very large particle, say $r = 10$ μm, 9 part-cm⁻² would be sufficient to explain the data. On the other hand, for 1-μm radius particles, a column density of order 1.5×10^3 part-cm⁻² would be required.

On the surface, one would not expect particulate radiation to represent a viable source for the observed radiation, in particular because of the highly structured emissivity that would be required. Nonetheless, this source cannot be ruled out completely.

The possibility that the observed radiation arises from exo-atmospheric sources must be considered. For example, the zodiacal light has been postulated to be made up of particles of "dirty quartz", and SiO and SiO₂ have spectral bands in the wavelength regions of the unidentified emitters. The observed variation in intensity vs time (or apparent observation position due to payload velocity) appears to argue against this explanation. Known infrared celestial sources such as stars, galaxies,

and so forth, were eliminated as candidate sources by comparison with AFCRL Infrared Sky Survey.²⁷

Another potential source would be the vibrational/rotational bands of interstellar molecules. The radiance of these bands is not readily amenable to prediction and satellite measurements would be of great value in determining their importance. Many interstellar molecules have been identified to date, for the most part through the identification of rotational transitions in the mm to cm wavelength region. A number of isotopic variations of these molecules has also been detected.

These molecules are typically found in interstellar molecular clouds. With the exception of H₂, which is by far the most abundant interstellar molecule, estimated line densities of these molecules are of order 3×10^{12} to 3×10^{16} part-cm⁻². The estimated CO line density falls at the upper end of this range while that for most other molecules falls at the lower. The typical kinetic temperatures of interstellar clouds are predicted to lie between approximately 20 to 125° K while observed rotational state temperatures have typically been found to fall between 4 to 45° K. It should be emphasized that the rotational and vibrational populations of these molecules should be severely collision limited.

Evidence of high altitude emissions in this wavelength region has been observed on two subsequent flights. Preliminary analysis of the 1974 LWIR CVF (with no auroral activity) shows evidence of an emission band around 9.3 μm with a slightly different band shape; however, the background continuum is not evident. Preliminary analysis²⁸ of a rocketborne LWIR radiometer flown during ICECAP 75 into an intense IBC III auroral breakup also indicates that above 100 km there are emissions in the 7 to 12 μm region at levels higher than predicted for ozone; however, the time history of the radiation showed an increasing value throughout the flight which is just the opposite of the 1973 LWIR CVF spectrometer. The radiometric measurements would not, however, rule out emissions from contaminant exhaust gases as it used a different boost rocket and the trajectory of any unwanted radiators could be quite different.

To resolve whether the emissions are due to possible instrumentation contaminants or exhaust gases or if they are indeed emissions from unidentified atmospheric or exo-atmospheric radiators will require additional experiments, preferably with higher spectral resolution for positive identification and using a "clean" booster or observation platform.

27. Walker, R. G. and Price, S. D. (1975) AFCRL Infrared Sky Survey, Volume I., Catalog of Observations at 4, 11, and 20 Microns, Environmental Research Papers, No. 522, AFCRL-TR-75-0373.

28. Nadile, R. M., AFGL, Private communications.

6. CONCLUSIONS

A liquid-helium-cooled, long-wavelength infrared (LWIR) spectrometer successfully obtained the first measurements of the infrared spectrum of the upper-atmospheric emissions between 7 and 24 μm .

All components of the rocket system performed well; however, the apogee obtained was approximately 9 km lower than predicted. This caused the clamshell closing and parachute deployment functions to be initiated at altitudes too low for completely successful execution. As a result, the spectrometer was damaged upon ground impact.

Excellent data were obtained from the LWIR spectrometer which was the primary payload sensor. The 3914 Å photometer provided a good measure of the intensity of the auroral form which was penetrated; however, the dust detector malfunctioned.

During an IBC II aurora, data were obtained on the 15- μm carbon dioxide emission from 65 to 150 km and on the 9.6- μm ozone emission between 45 and 100 km. The data showed that the most accurate models at the time of the flight were in error by as much as two orders of magnitude leading to a revision of the theoretical predictions. In addition, emission data on the long wavelength wing of the 6.3- μm water band between 6.7 and 7.6 μm were obtained between 50 and 75 km.

Above 100 km, significant unidentified emission was observed at 9.3 μm with weaker features at 6.9, 7.3, 8.0, 11.1, and 12.3 μm . All these emissions showed a marked asymmetry between ascent and descent. Identification of the species which produce this observed radiation has not been accomplished at this time. Several possible sources have been investigated including atmospheric and exo-atmospheric radiators along with contaminants introduced by the measuring system or rocket exhaust. A complete investigation of the spectrometer optics and electronics has shown the emissions are not internally generated and are caused by an external source or sources.

References

1. Stair, A.T., Jr., Ulwick, J.C., Baker, K.D. and Baker, D.J. (1975) Rocket-borne observations of atmospheric infrared emissions in the auroral region, Atmospheres of Earth and Planets, edited by B.M. McCormac (D. Reidel, Dordrecht-Holland), pp 335-346.
2. Condron, T.P. (1973) Calibration of a Liquid Helium Cooled CVF Radiometer in a Warm Environment, AFCRL Instrumentation Papers, No. 199, AFCRL-TR-73-0480.
3. Rogers, J.W. (1975) Instrumentation Analysis and Data Processing for Rocket-borne LWIR Spectrometers (With Application to Rocket A18, 006-2 of 22 March 1973), Environmental Research Papers, No. 539, AFCRL-TR-75-0535, HAES Rept No. 23.
4. ICECAP '73 Field Requirements and Procedures (1973) SDC TM-620, Revision D, Space Data Corporation, Phoenix, Arizona, 6 March 1973.
5. Wyatt, C.L. (1971) Infrared Helium-Cooled Circular-Variable Spectrometer Model HS-1, Final Report, AFCRL-71-0340, Contract No. F19628-67-C-0340, Utah State University, Logan, Utah, September 1971.
6. Wyatt, C.L. and Baker, D.J. (1975) Development of a Liquid-Helium Cooled Rocketborne Spectrometer, Scientific Report No. 2, AFCRL-TR-75-0164, Contract No. F19628-73-C-0048, Utah State University, Logan, Utah, February 1975.
7. Wyatt, C.L. (1975) Infrared Spectrometer; Liquid-Helium-Cooled Rocketborne Circular-Variable Filter, Applied Optics, 14, No. 12:3086-3091.
8. Stair, A.T., Jr., Wheeler, N.B., Baker, D.J., and Wyatt, C.L. (1973) Cryogenic IR spectrometer for rocketborne measurements, NEREM 73 Record, IEEE Catalog No. 73 CHO-841-7 NEREM, pp 80-89.
9. Trajectory Report, Rocket No. A18-006-2 (1973) Analysis and simulation branch, AFCRL Computation Center.
10. Aspect Report, Rocket No. A18-006-2 (1974) Aspect Report Number 4531-9, Analysis and Simulation Branch, AFCRL Computation Center.

References

11. Romick, G. J. (1975) Report of the Geophysical Description and Available Data Associated with Rocket PF-BB-53, Scientific Rpt No. 2, AFCRL-TR-75-0040, Contract No. F19628-74-C-0188, Geophysical Institute, University of Alaska, January 1975.
12. Kofsky, I. L., Meriwether, J. W., Schroeder, J. W., and Sluder, R. B. (1974) Data Reduction and Auroral Characterizations of ICECAP, HAES Report No. 4, Final Report, DNA 3511F, Contract No. DNA001-73-C-0027, Photometrics, Inc., Lexington, Mass., September 1974.
13. Baron, M. and Chang, N. J. (1975) ICECAP '73A - Chatanika Radar Results, HAES Report No. 15, Topical Report, DNA 3531T, Contract No. DNA 001-74-C-0167, Stanford Research Institute, Menlo Park, California, April 1975.
14. Corbin, V. L., Dalgarno, A., Degges, T. C., House, F. B., Lilienfeld, P., Ohring, G., and Oppel, G. D. (1969) Atmospheric Radiance Models for Limb-Viewing Geometry in the Five To Twenty-Five Micron Spectral Region, Final Report, AFCRL-TR-0552, Contract No. F19628-69-C-0268, Honeywell, Inc.
15. Degges, T. C. (1972) A High Altitude Radiance Model, AFCRL-TR-72-0273, Visidyne Corporation, Burlington, Mass.
16. Degges, T. C. (1974) A High Altitude Radiance Model, Final Report, AFCRL-TR-74-0606, Contract No. F19628-72-C-0330, Visidyne Corporation, Burlington, Mass.
17. Roble, R. G. and Hays, P. B. (1974) On determining the ozone number density distribution from OAO-2 Stellar Occultation Measurements, Planet. Space Sci., 22:1337-1340.
18. Kumer, J. B. and James, T. C. (1974) CO₂ and N₂ vibrational temperatures in the 50 < Z < 130 km altitude range, J. Geophys. Res., 79:638-648.
19. Kumer, J. B. (1974) Atmospheric Non-LTE CO₂ ν_2 vibrational temperatures and radiances, EOS, 55:375.
20. James, T. C. and Kumer, J. B. (1973) Fluorescence of CO₂ near 4.3 microns: Application to daytime limb radiance calculations, J. Geophys. Res., 78:8320-8329.
21. Murcray, D. G., Barker, D. B., Brooks, J. M., Kosters, J. J., Murcray, F. H., and Williams, W. J. (1972) Atmospheric Emissions at High Latitudes, Final Report, Contract No. F19628-71-C-0171, University of Denver, Denver, Colorado, AFCRL-TR-72-0353.
22. Conrath, B. J., Hanel, R. A., Kunde, V. G., and Prabhakara, C. (1970) The infrared interferometer experiment on NIMBUS 3, J. Geophys. Res., 75:5831-5857.
23. Barnett, J. J., Houghton, J. T., Morgan, C. G., Pick, D. R., Rogers, C. D., Williamson, E. J., Cross, M. J., Flower, D., Peckham, G., and Smith, S. D. (1973) Stratospheric observations from NIMBUS 5, Nature, 245:141-143.
24. Stair, A. T., Jr., Ulwick, J. C., Baker, D. J., Wyatt, C. L., and Baker, K. D. (1974) Altitude profiles of infrared radiance of O₃ (9.6 μ m) and CO₂ (15 μ m), Geophysical Research Letters, 1, No. 3:117-118.
25. Bishop, R. H., Han, R. Y., Shaw, A. W., and Megill, L. R. (1973) Infrared Radiance Model for the Aurorally Disturbed Atmosphere, Final Report, AFCRL-TR-73-0527, Contract No. F19628-71-C-0257, Utah State University, Logan, Utah.

References

26. Caledonia, G. E. and Wray, K. L. (1974) Investigation of Auroral Phenomena and Light Scattering Models, Final Report, PSI-TR-5, Subcontract No. 129234B to Utah State University, Contract No. F19628-73-C-0048, Physical Sciences, Inc., Wakefield, Mass.
27. Walker, R. G. and Price, S. D. (1975) AFCRL Infrared Sky Survey, Volume I., Catalog of Observations at 4, 11, and 20 Microns, Environmental Research Papers, No. 522, AFCRL-TR-75-0373.
28. Nadile, R. M., AFGL, Private communications.

Appendix A

Spectral Data Scans Obtained During the Flight

This appendix contains all the usable data obtained during the flight. Individual scans are shown at altitudes below 104 km in Figures A1 through A11 (96.3 to 103.2 km) during ascent and in Figures A77 through A151 (102.9 to 45.6 km) during descent. At the higher altitudes, scans averaged over 2.5 km increments are shown in Figures A17 through A43 during ascent and Figures A44 through A76 during descent.

For individual scans, the scan number, time, and altitude are shown at the top of the figures. The inclusive scan numbers, times, and altitudes are shown for the averaged scans. The numbers in parentheses indicate the number of usable scans and the total number of scans in the 2.5-km increment being averaged. The spectral intensity values are in $\text{W cm}^{-2} \text{sr}^{-1} \mu\text{m}^{-1}$, with the exponent shown in the upper right-hand corner of the figure. The clipping of the $15\text{-}\mu\text{m CO}_2$ below 67 km is caused by amplifier saturation.

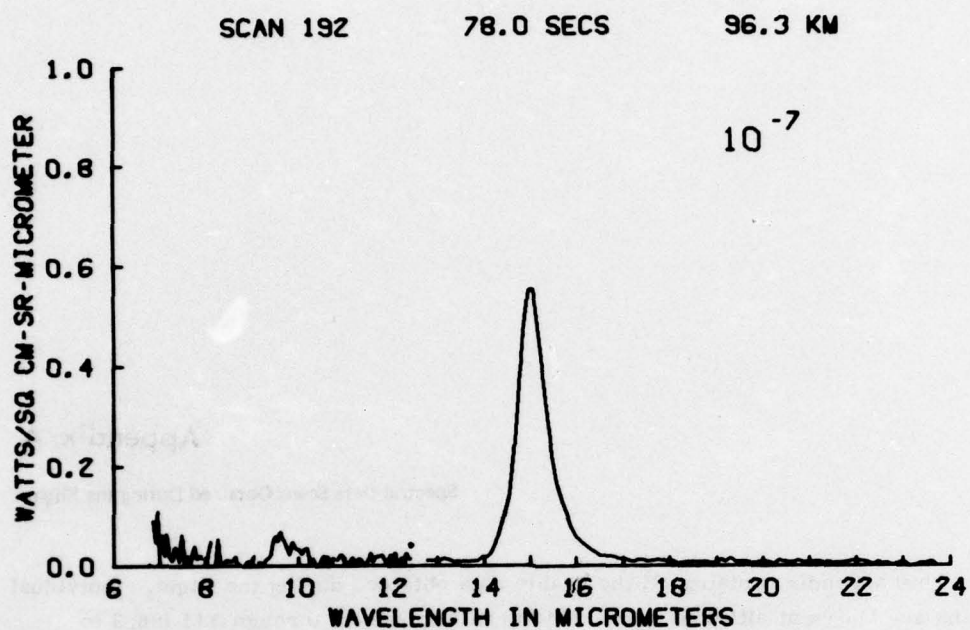


Figure A1

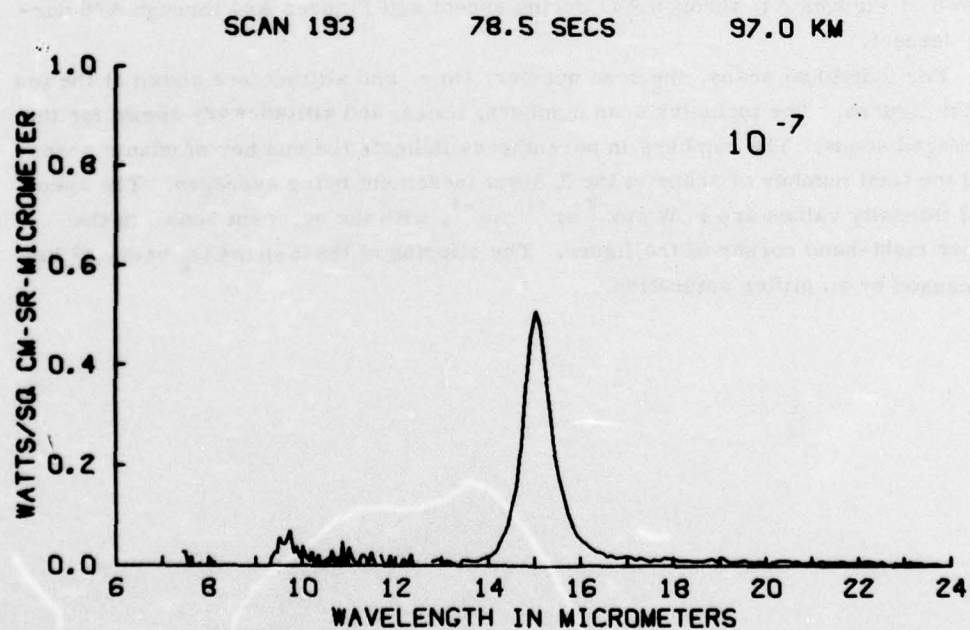


Figure A2

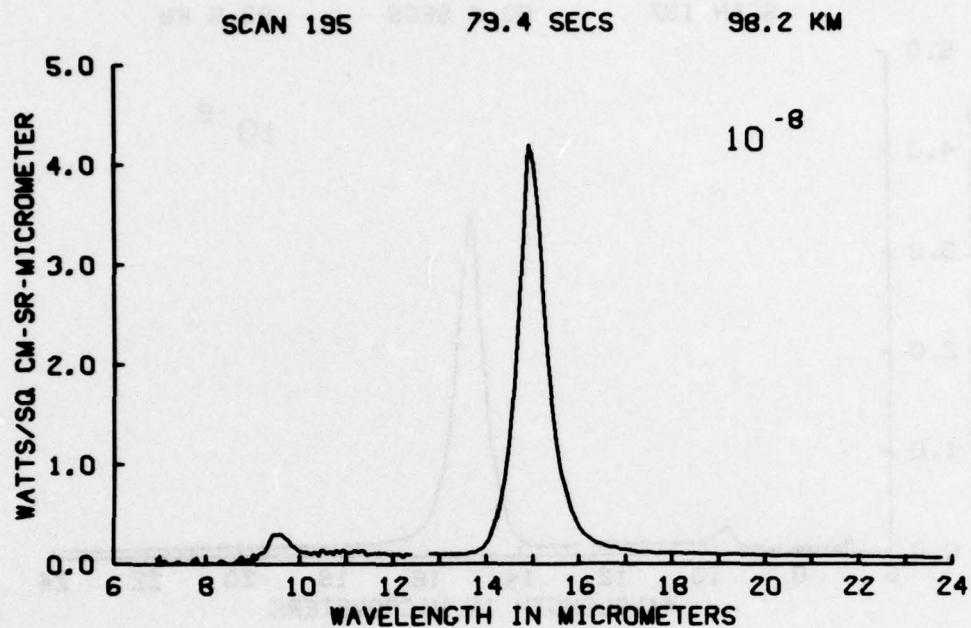


Figure A3

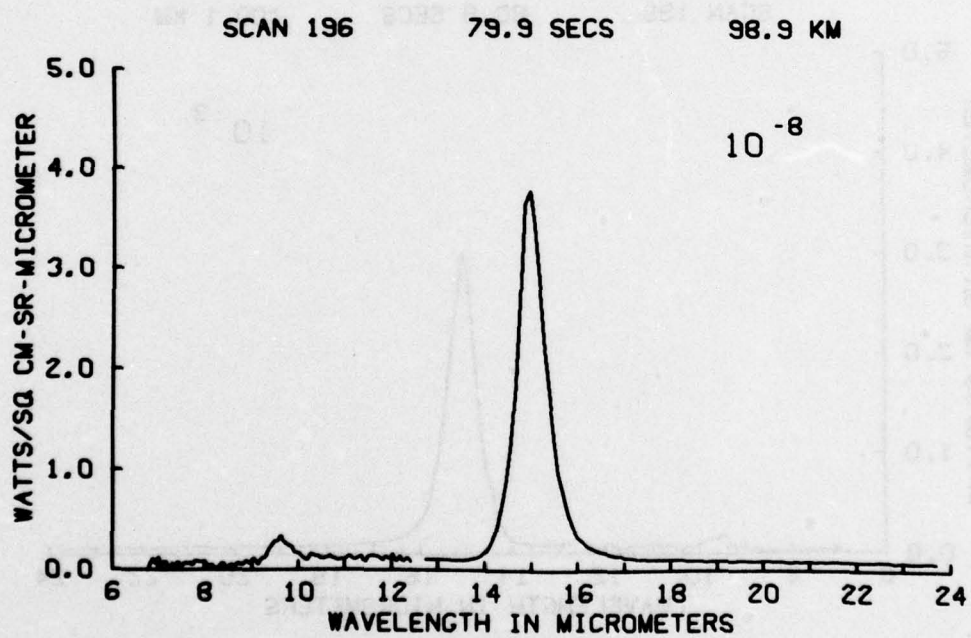


Figure A4

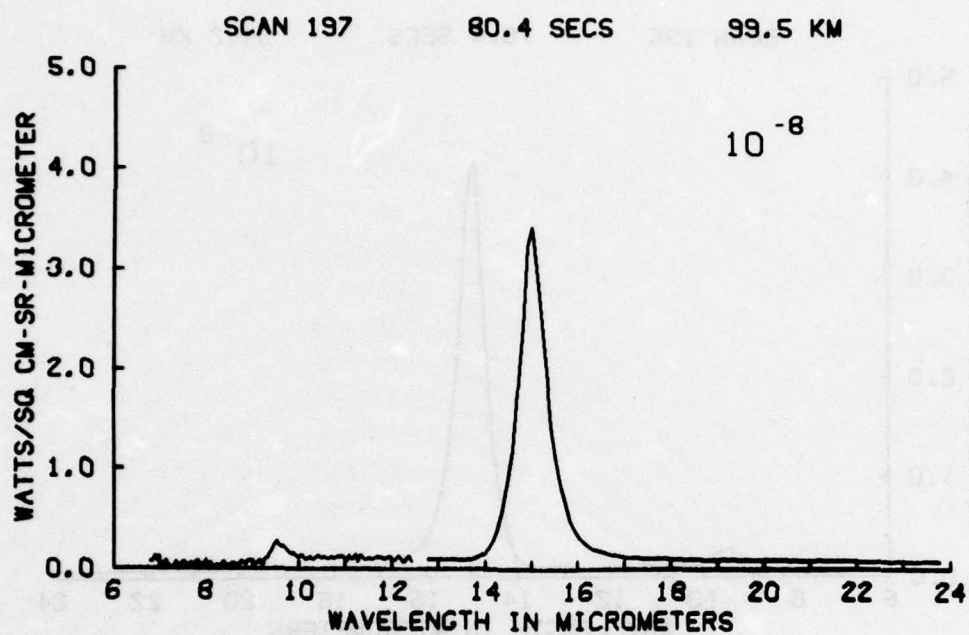


Figure A5

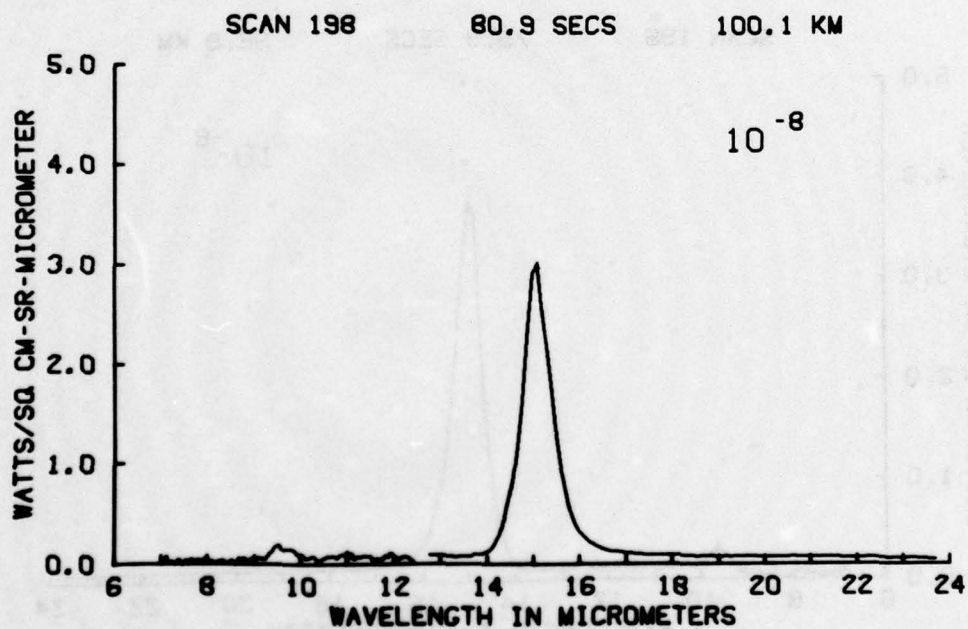


Figure A6

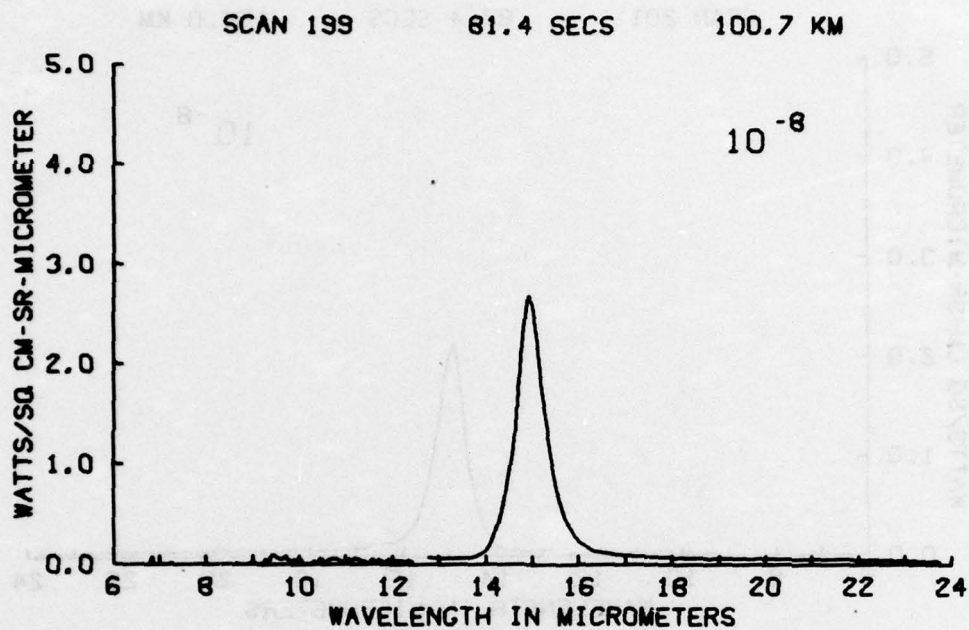


Figure A7

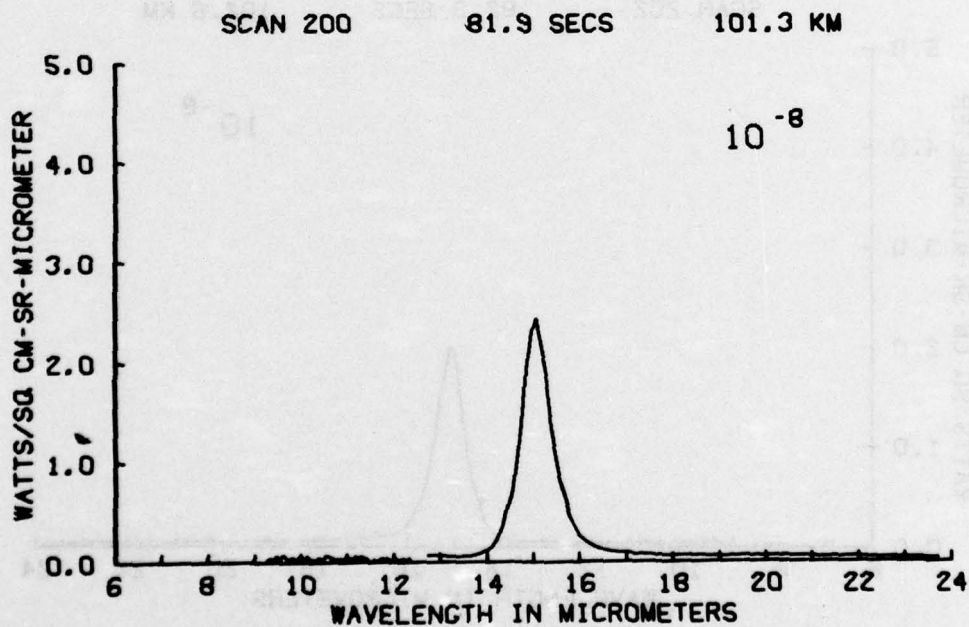


Figure A8

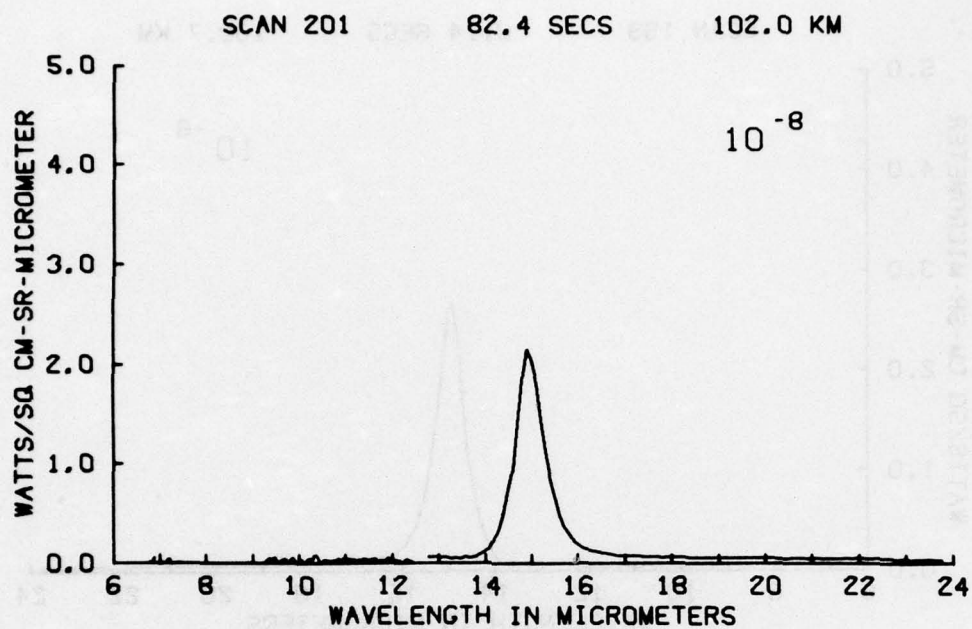


Figure A9

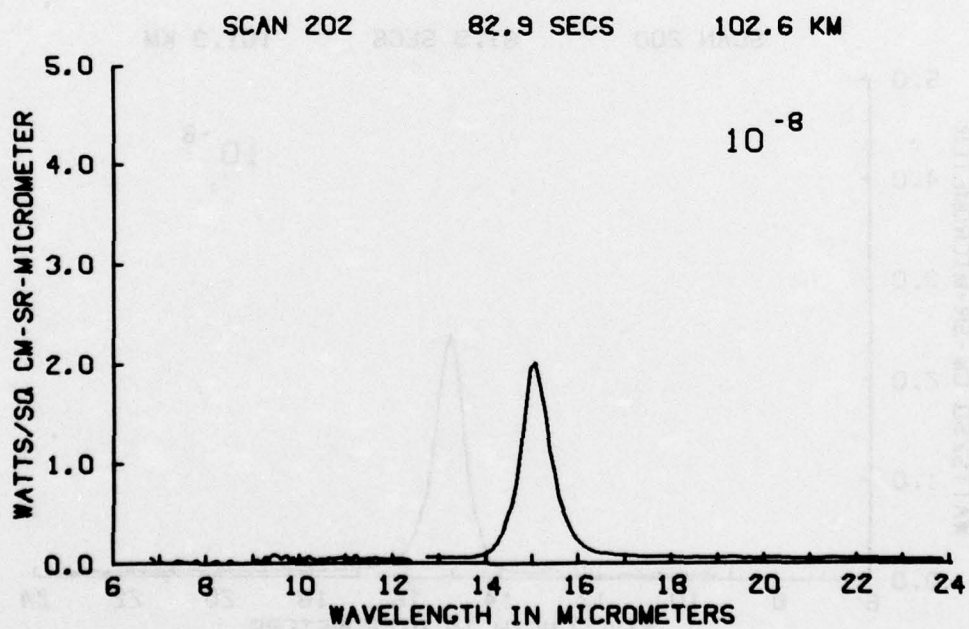


Figure A10

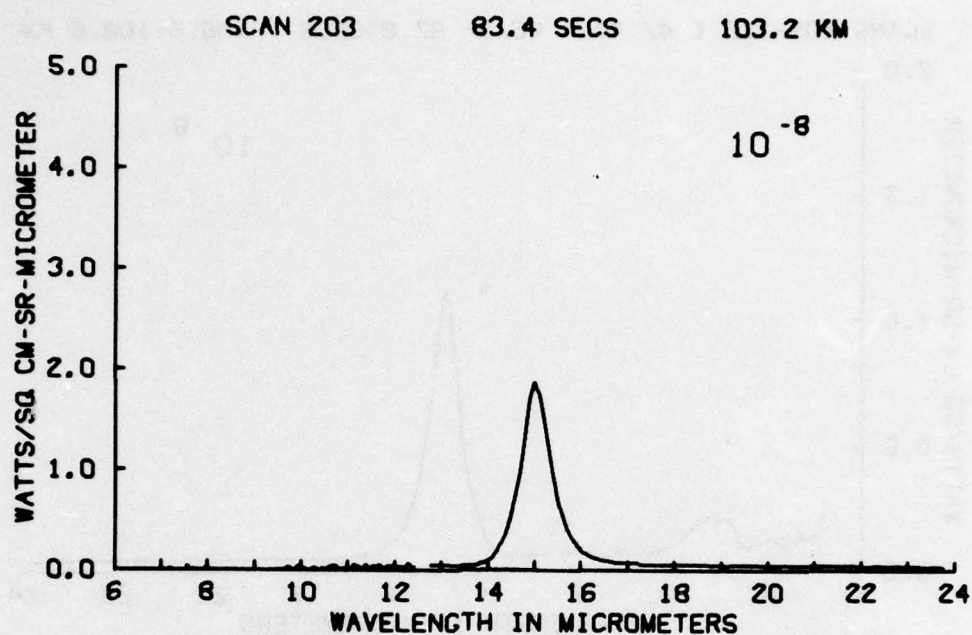


Figure A11

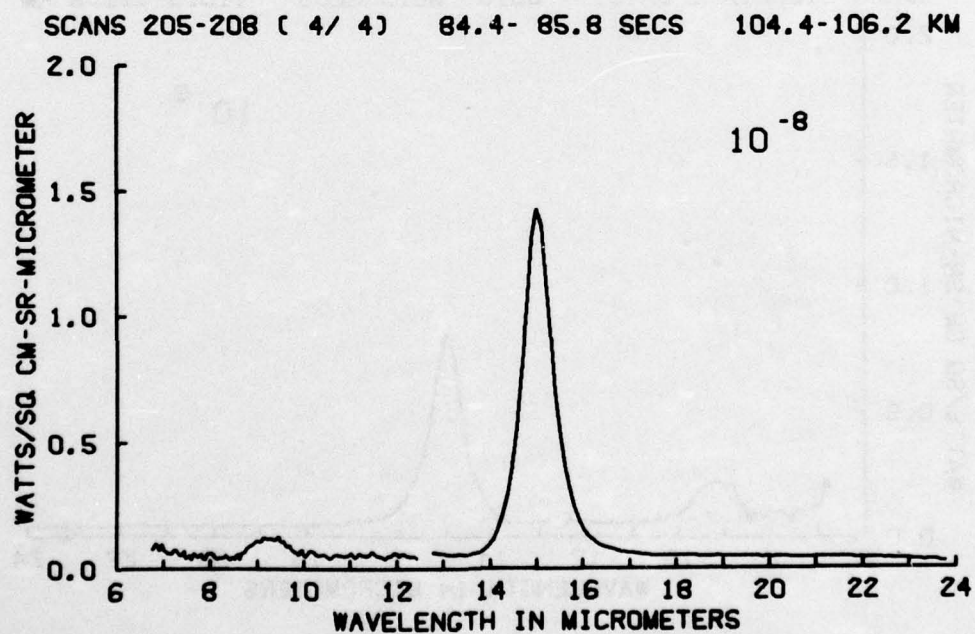


Figure A12

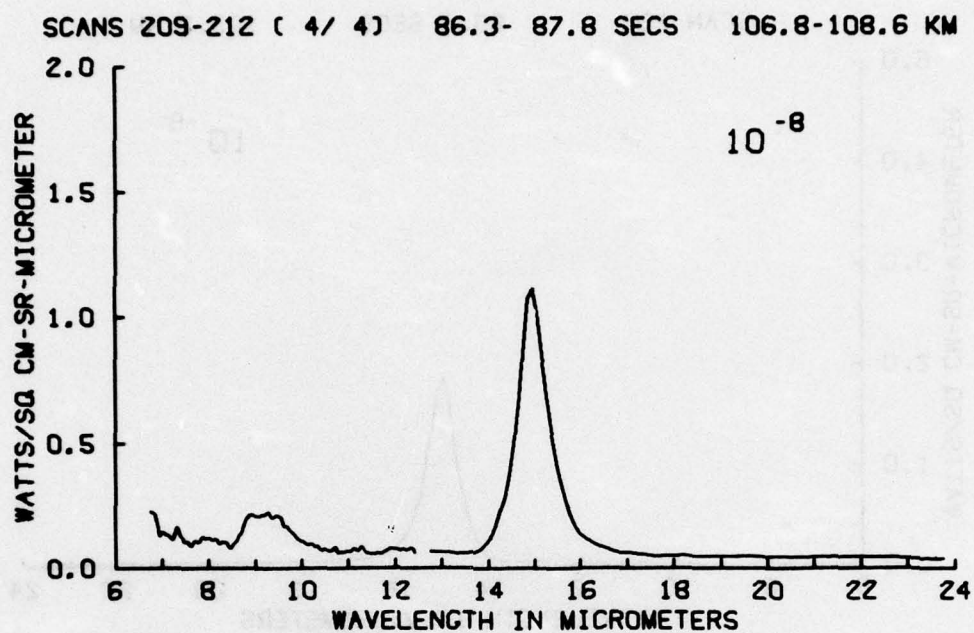


Figure A13

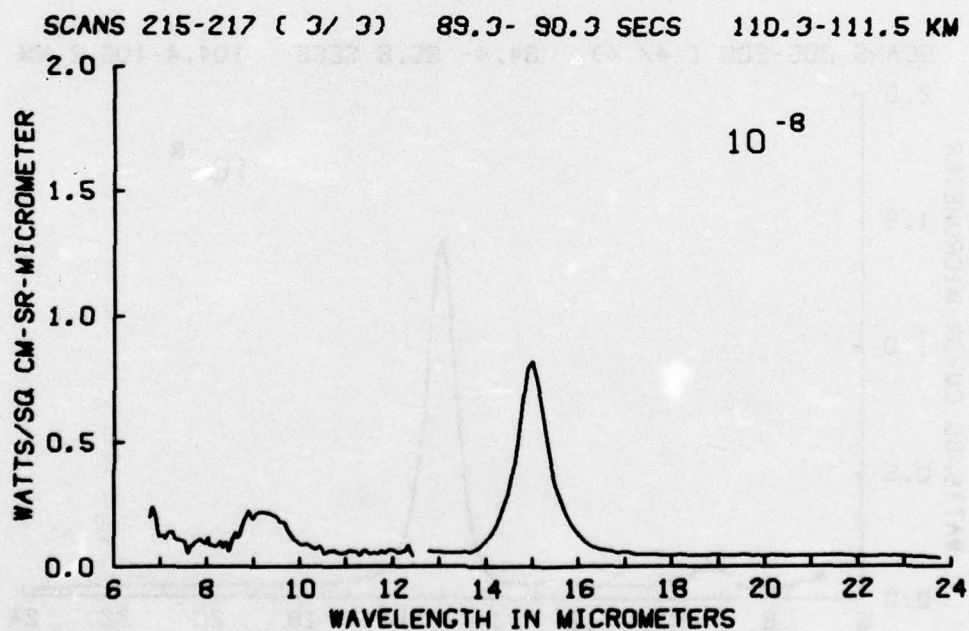


Figure A14

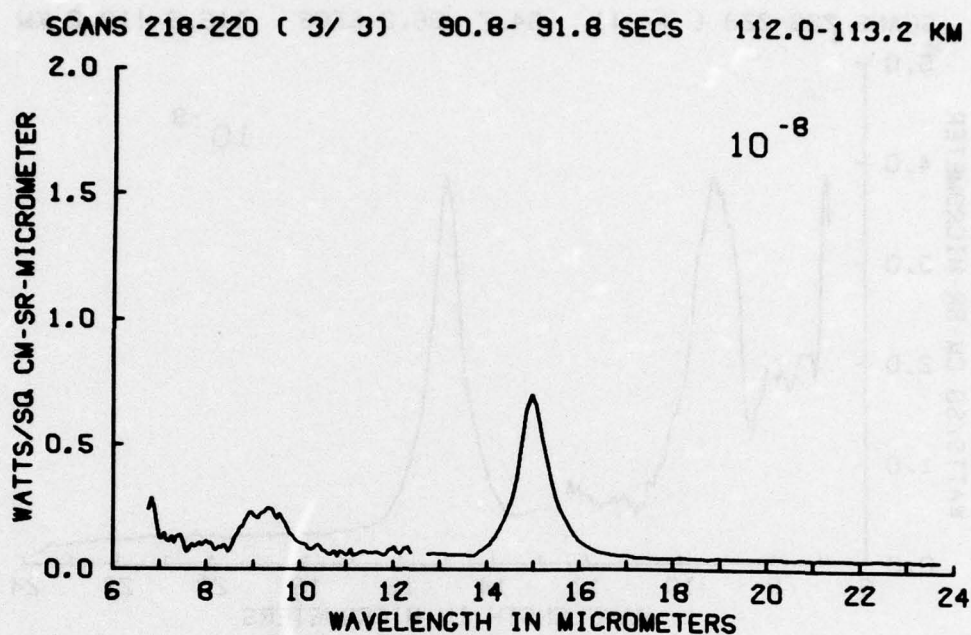


Figure A15

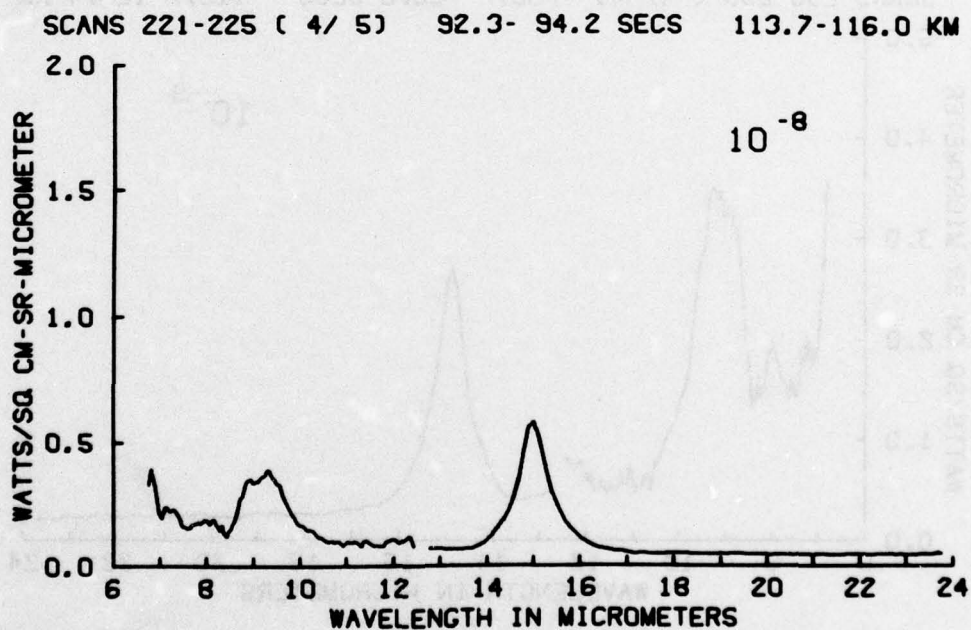


Figure A16

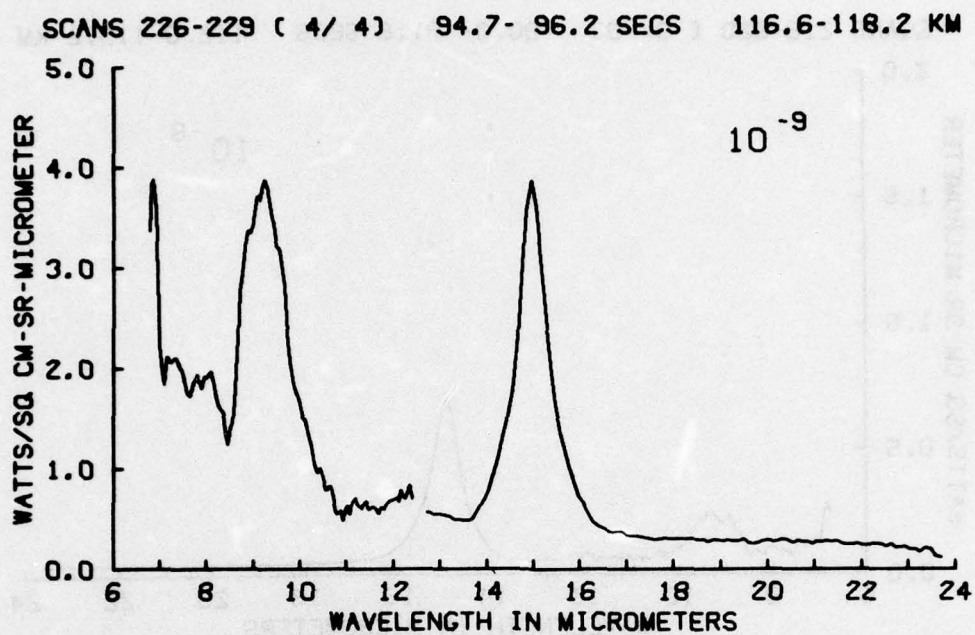


Figure A17

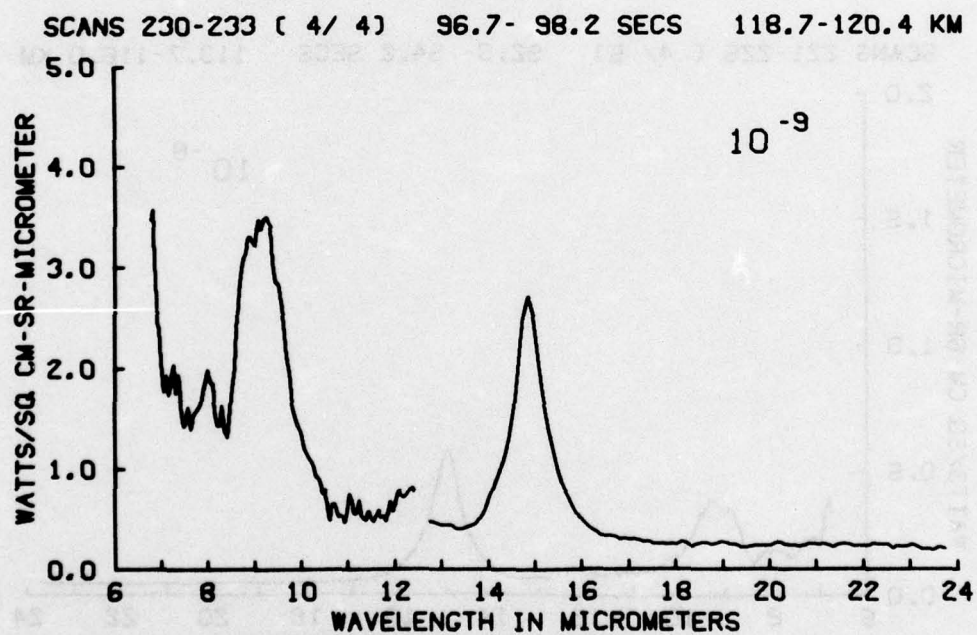


Figure A18

SCANS 235-239 (5/ 5) 99.2-101.1 SECS 121.4-123.6 KM

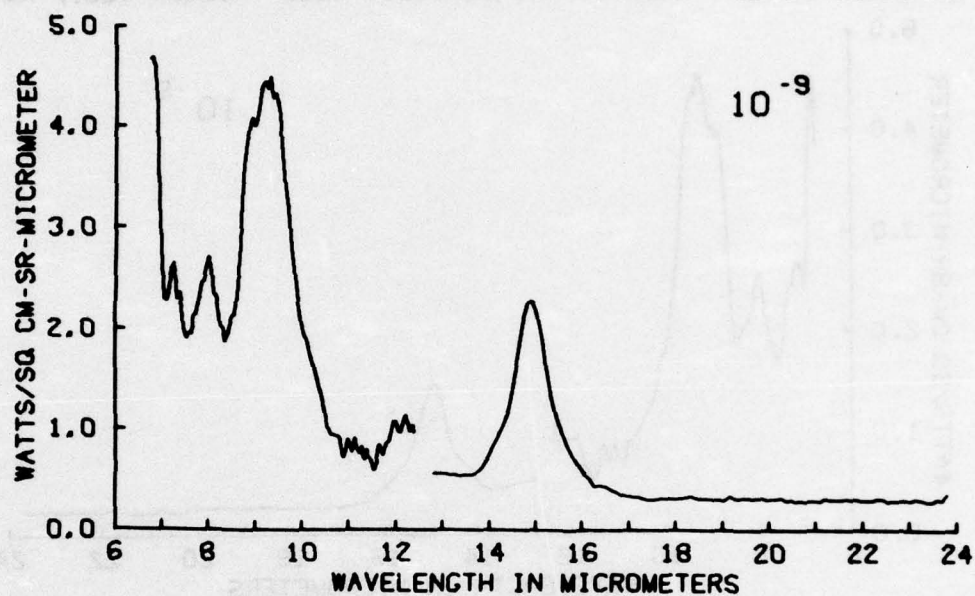


Figure A19

SCANS 240-243 (4/ 4) 101.6-103.1 SECS 124.1-125.6 KM

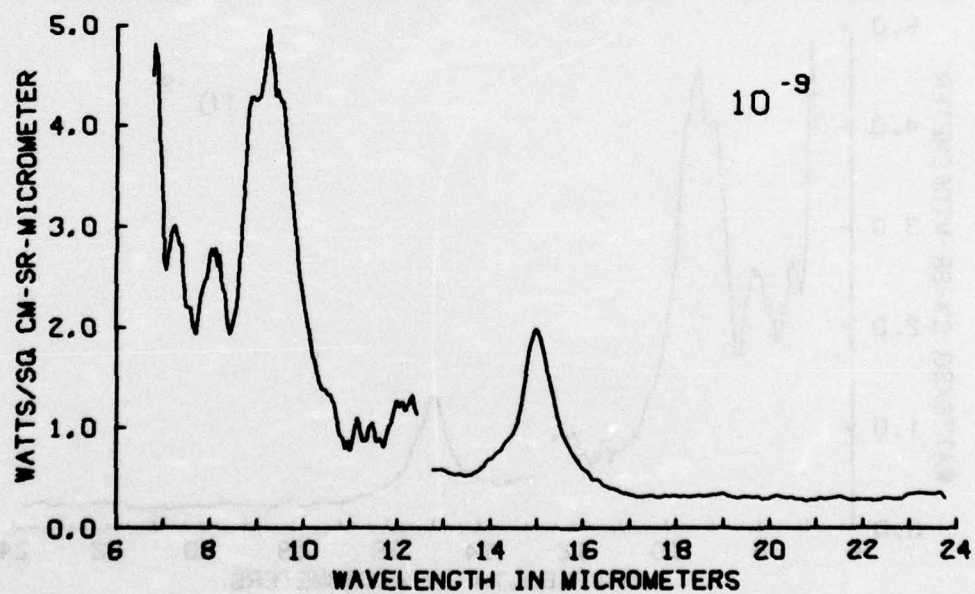


Figure A20

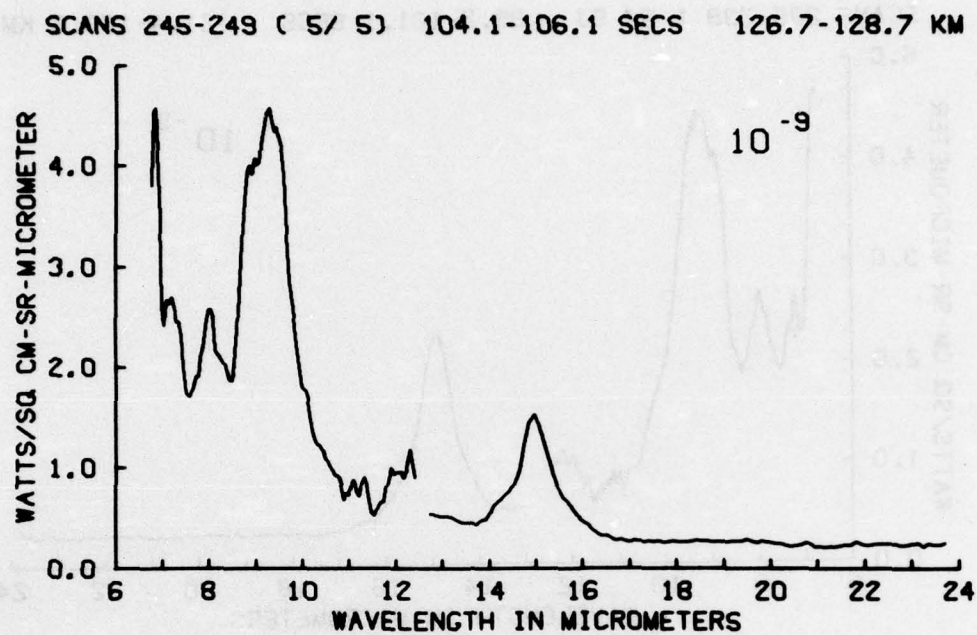


Figure A21

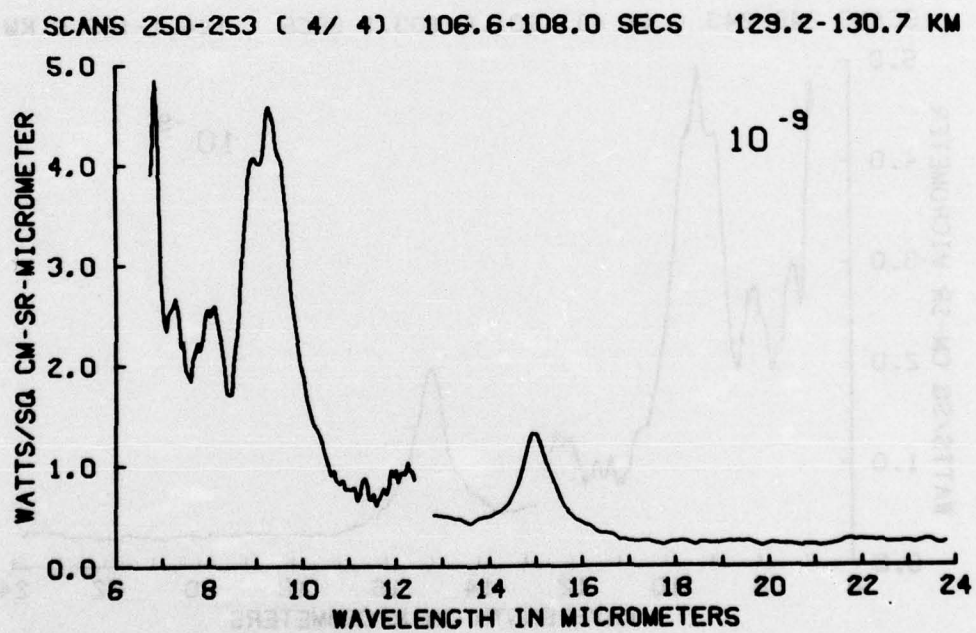


Figure A22

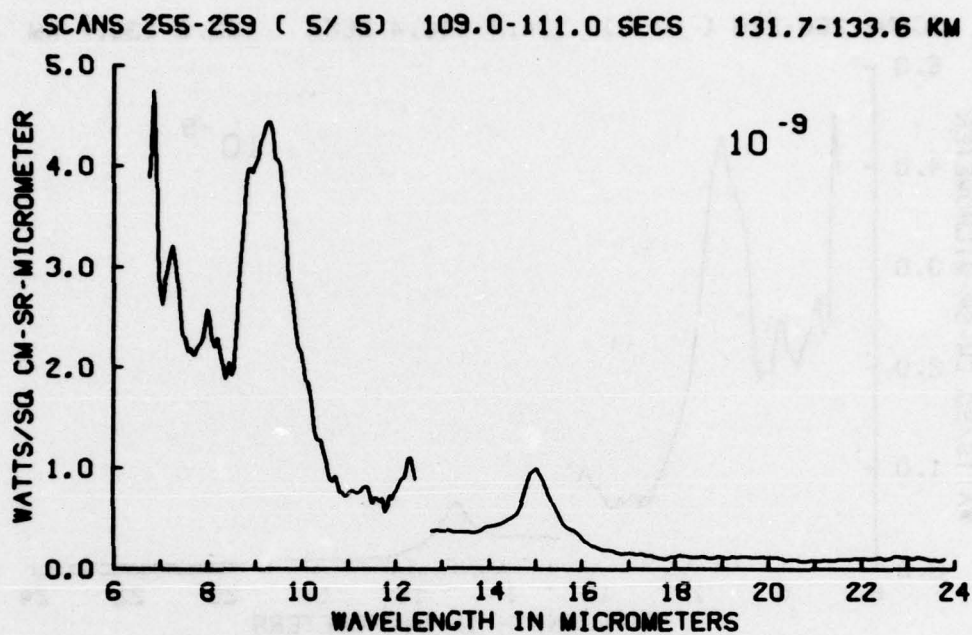


Figure A23

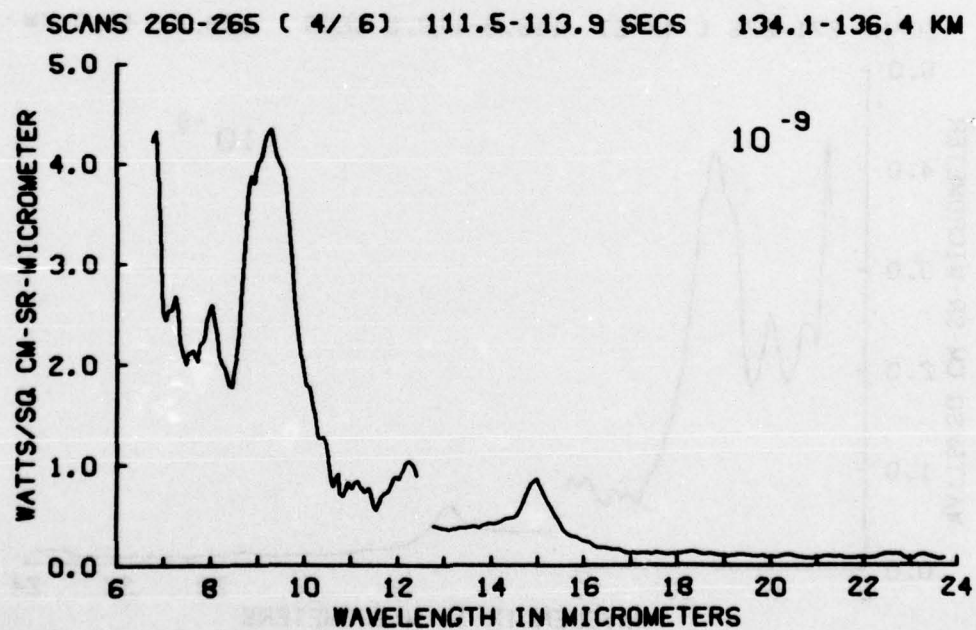


Figure A24

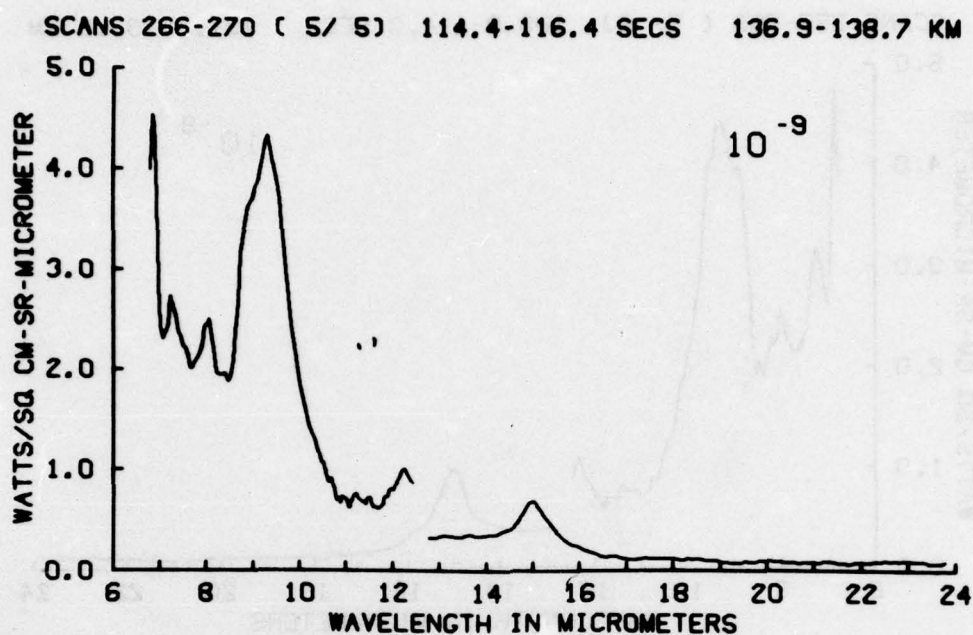


Figure A25

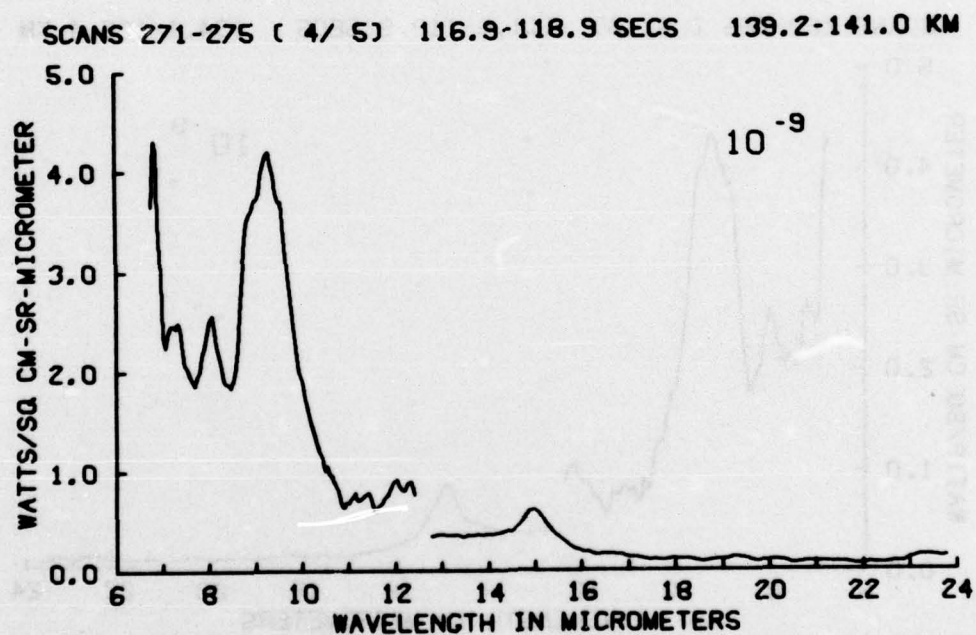


Figure A26

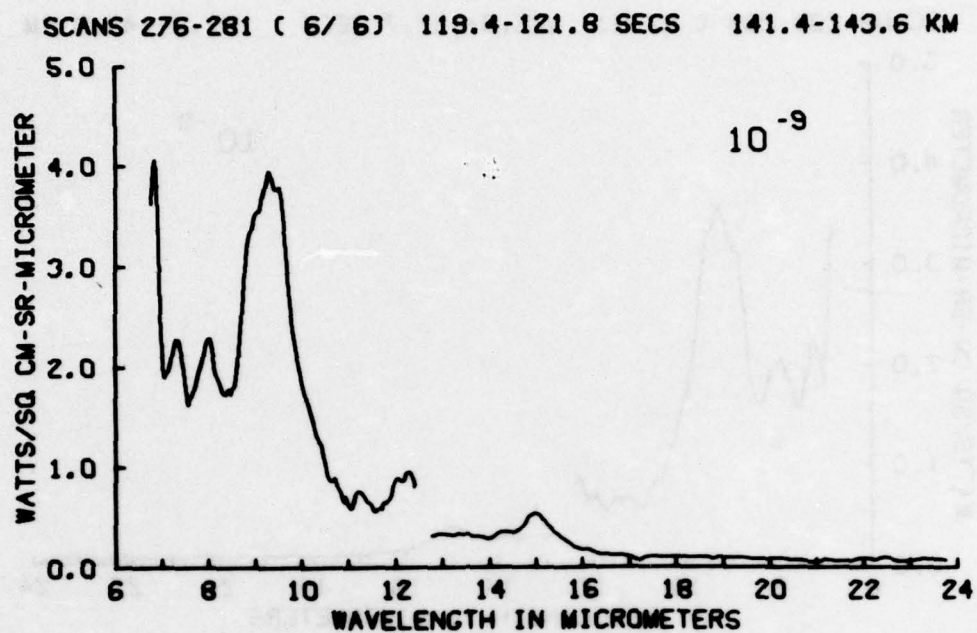


Figure A27

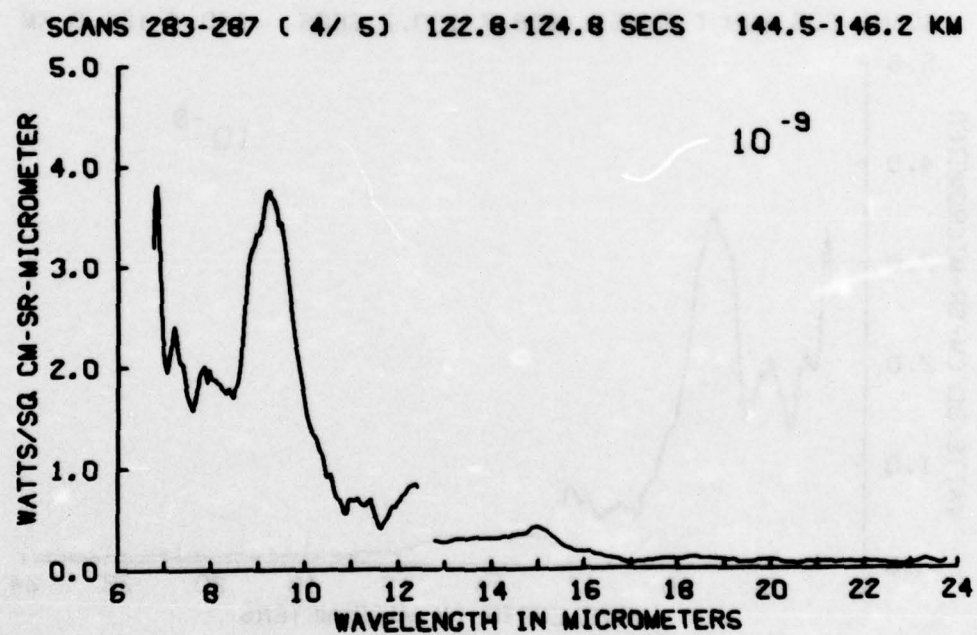


Figure A28

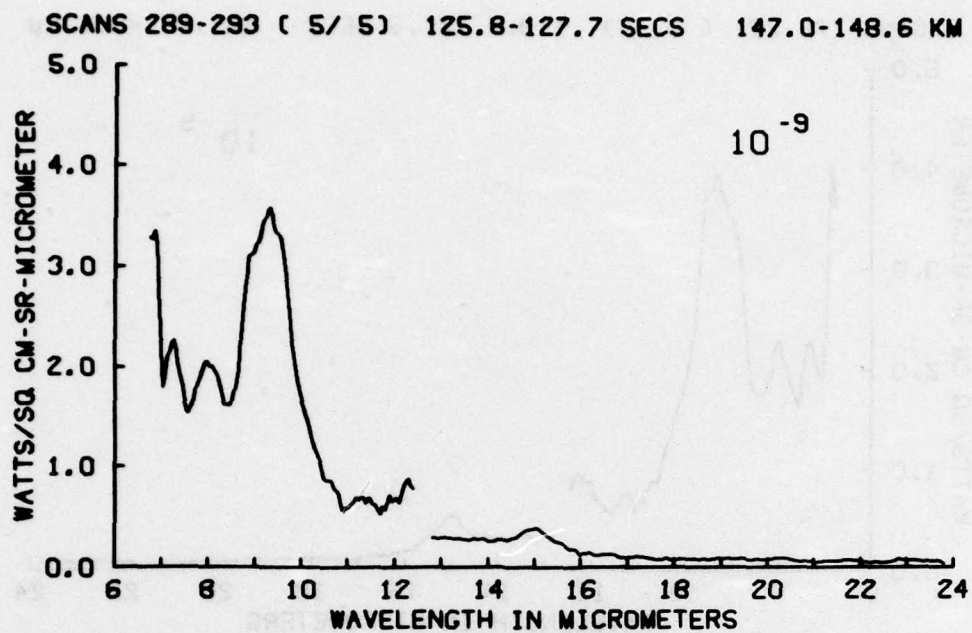


Figure A29

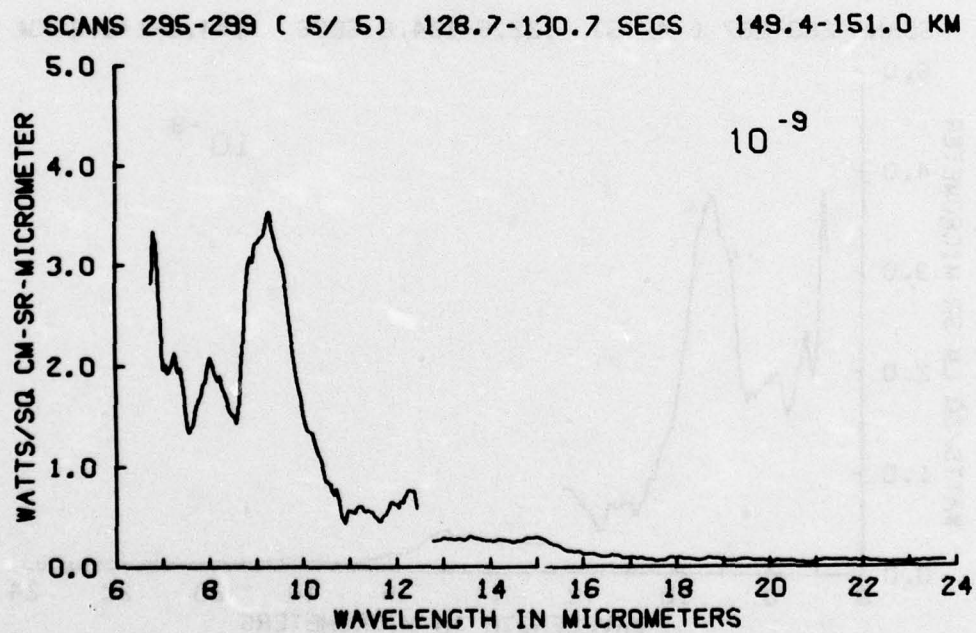


Figure A30

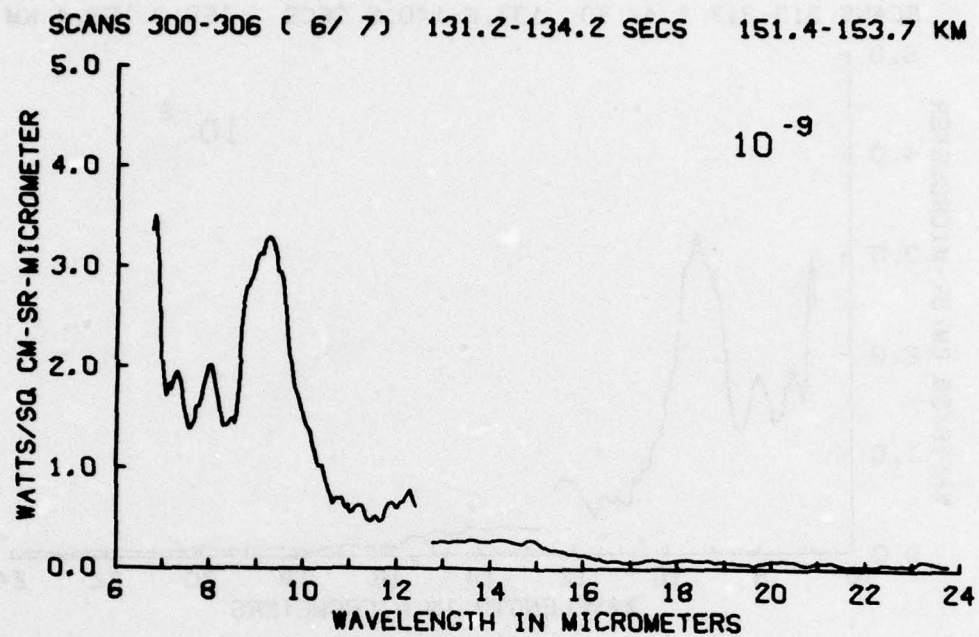


Figure A31

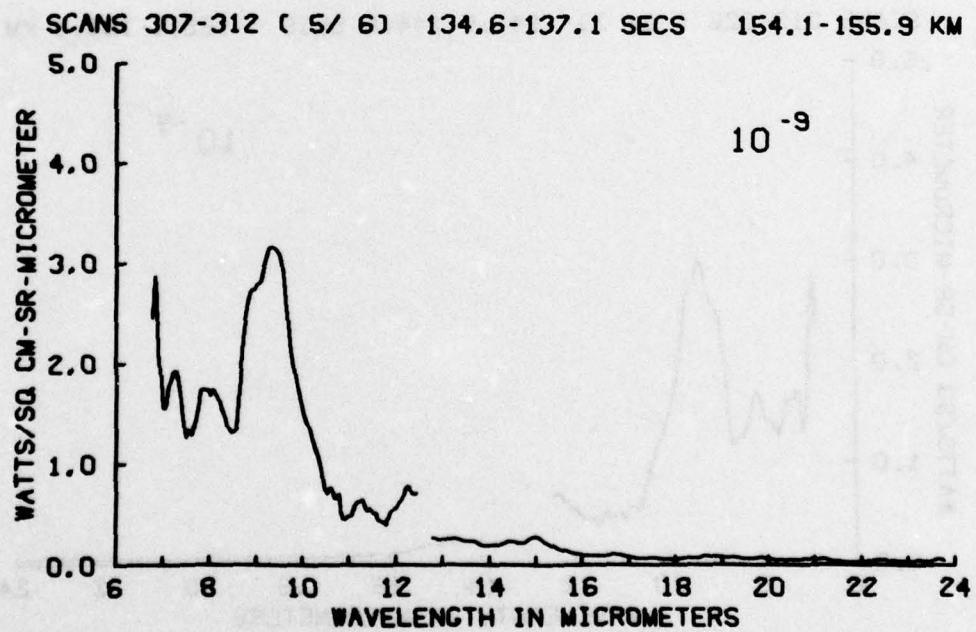


Figure A32

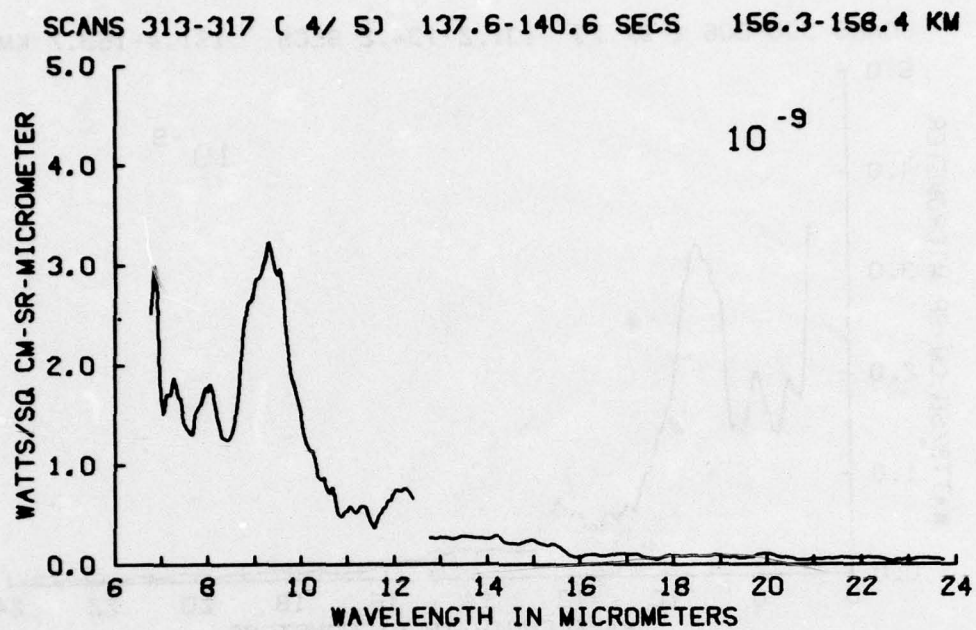


Figure A33

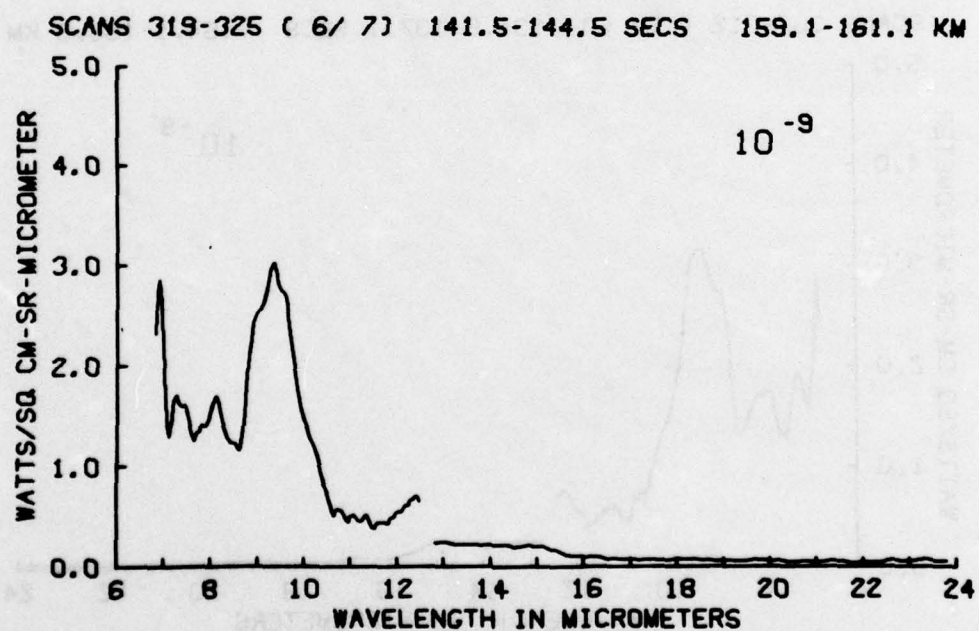


Figure A34

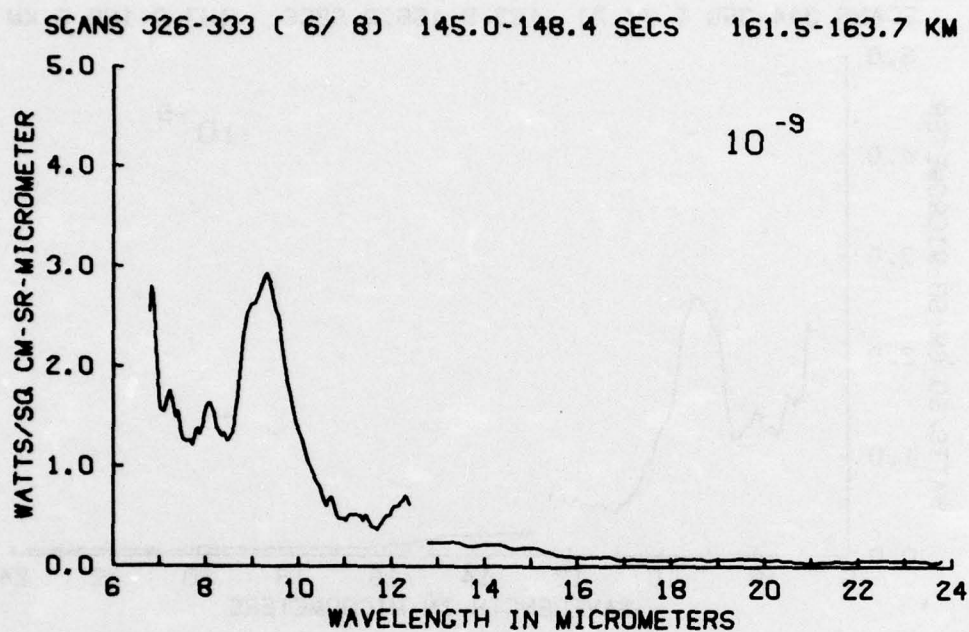


Figure A35

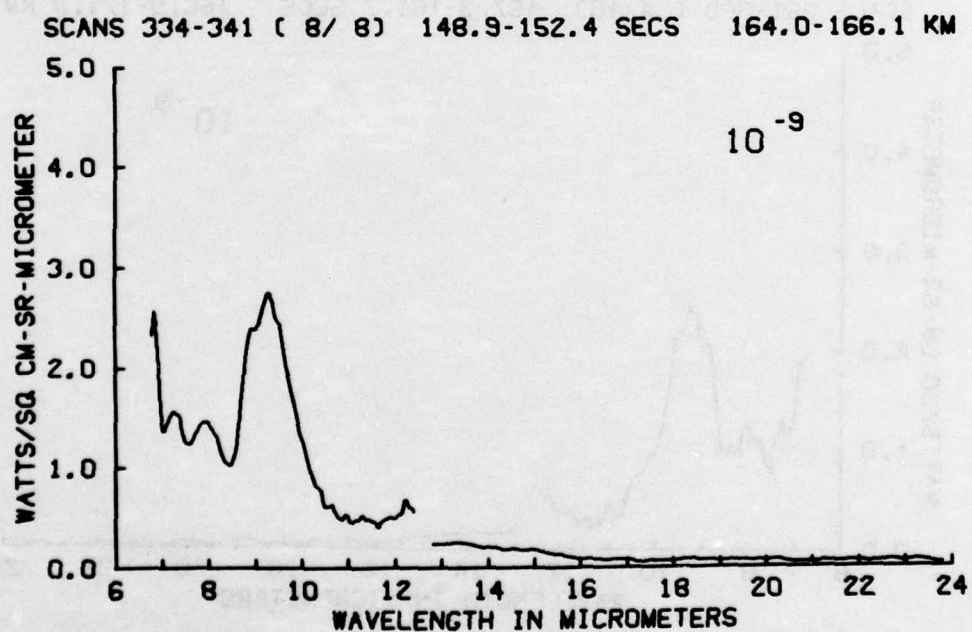


Figure A36

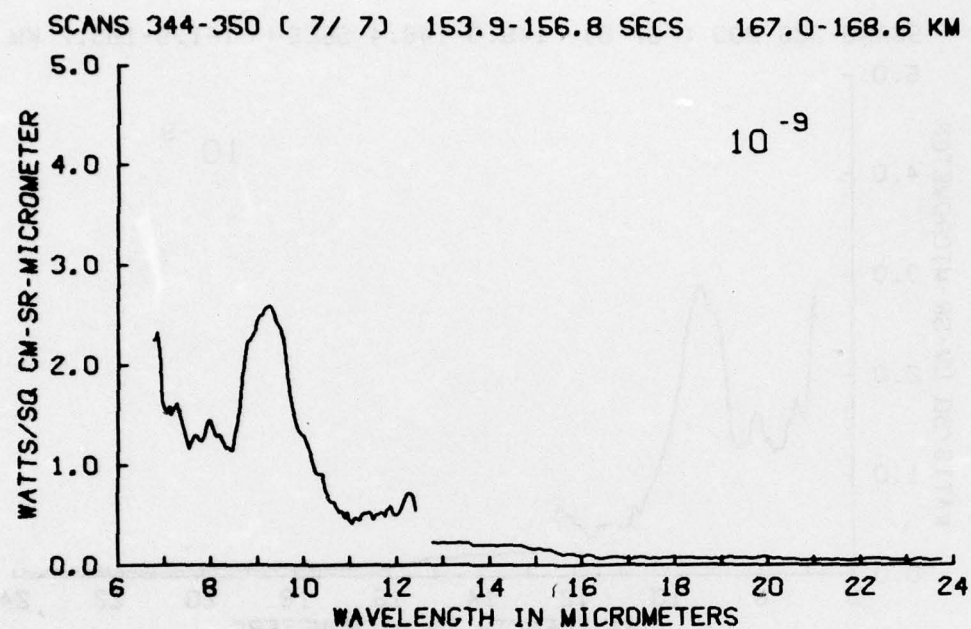


Figure A37

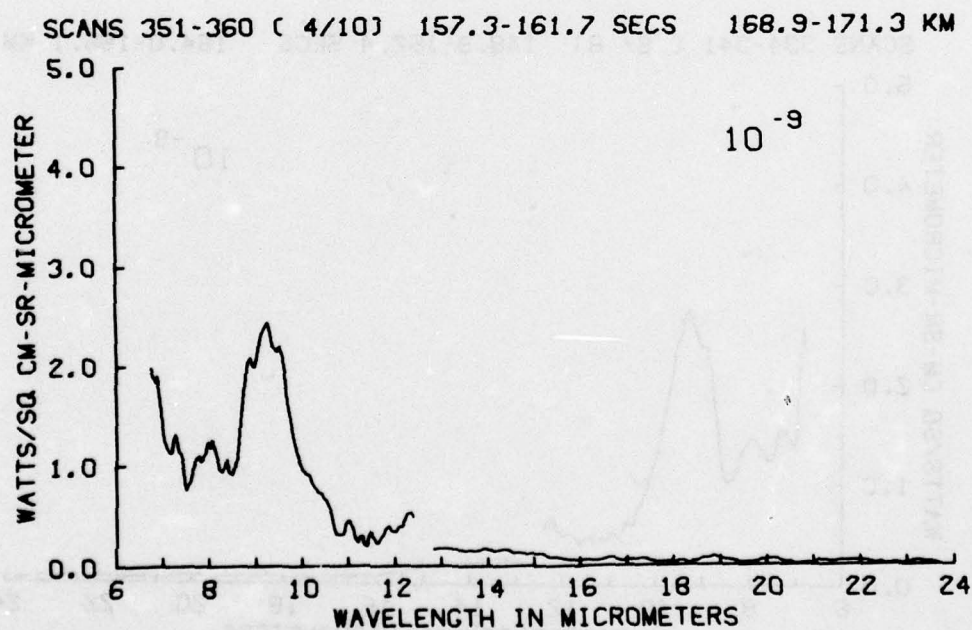


Figure A38

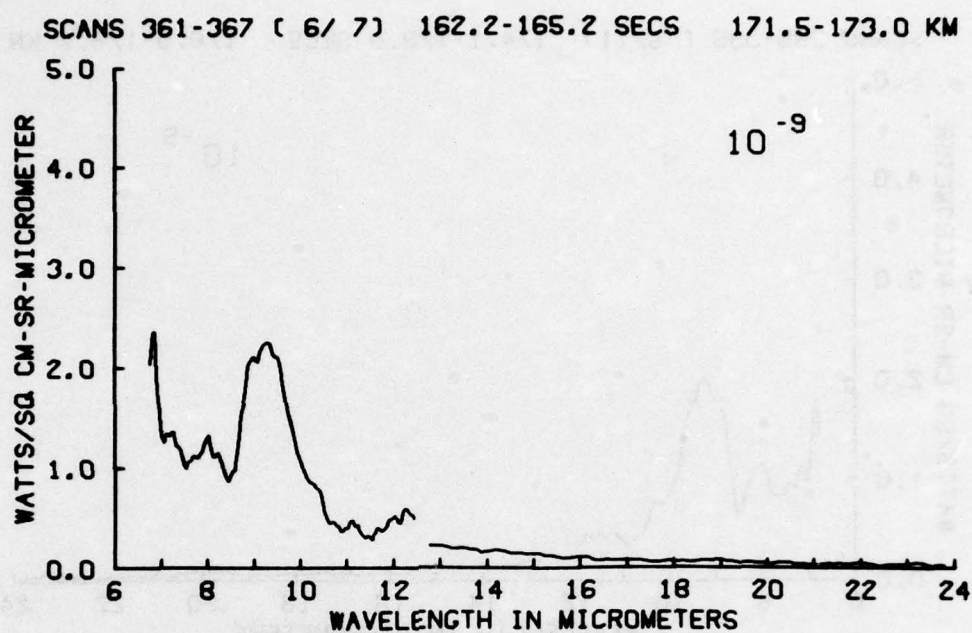


Figure A39

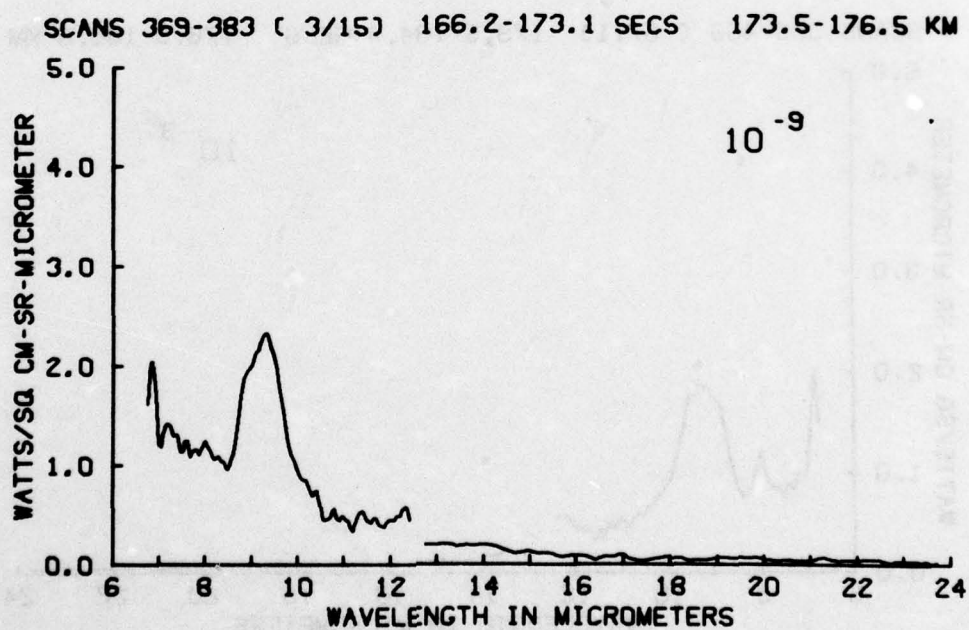


Figure A40

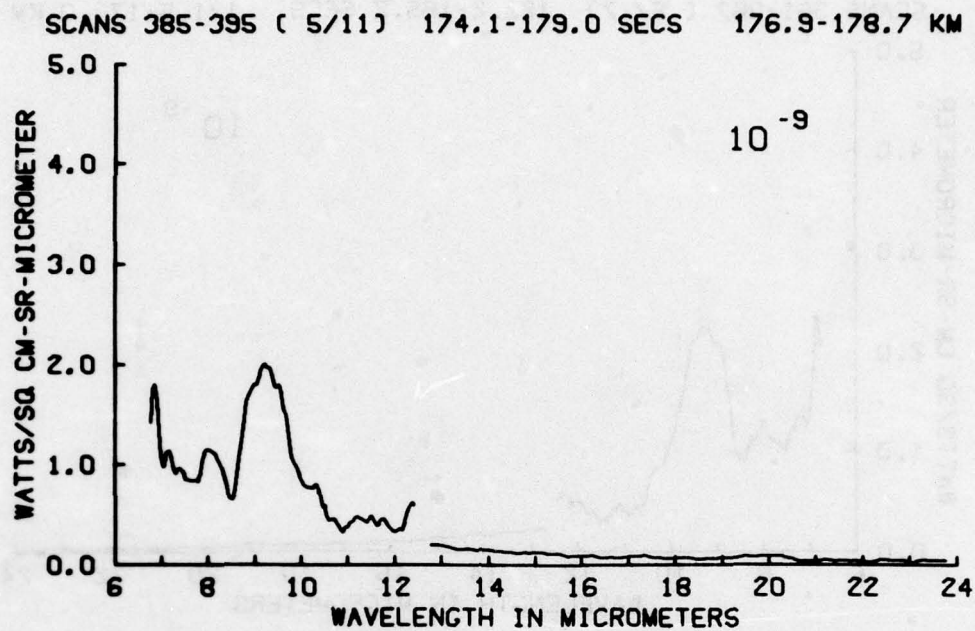


Figure A41

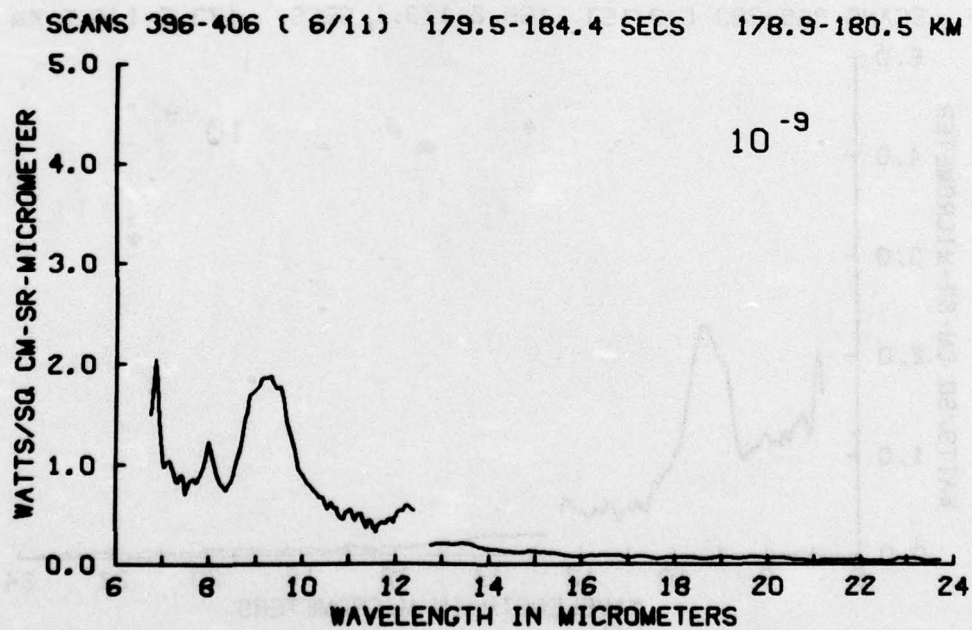


Figure A42

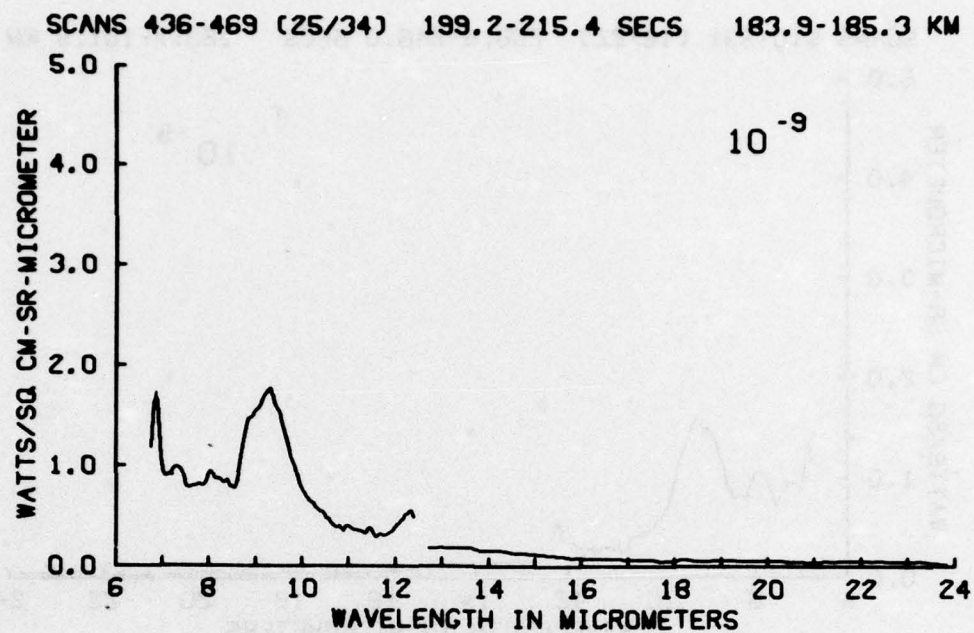


Figure A43

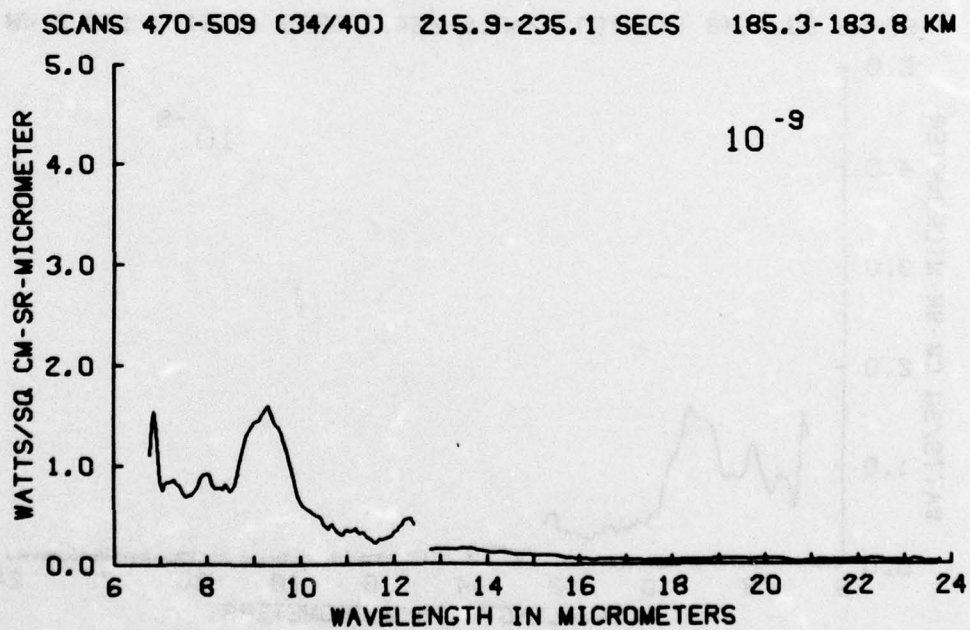


Figure A44

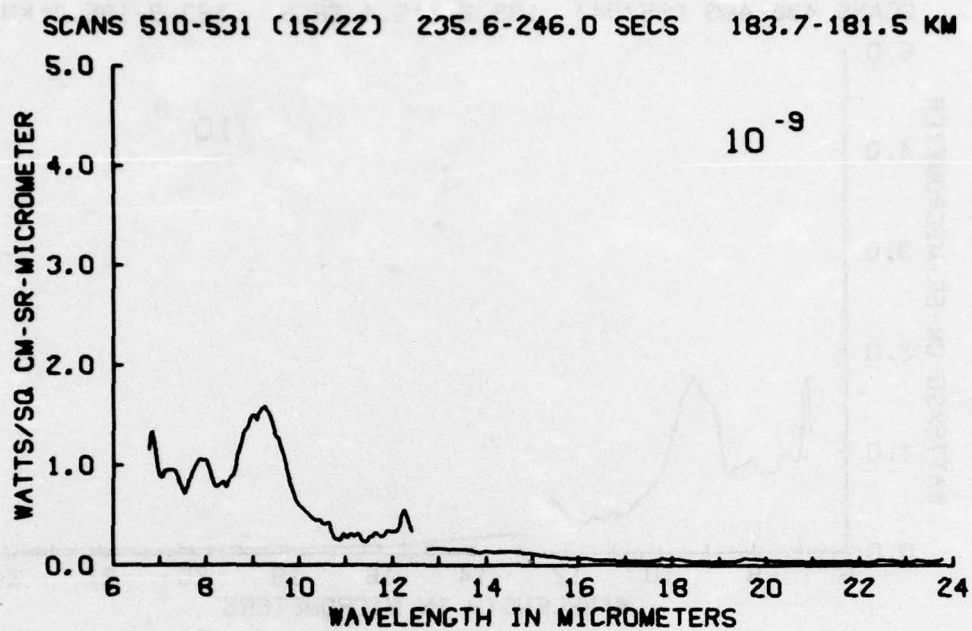


Figure A45

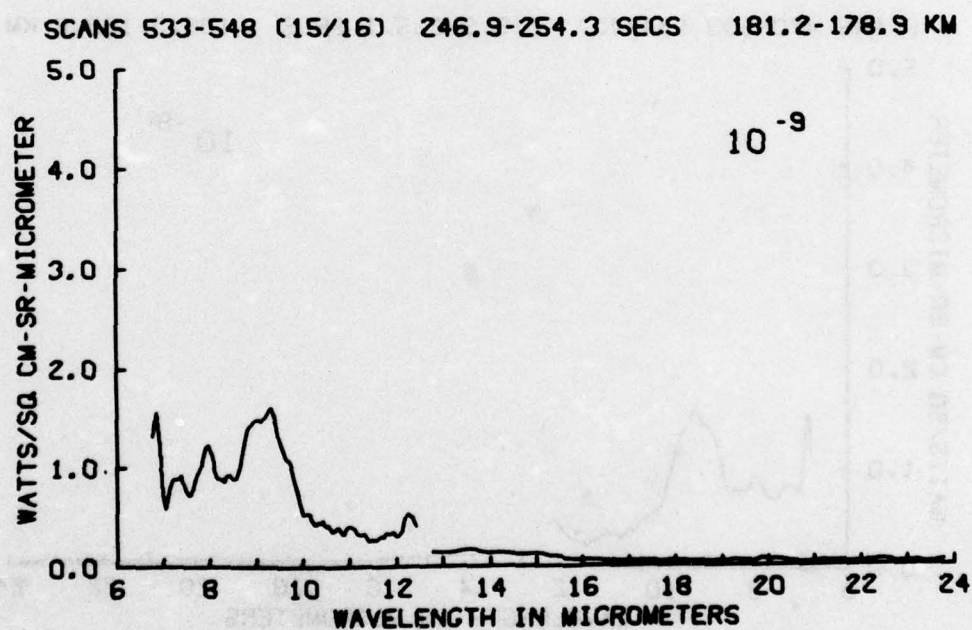


Figure A46

SCANS 549-561 (12/13) 254.8-260.7 SECS 178.7-176.5 KM

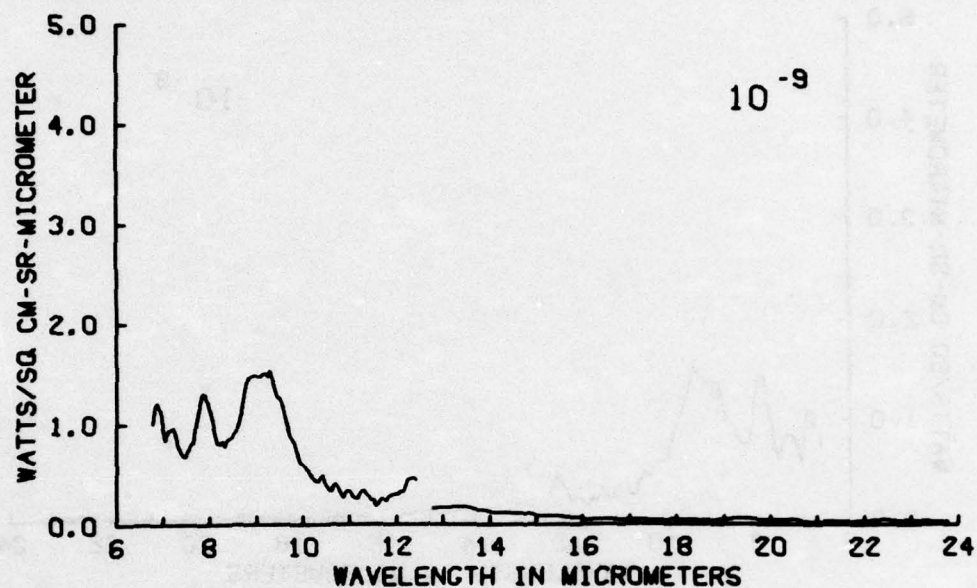


Figure A47

SCANS 563-573 (10/11) 261.7-266.6 SECS 176.1-174.0 KM

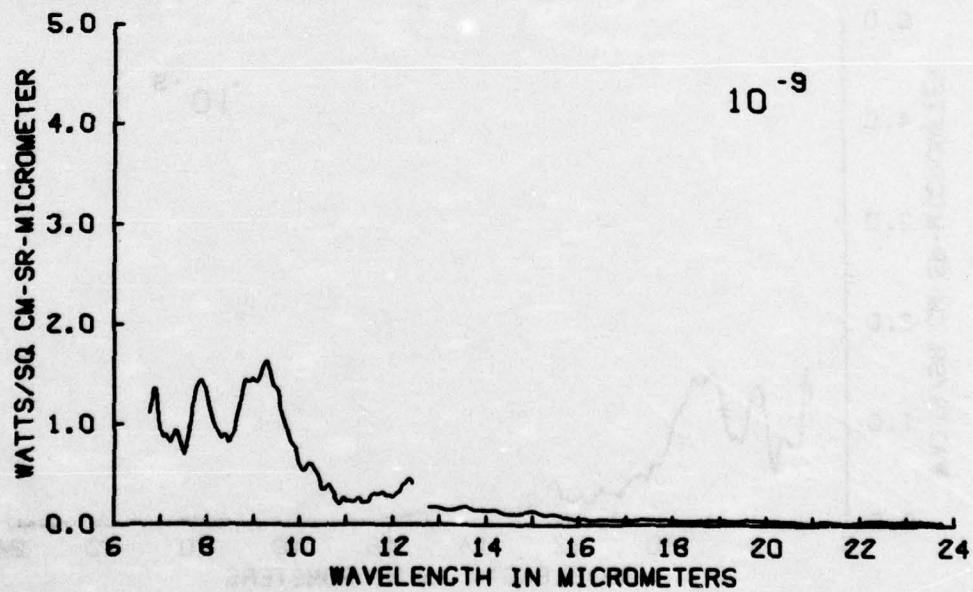


Figure A48

SCANS 574-584 (10/11) 267.1-272.0 SECS 173.7-171.3 KM

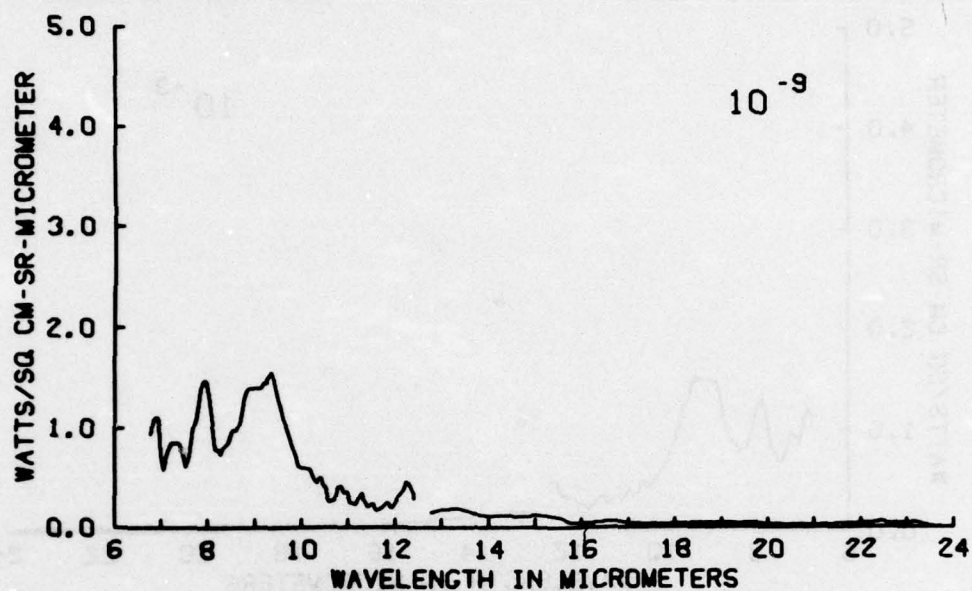


Figure A49

SCANS 585-593 (8/ 9) 272.5-276.5 SECS 171.1-169.0 KM

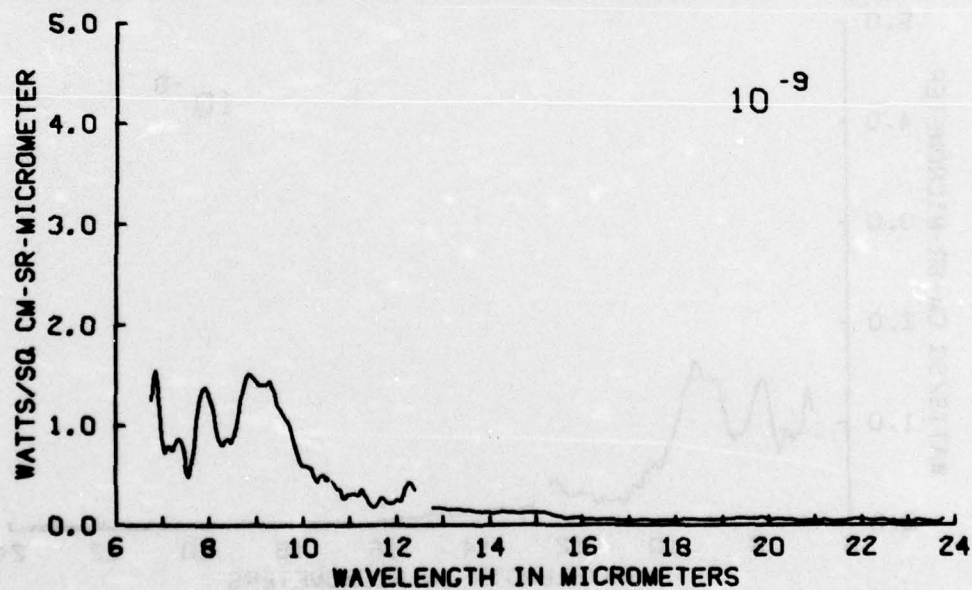


Figure A50

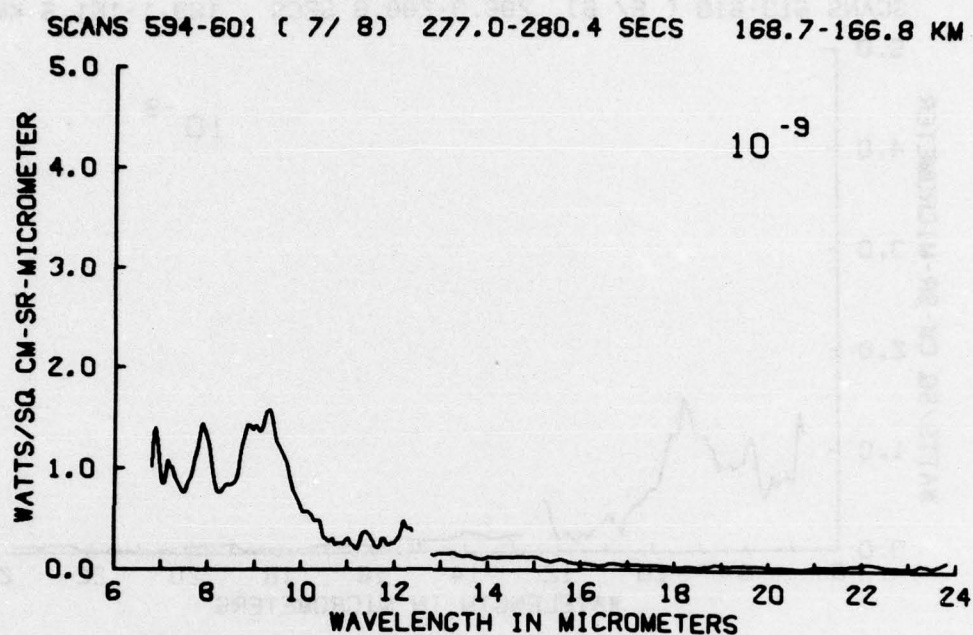


Figure A51

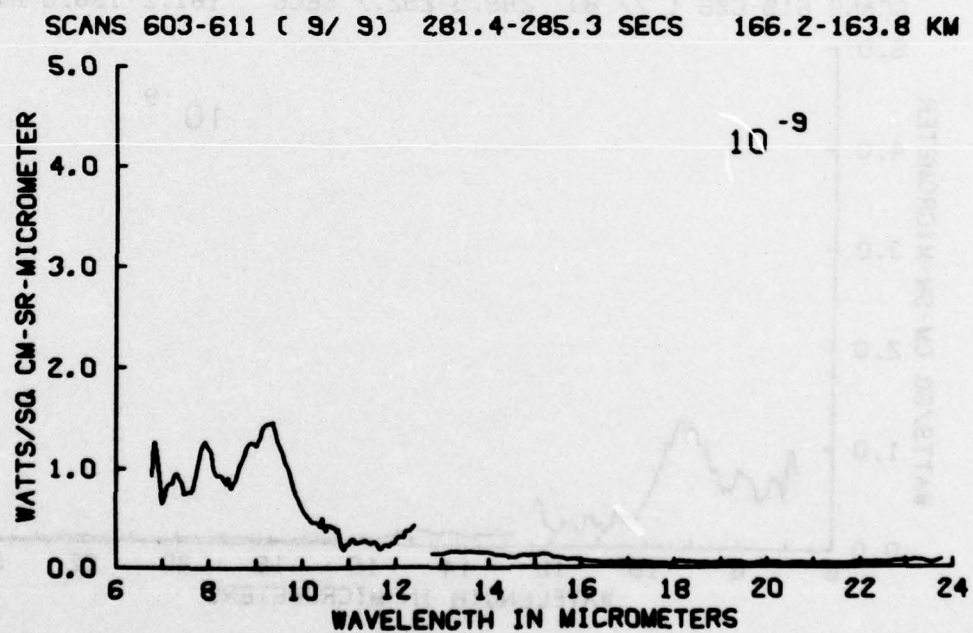


Figure A52

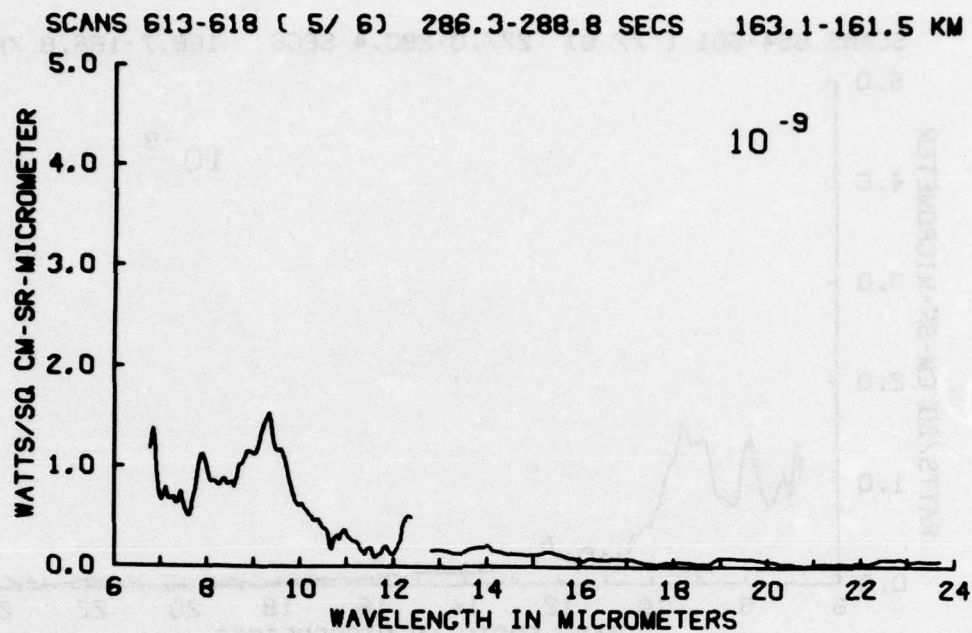


Figure A53

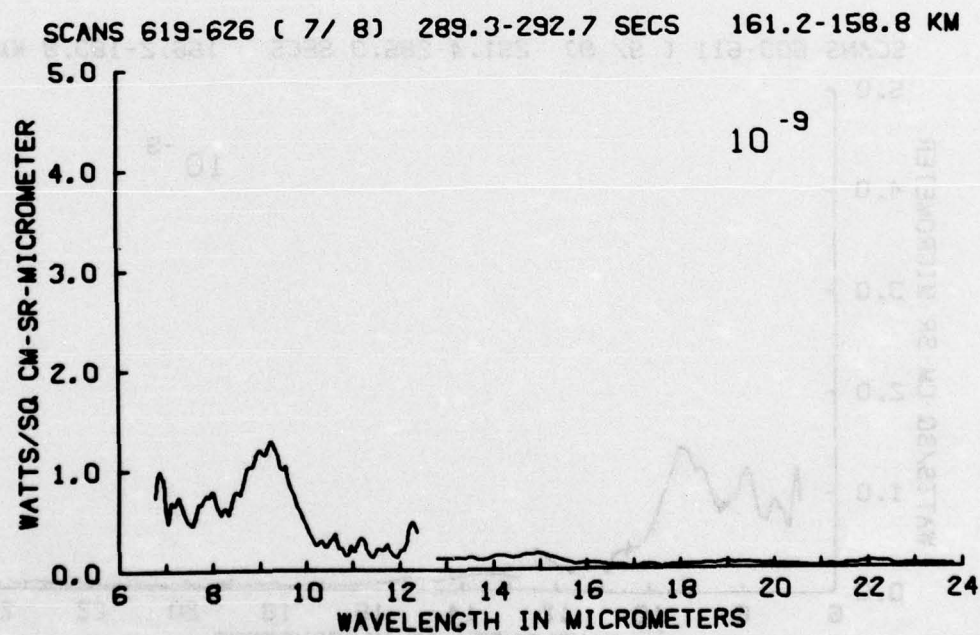


Figure A54

SCANS 627-633 (5/ 7) 293.2-296.1 SECS 158.5-156.3 KM

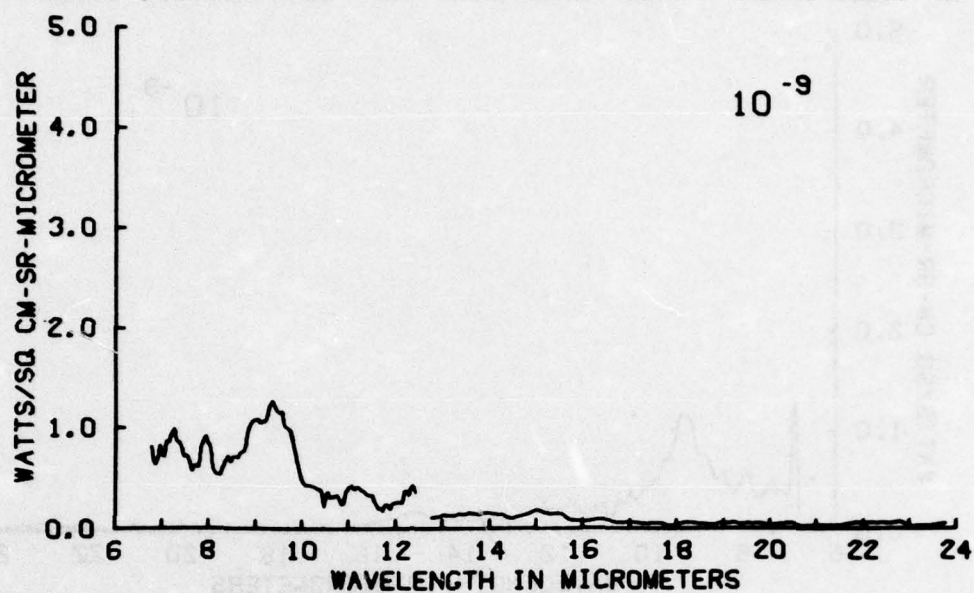


Figure A55

SCANS 634-640 (7/ 7) 296.6-299.6 SECS 156.0-153.8 KM

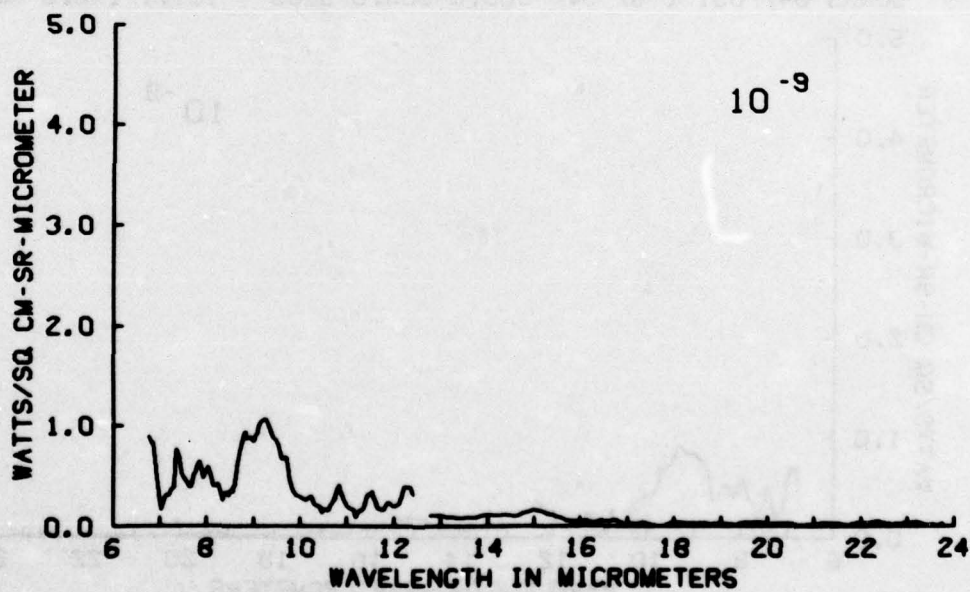


Figure A56

SCANS 641-646 (5/ 6) 300.1-302.5 SECS 153.4-151.4 KM

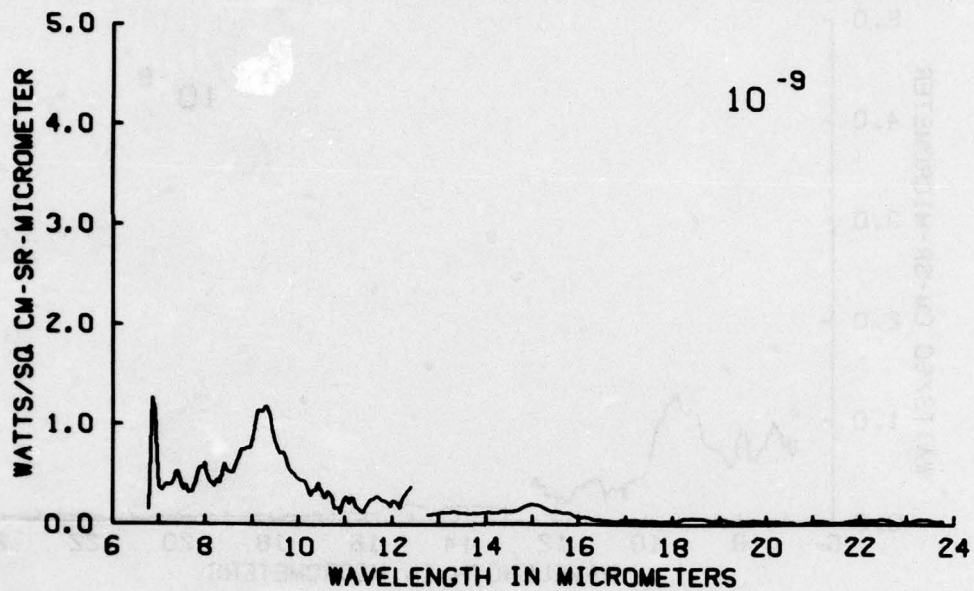


Figure A57

SCANS 647-651 (5/ 5) 303.0-305.0 SECS 151.1-149.5 KM

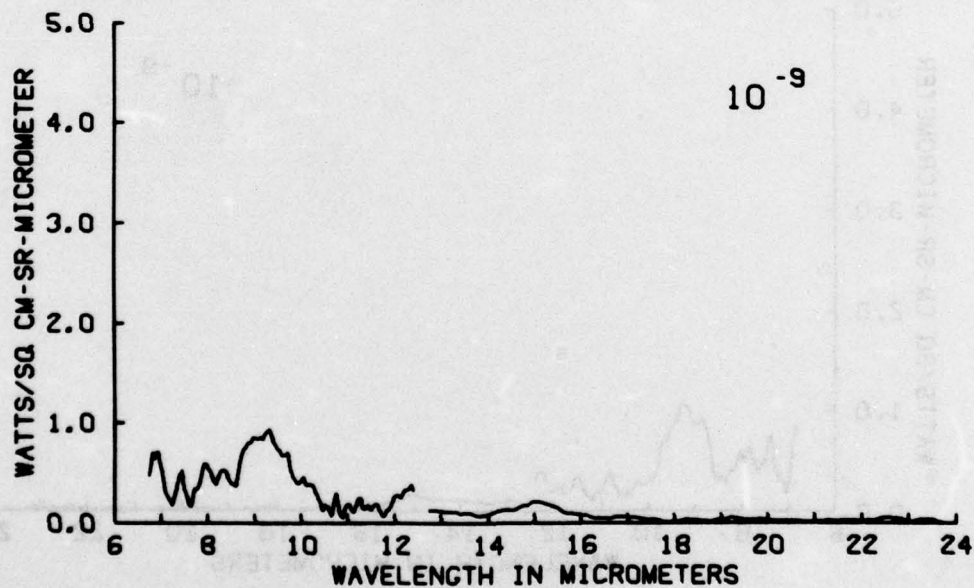


Figure A58

SCANS 653-658 (6/ 6) 306.0-308.4 SECS 148.7-146.6 KM

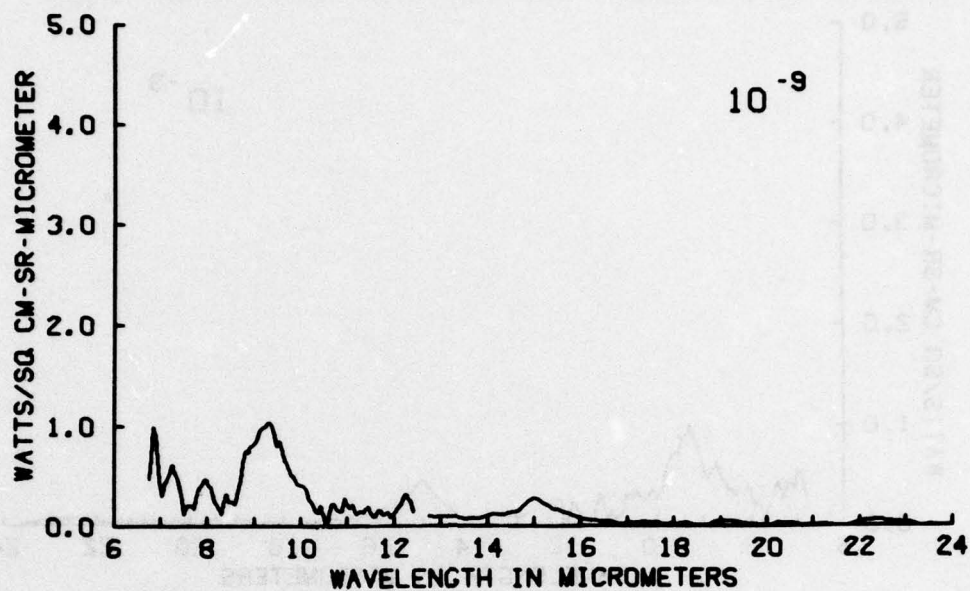


Figure A59

SCANS 659-664 (5/ 6) 308.9-311.4 SECS 146.2-144.0 KM

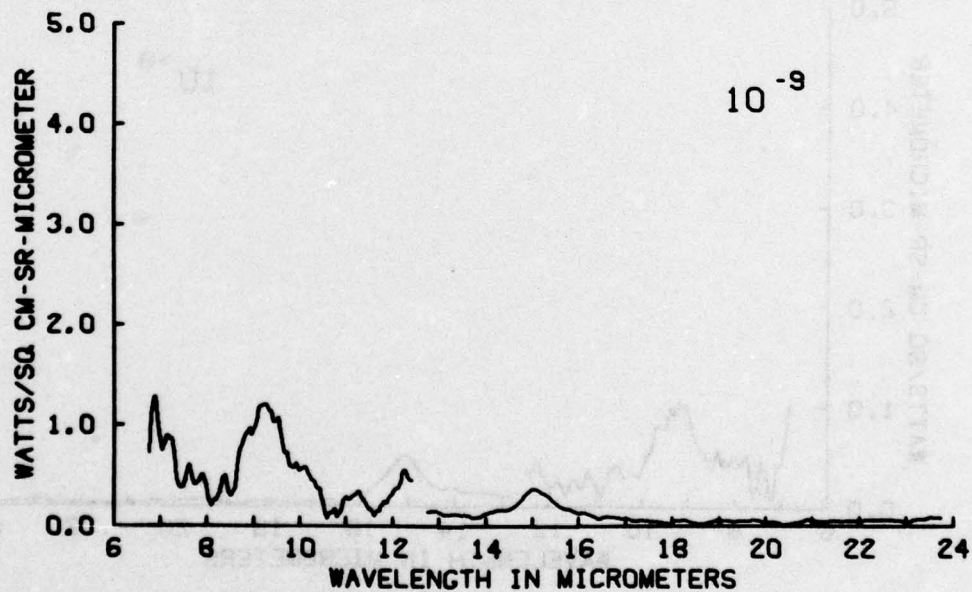


Figure A60

SCANS 665-667 (3/ 3) 312.9-313.9 SECS 142.7-141.9 KM

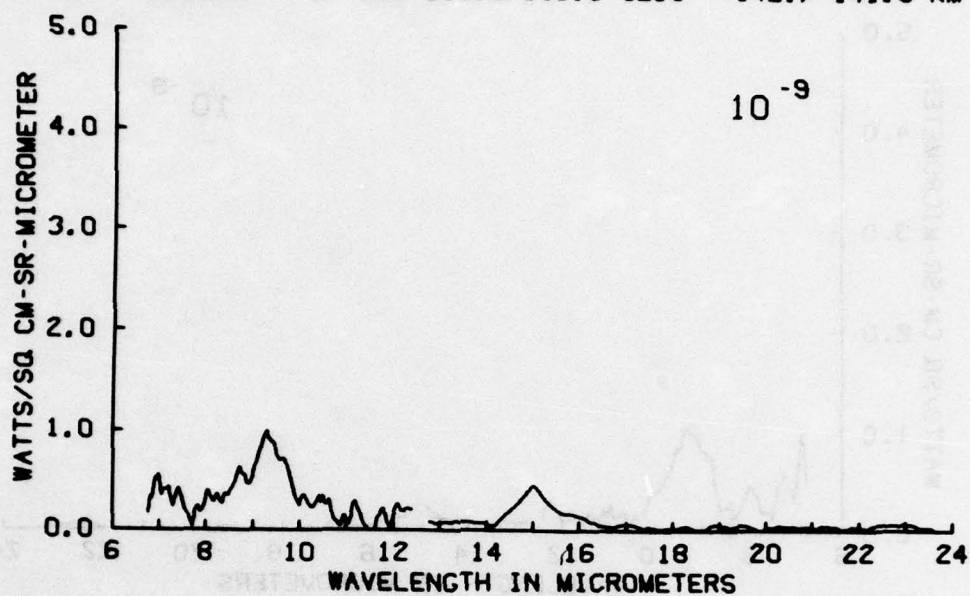


Figure A61

SCANS 669-674 (4/ 6) 314.8-317.3 SECS 141.0-138.7 KM

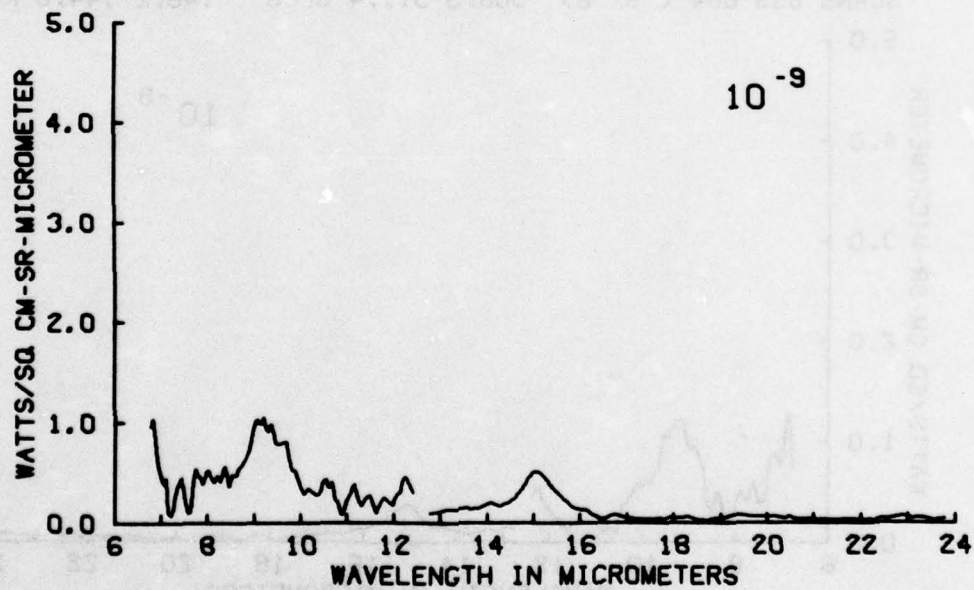


Figure A62

SCANS 675-679 (5/ 5) 317.8-319.8 SECS 138.2-136.4 KM

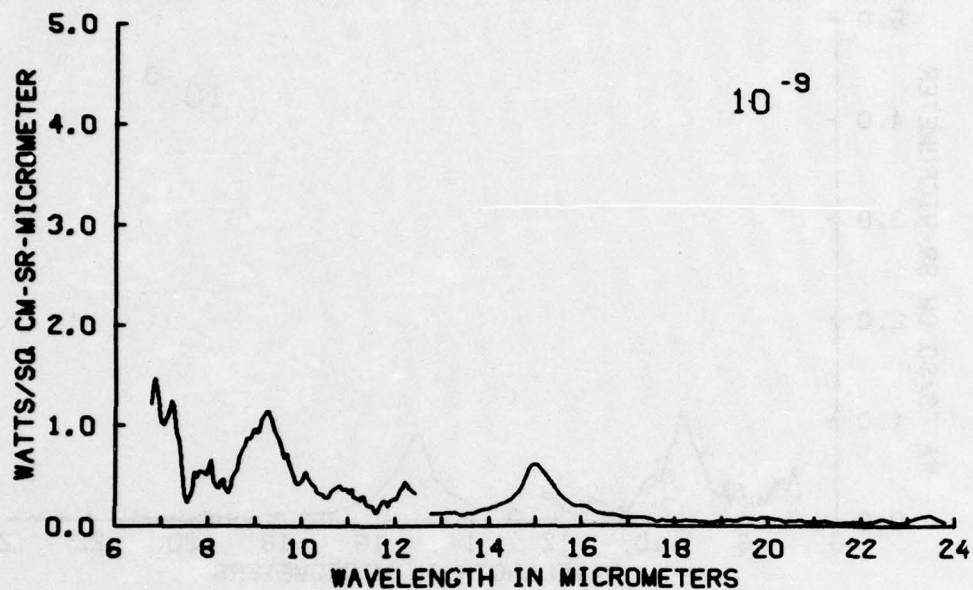


Figure A63

SCANS 681-684 (4/ 4) 320.7-322.2 SECS 135.4-134.0 KM

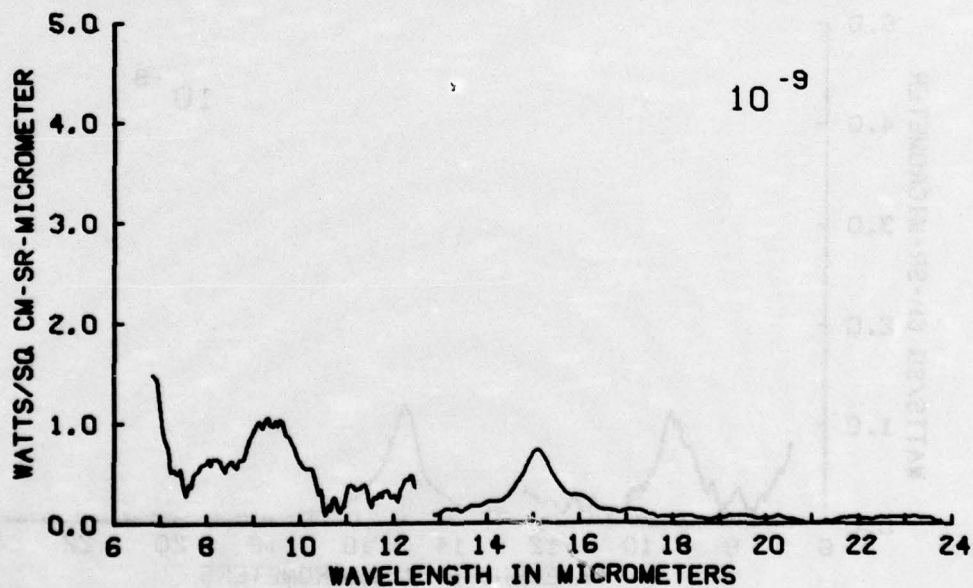


Figure A64

SCANS 685-689 (5/ 5) 322.7-324.7 SECS 133.5-131.6 KM

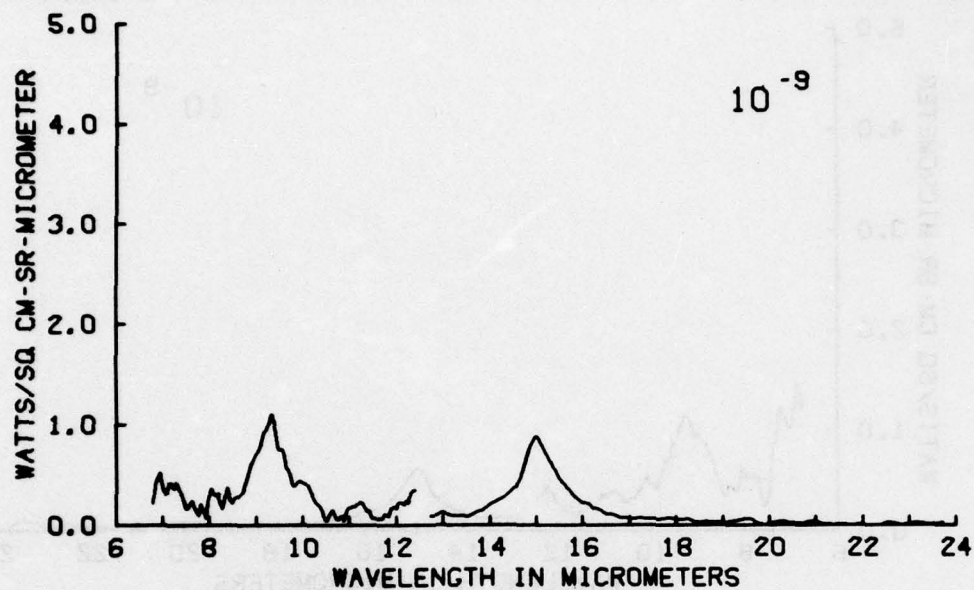


Figure A65

SCANS 691-694 (4/ 4) 325.7-327.1 SECS 130.6-129.1 KM

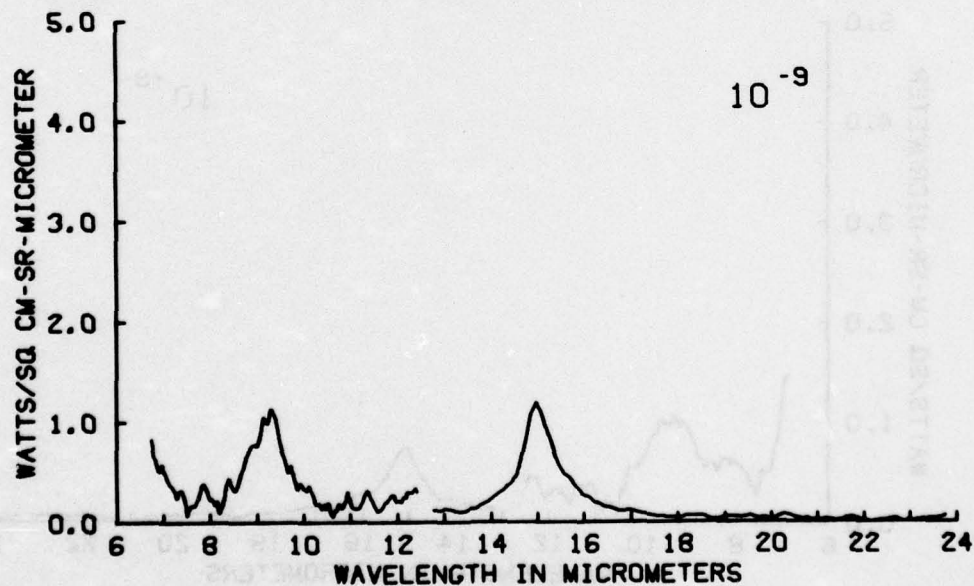


Figure A66

SCANS 695-699 (5/ 5) 327.6-329.6 SECS 128.6-126.5 KM

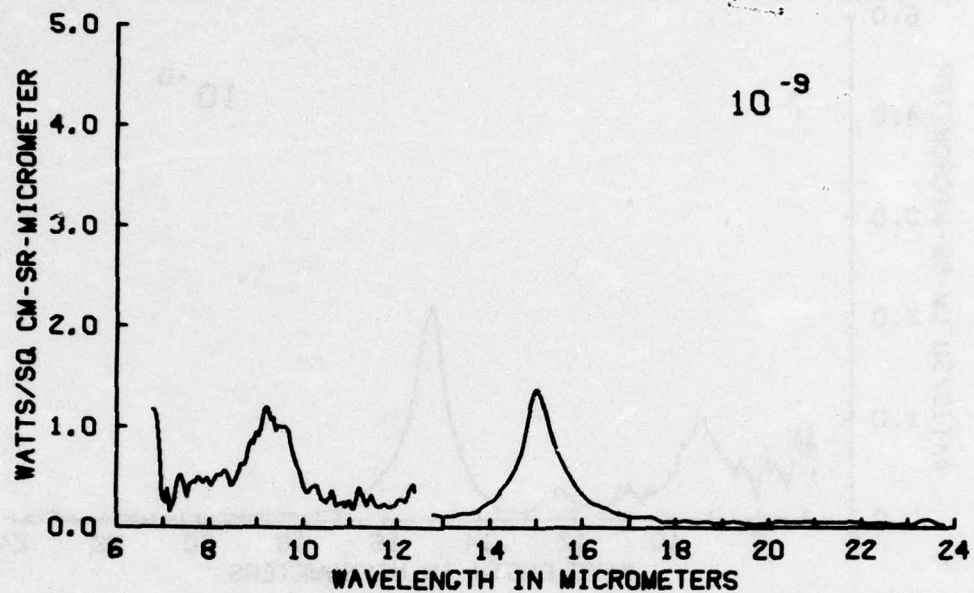


Figure A67

SCANS 701-704 (4/ 4) 330.6-332.1 SECS 125.5-123.9 KM

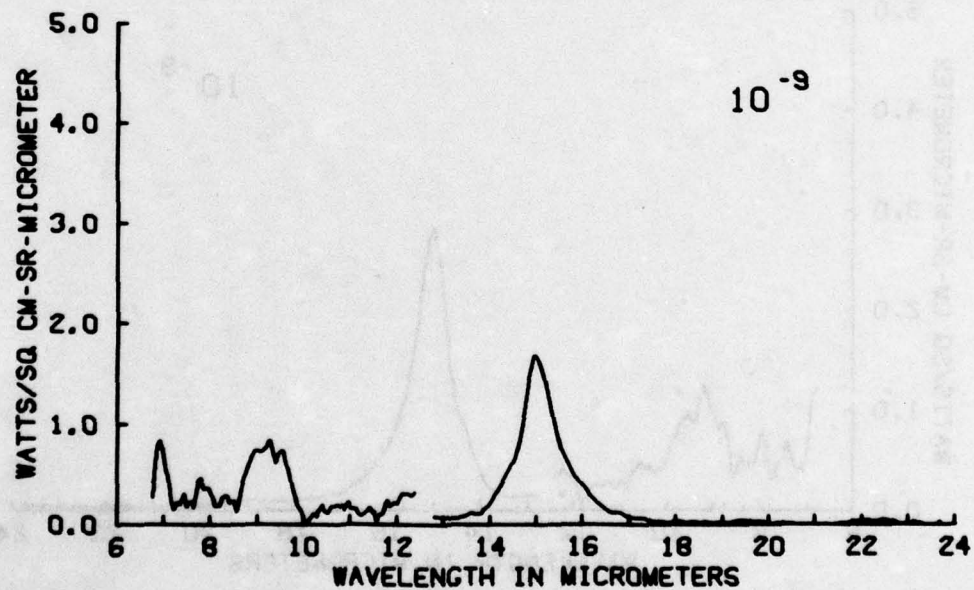


Figure A68

SCANS 705-708 (4/ 4) 332.6-334.0 SECS 123.4-121.8 KM

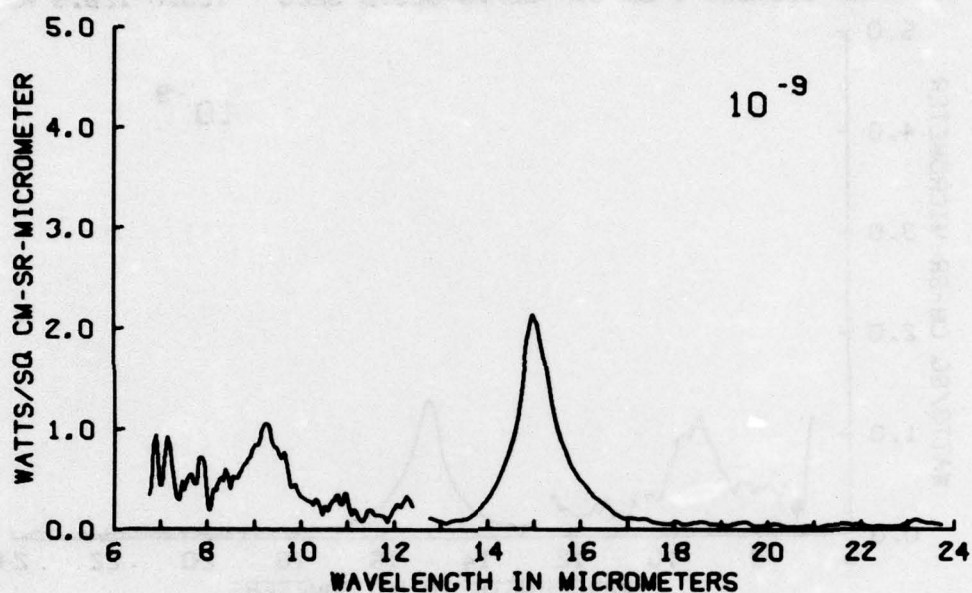


Figure A69

SCANS 709-713 (4/ 5) 334.5-336.5 SECS 121.3-119.1 KM

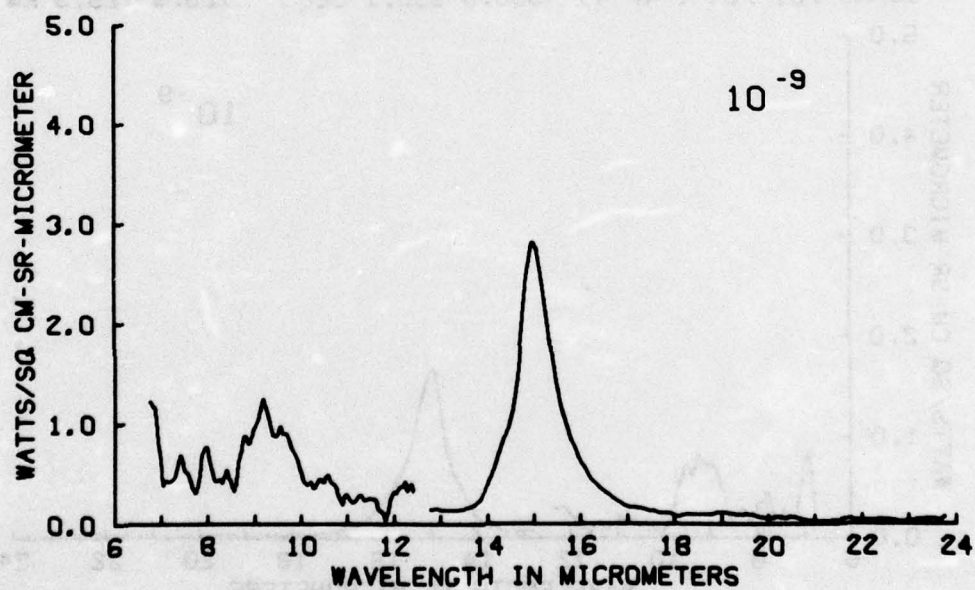


Figure A70

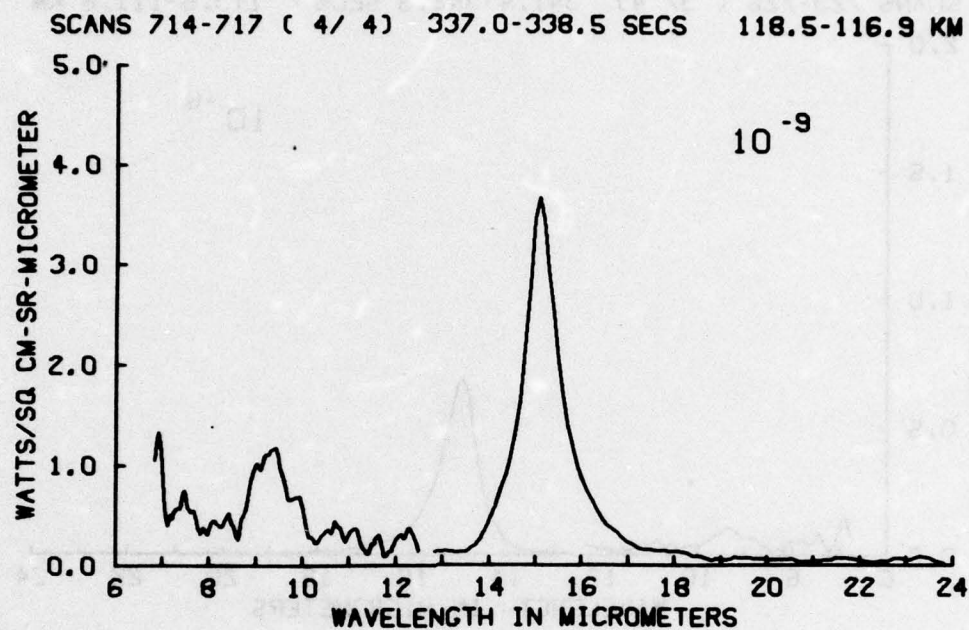


Figure A71

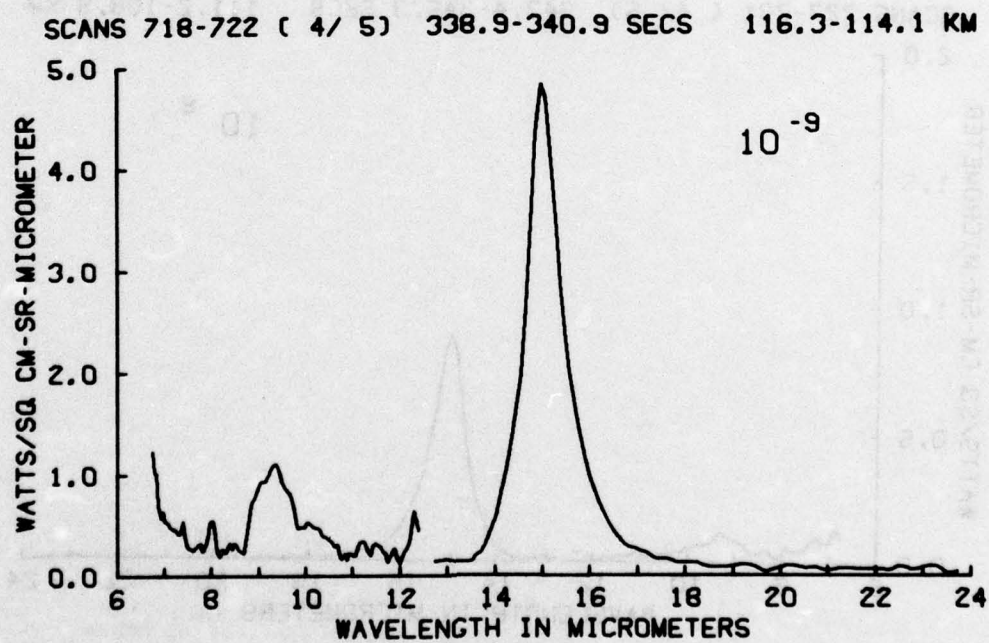


Figure A72

SCANS 723-726 (3/ 4) 341.4-342.9 SECS 113.5-111.8 KM

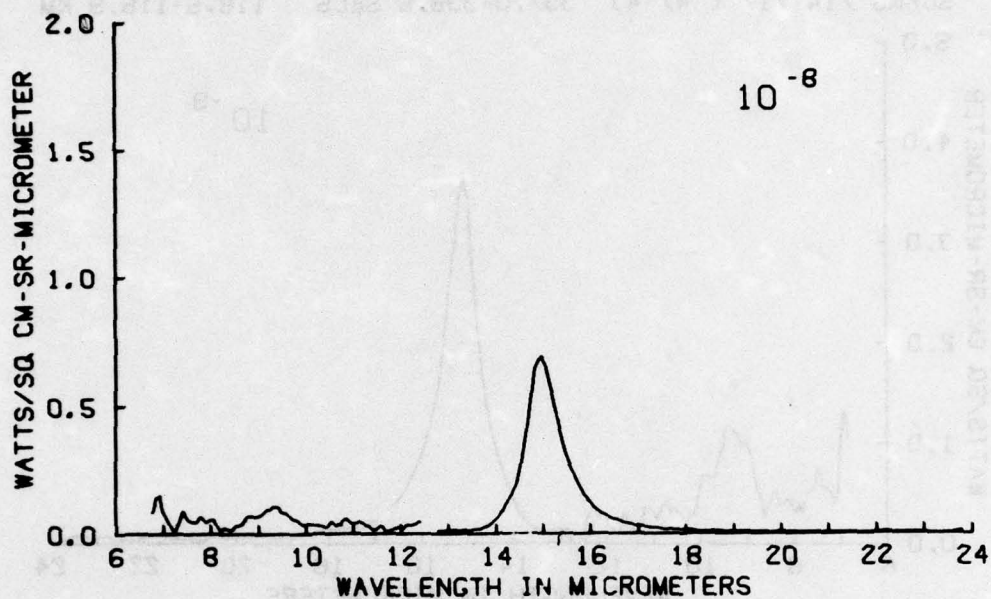


Figure A73

SCANS 727-731 (4/ 5) 343.4-345.3 SECS 111.2-108.9 KM

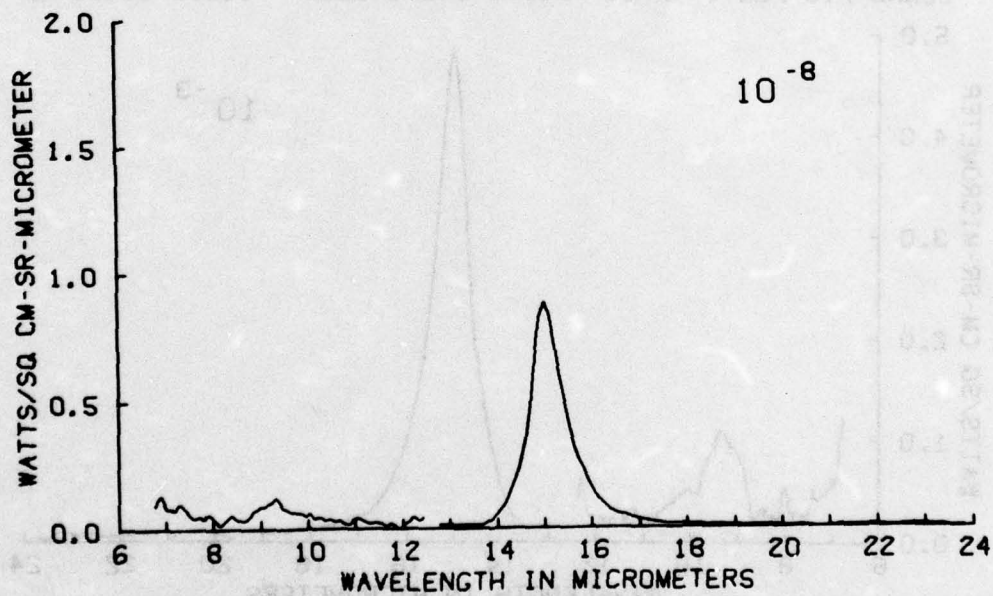


Figure A74

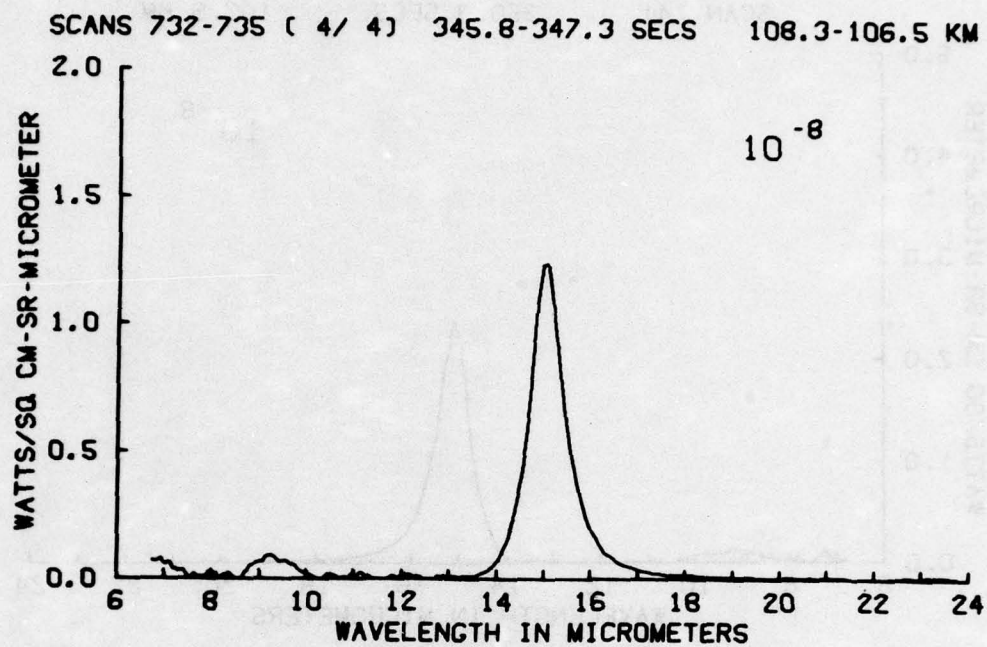


Figure A75

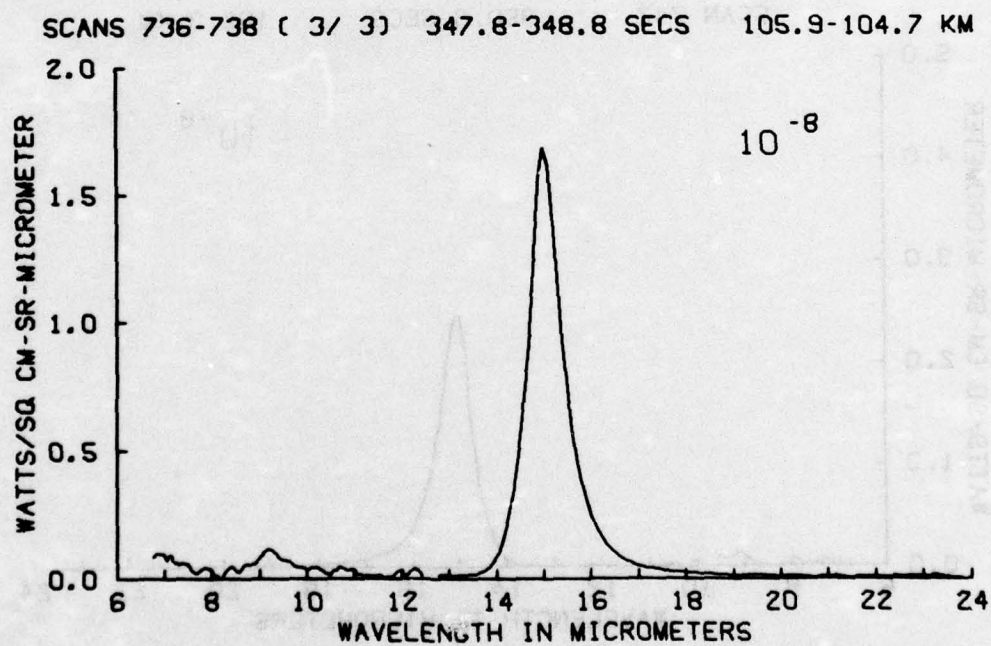


Figure A76

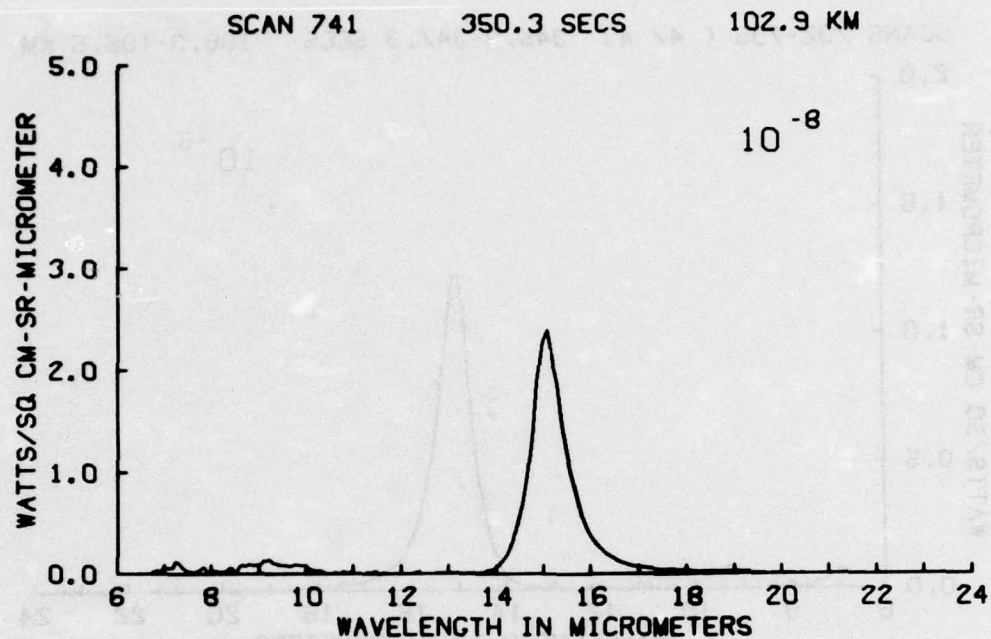


Figure A77

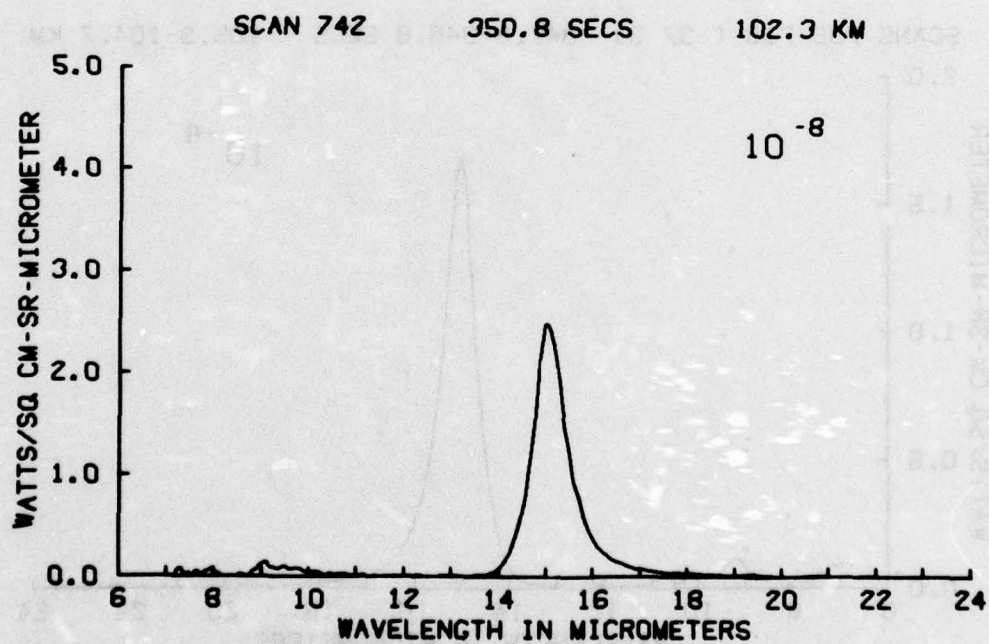


Figure A78

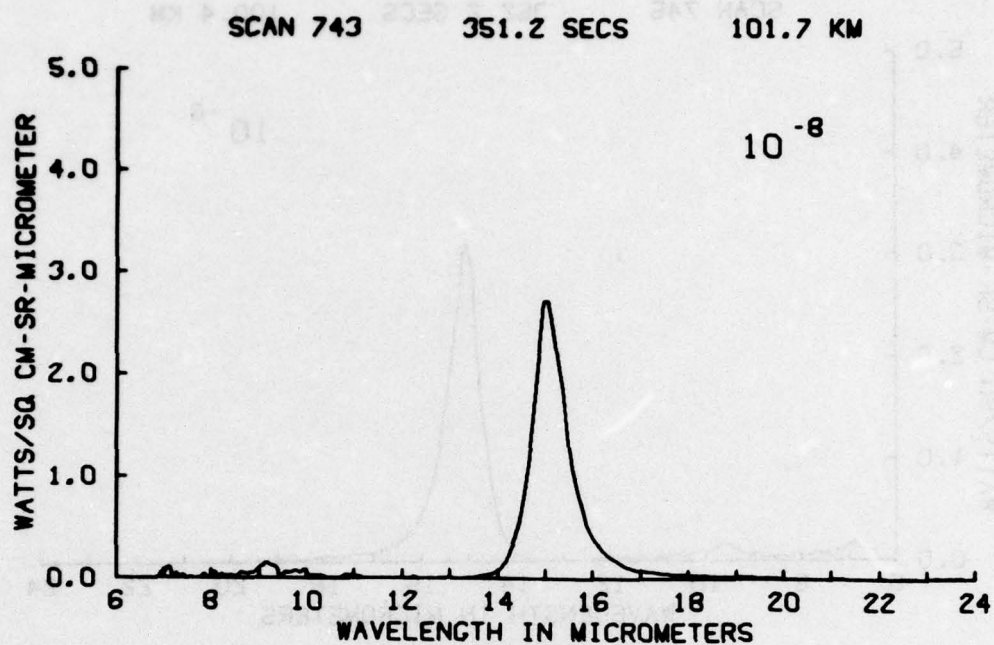


Figure A79

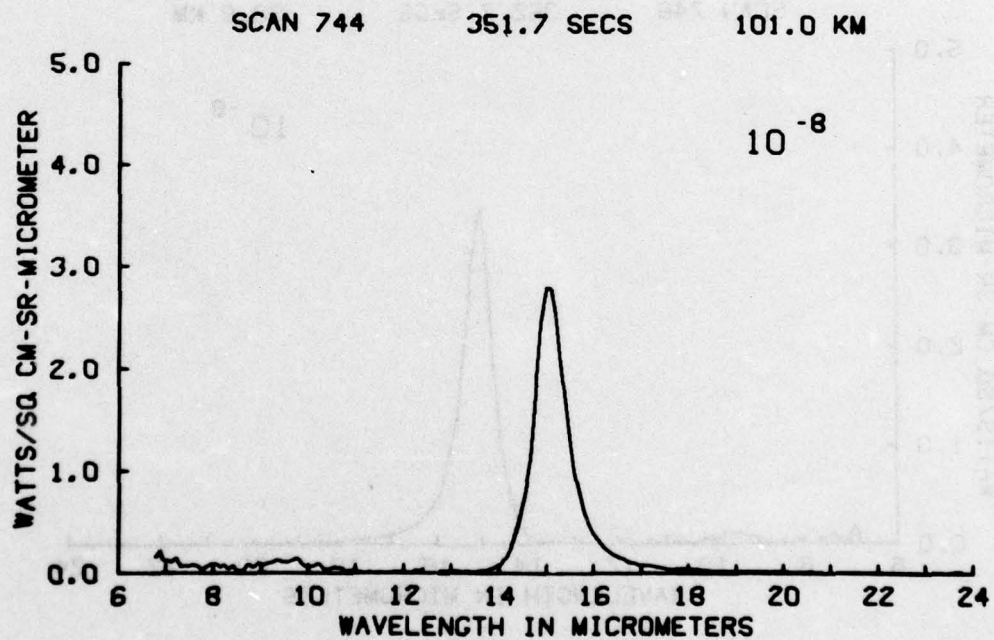


Figure A80

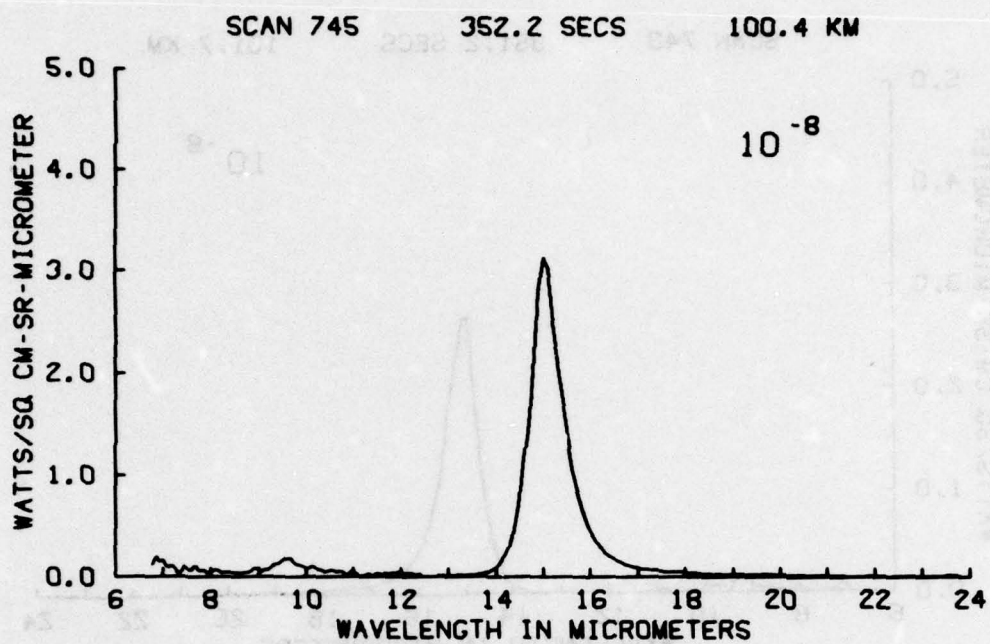


Figure A81

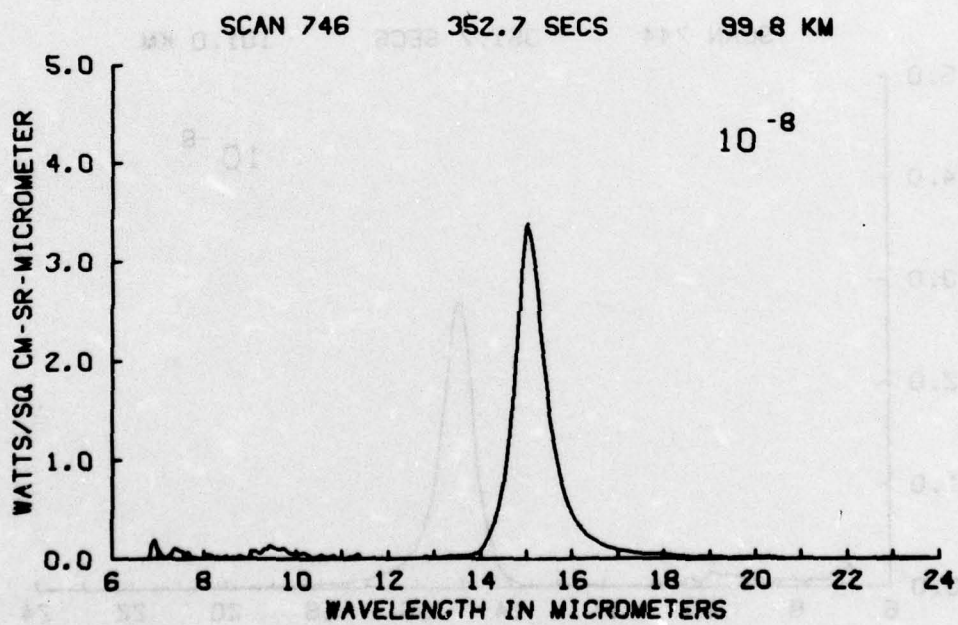


Figure A82

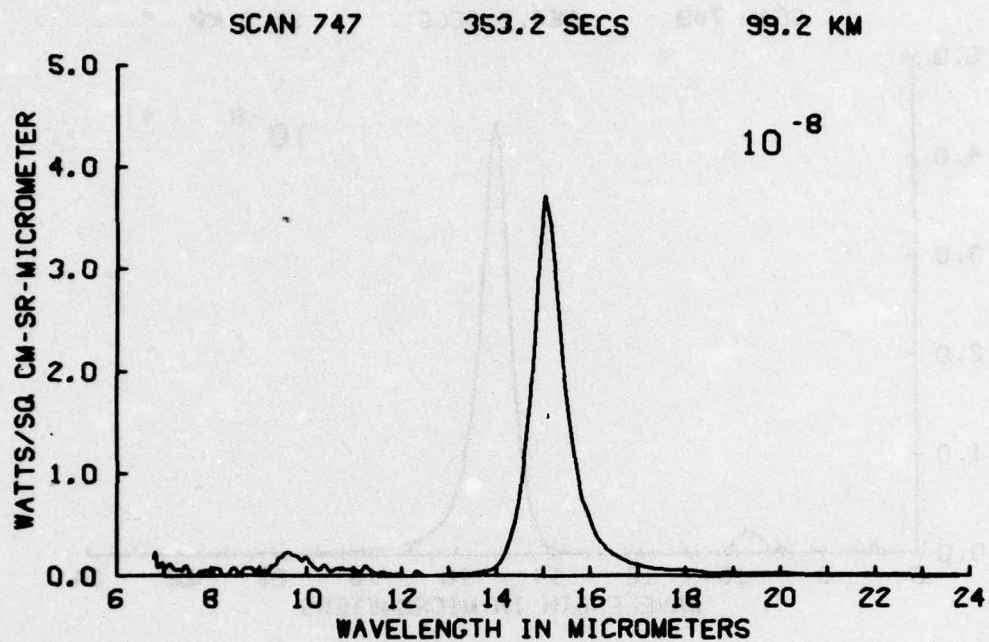


Figure A83

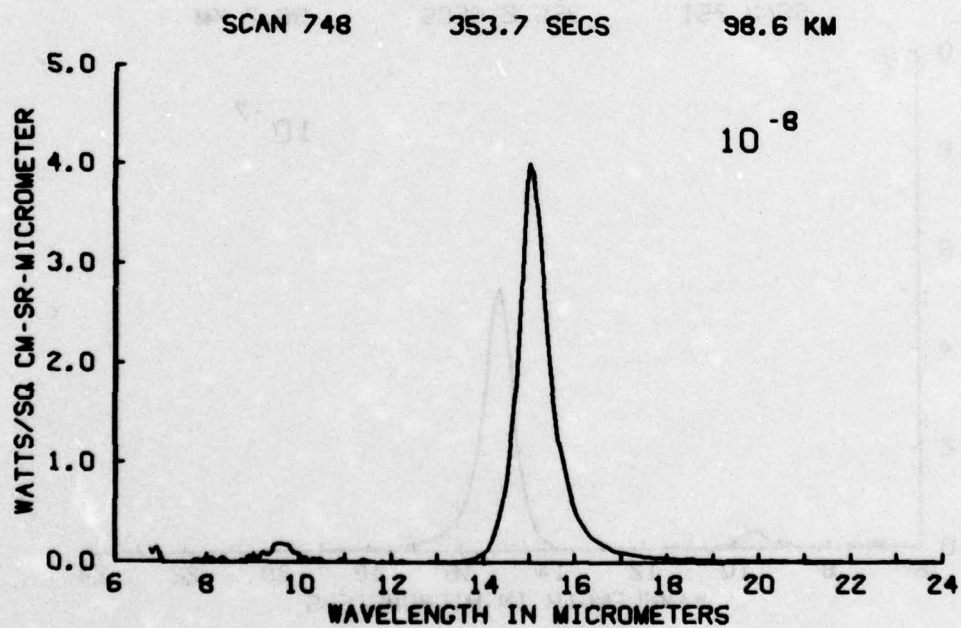


Figure A84

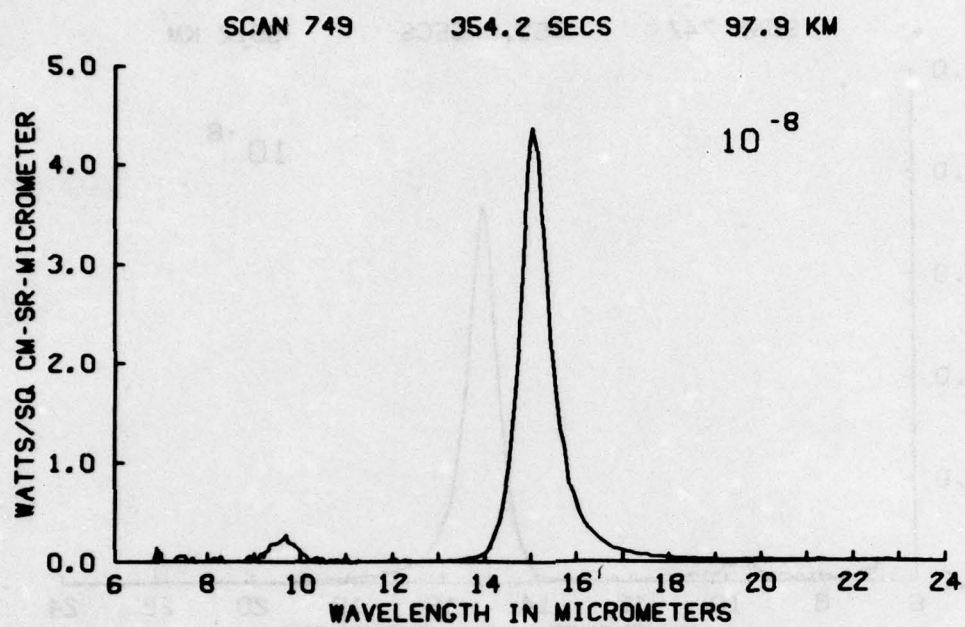


Figure A85

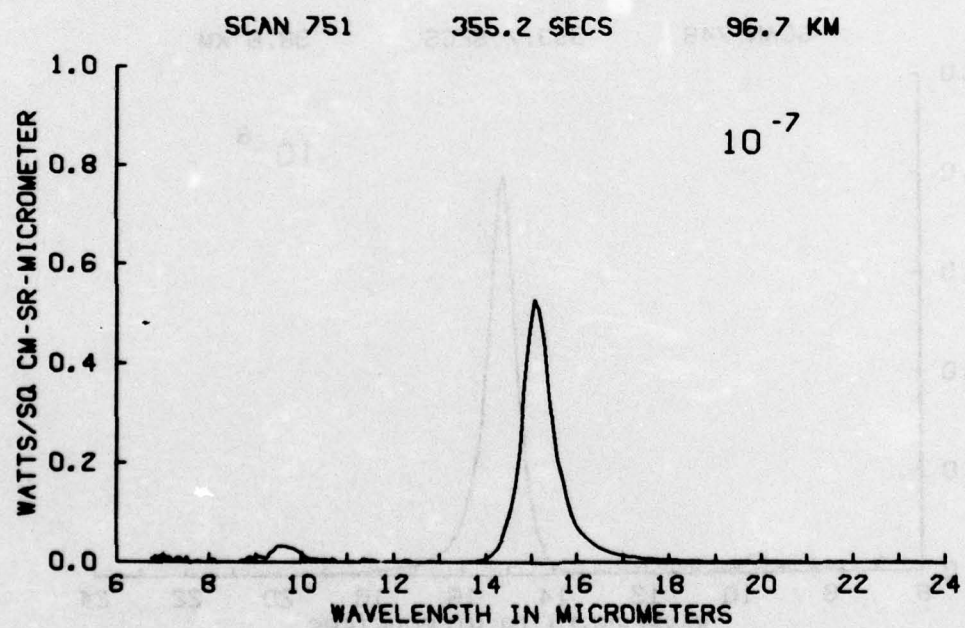


Figure A86

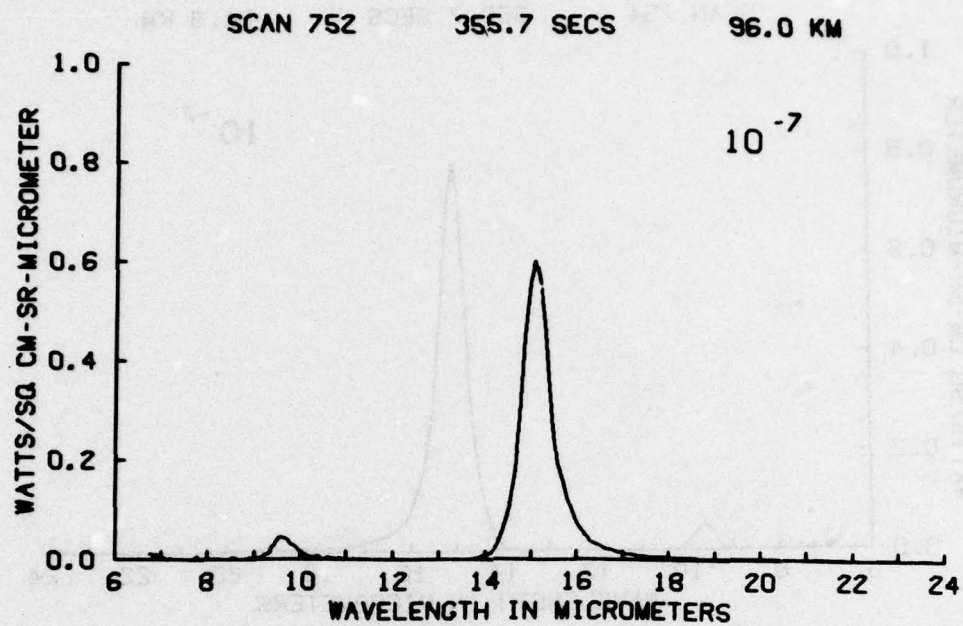


Figure A87

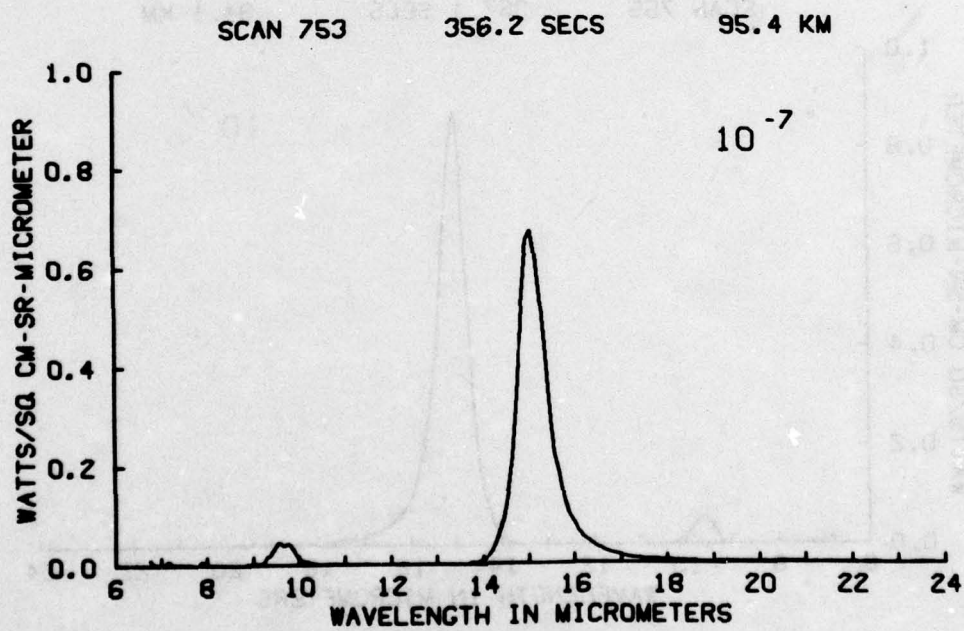


Figure A88

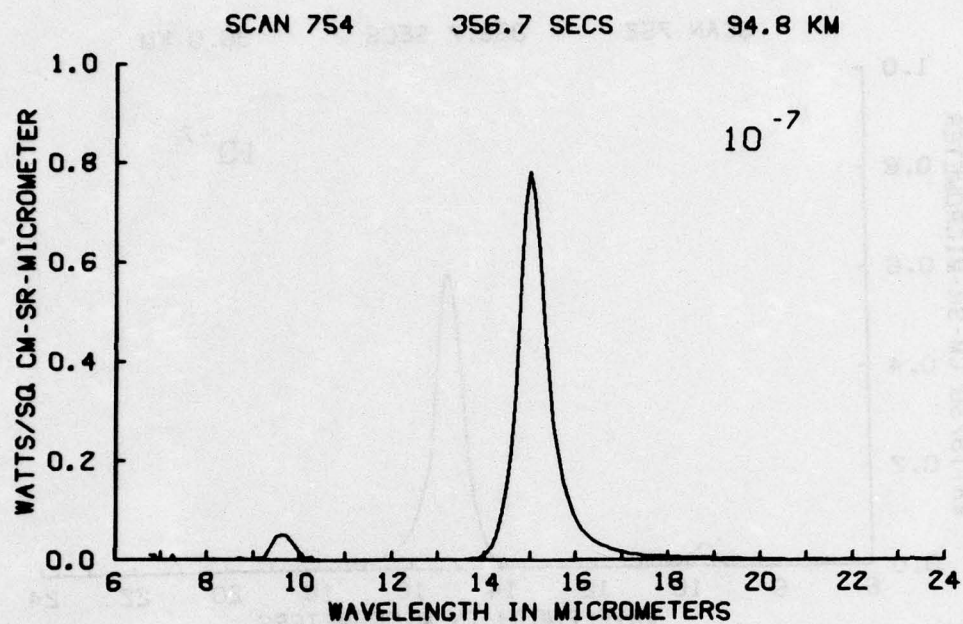


Figure A89

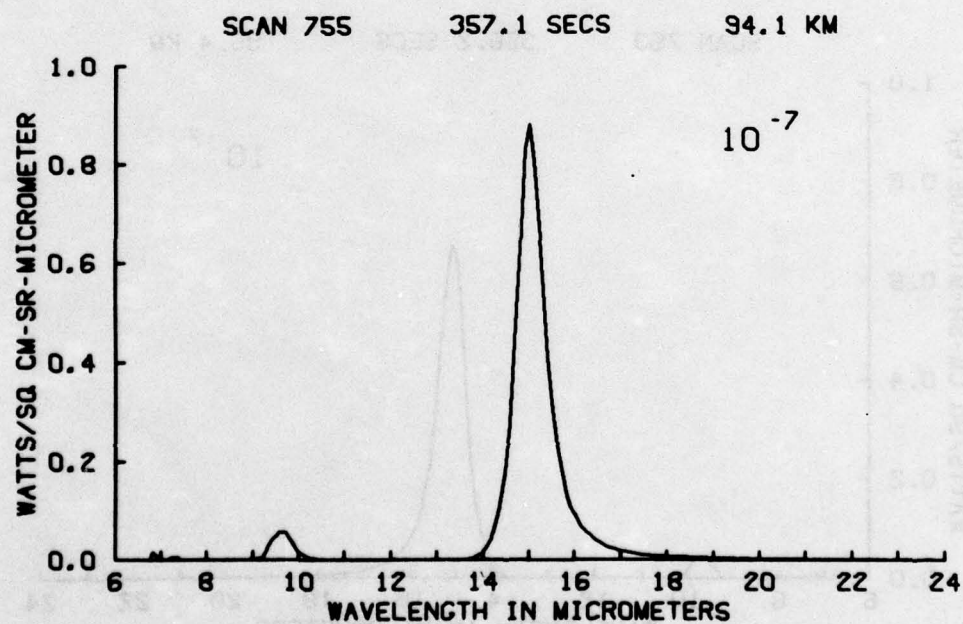


Figure A90

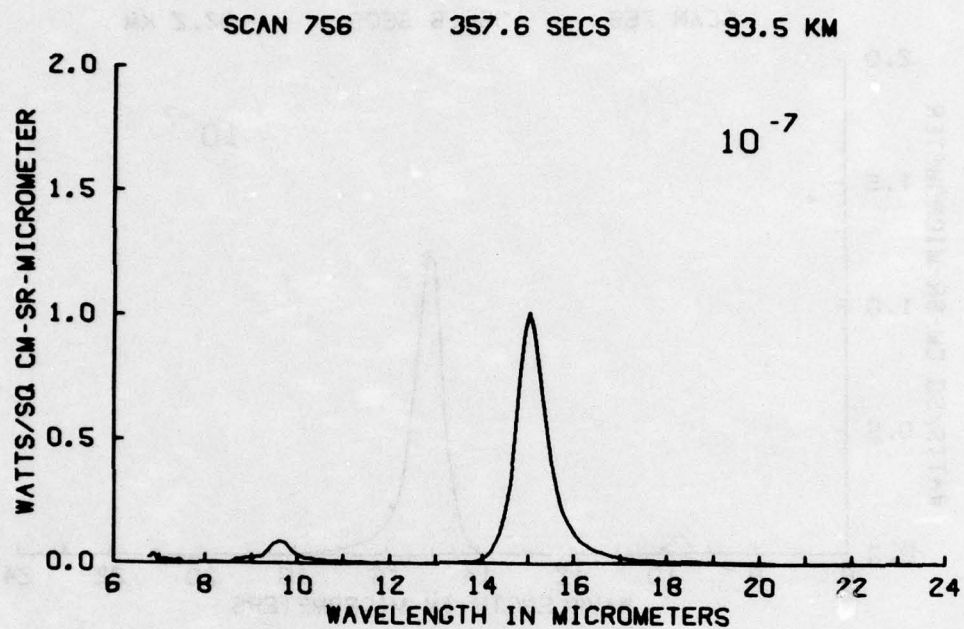


Figure A91

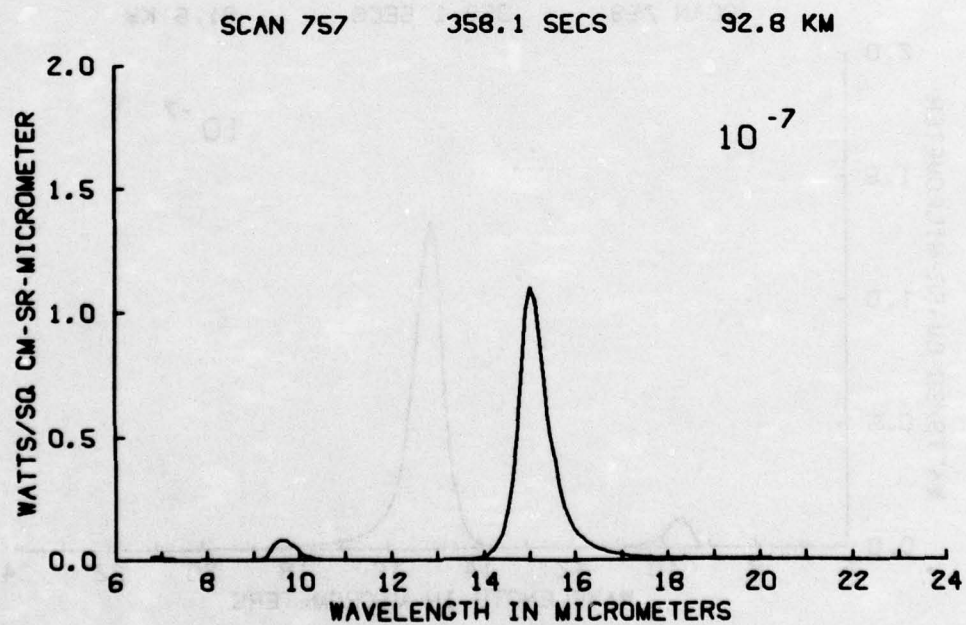


Figure A92

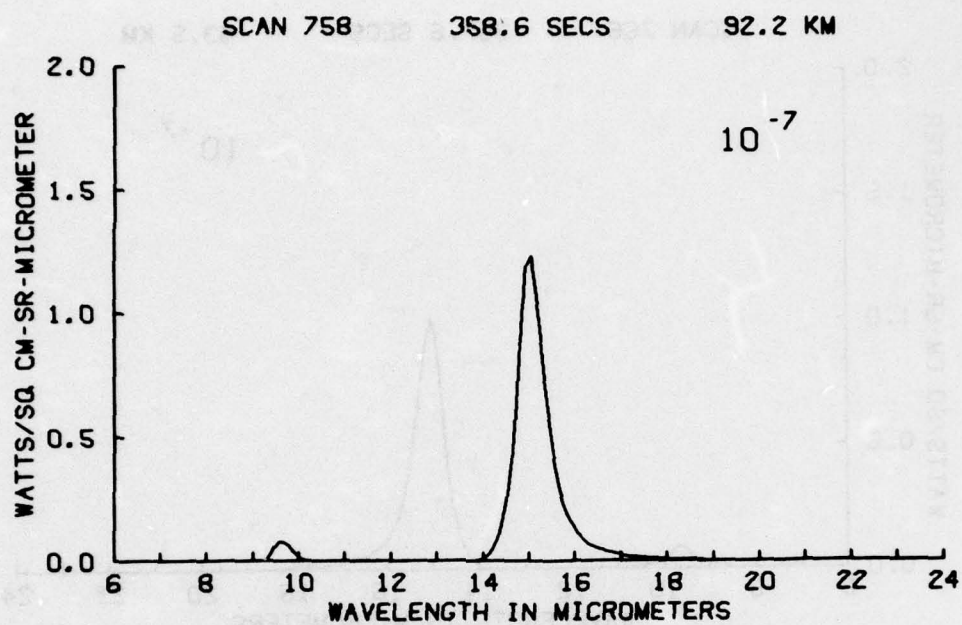


Figure A93

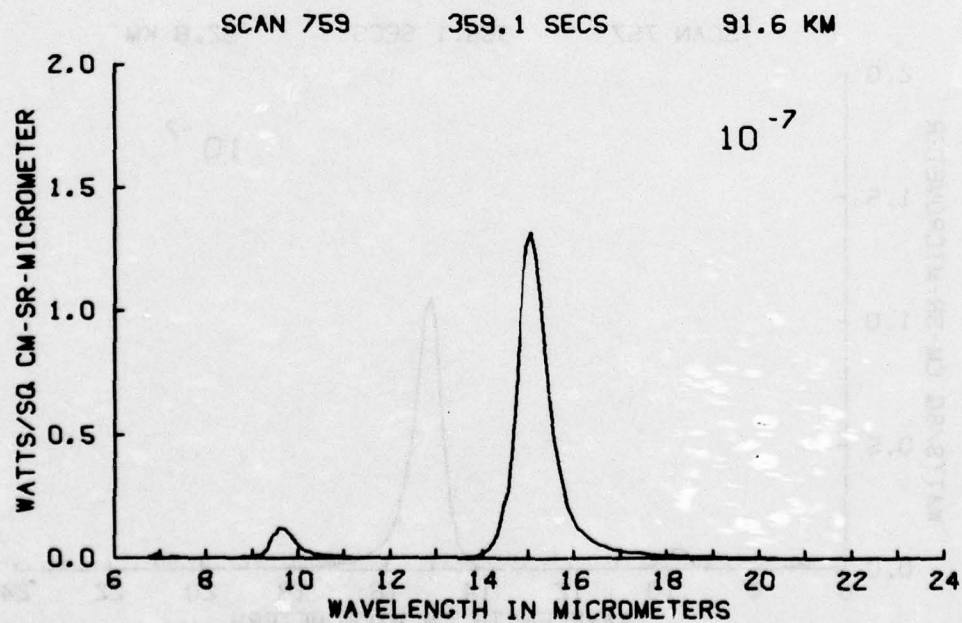


Figure A94

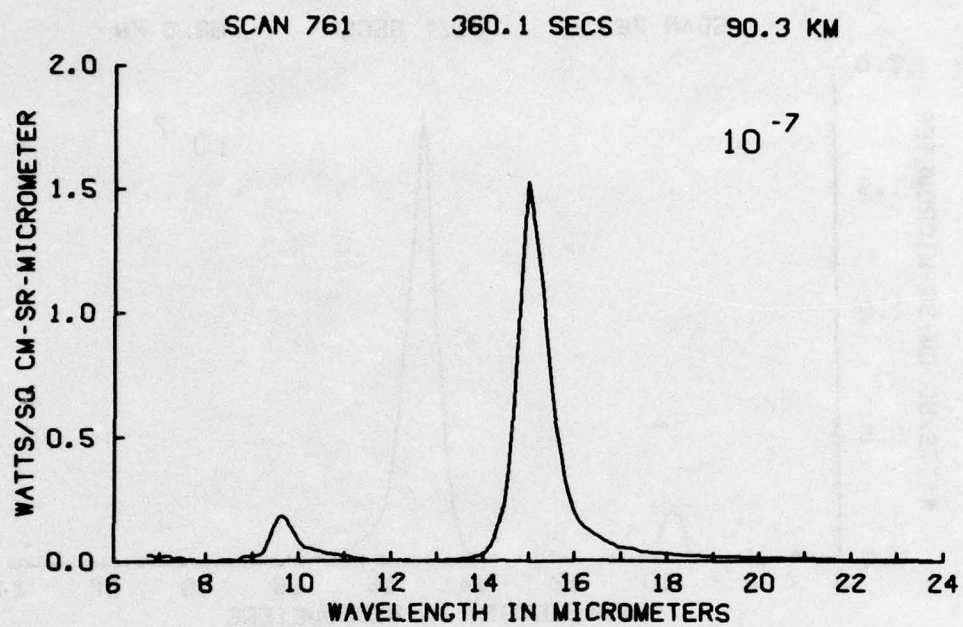


Figure A95

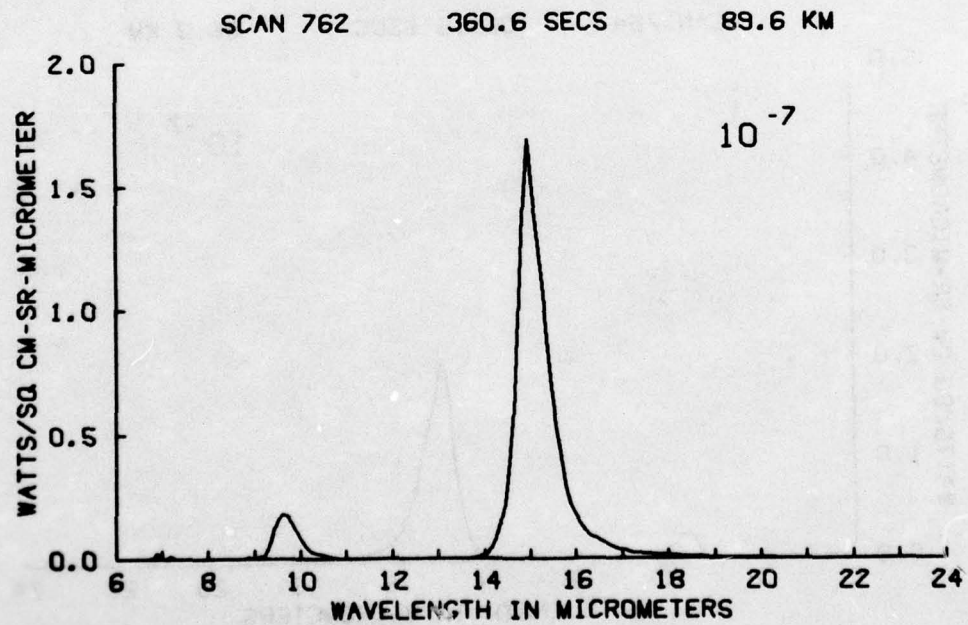


Figure A96

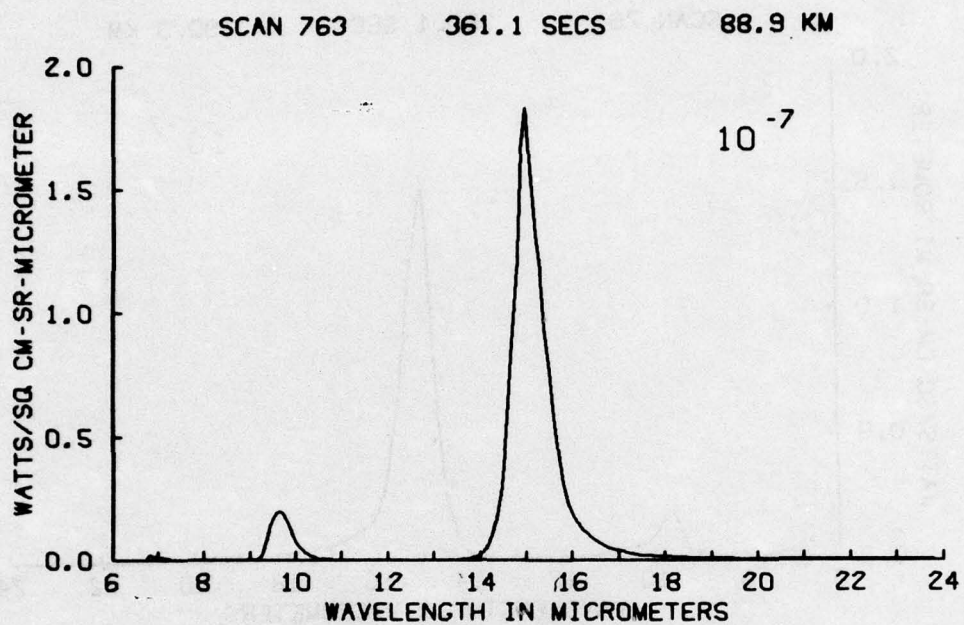


Figure A97

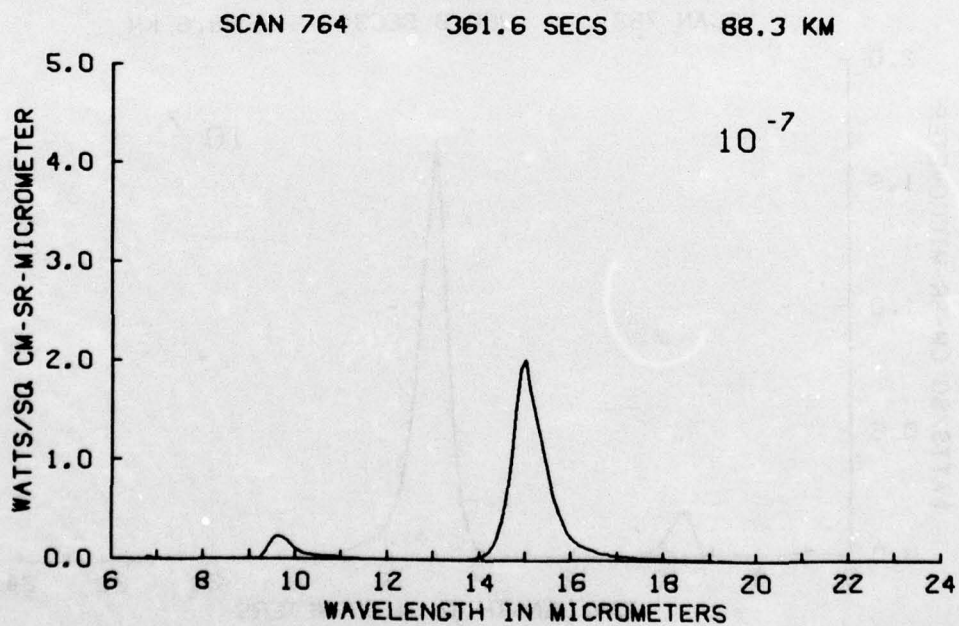


Figure A98

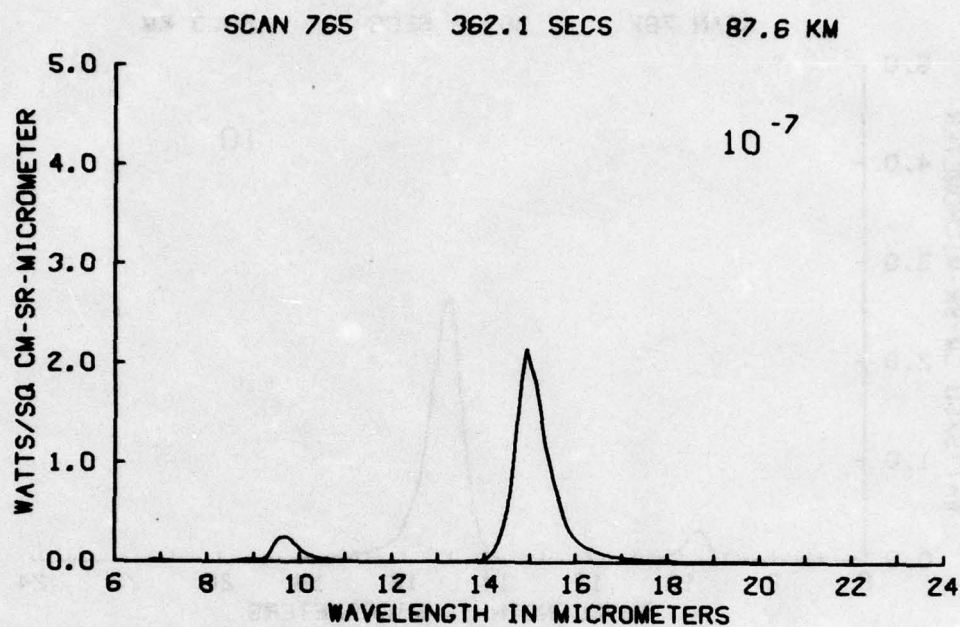


Figure A99

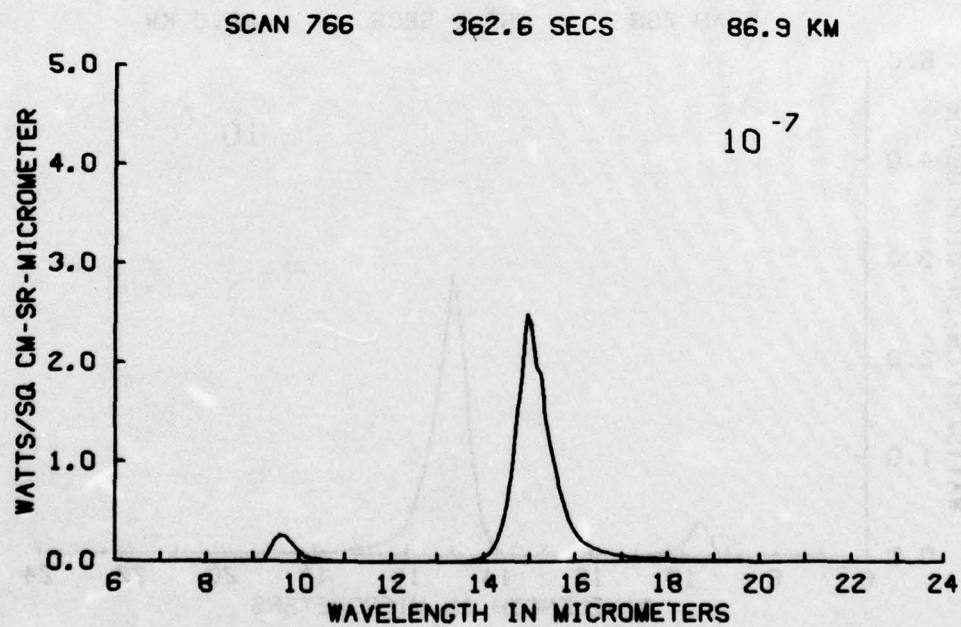


Figure A100

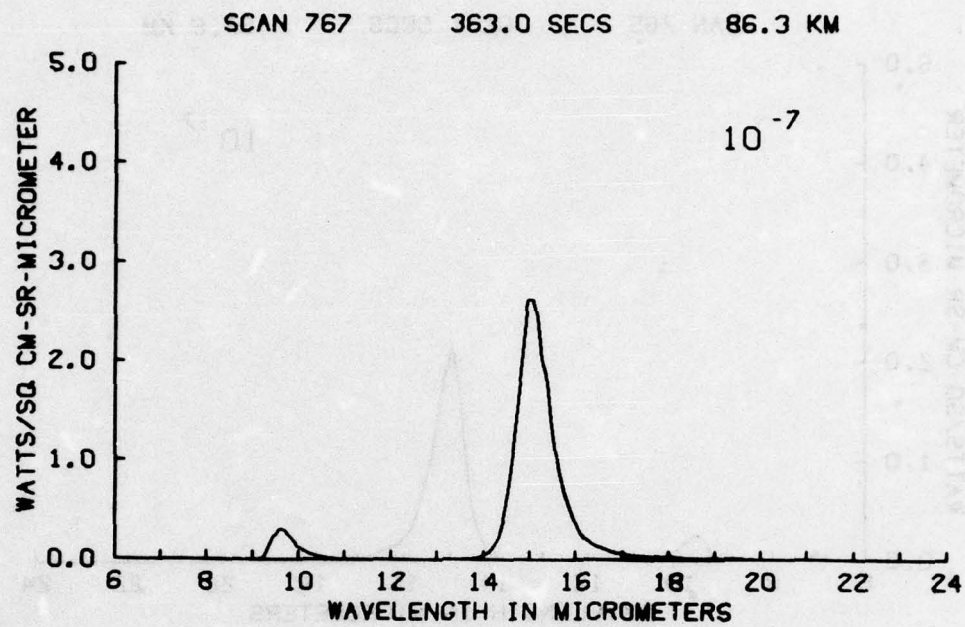


Figure A101

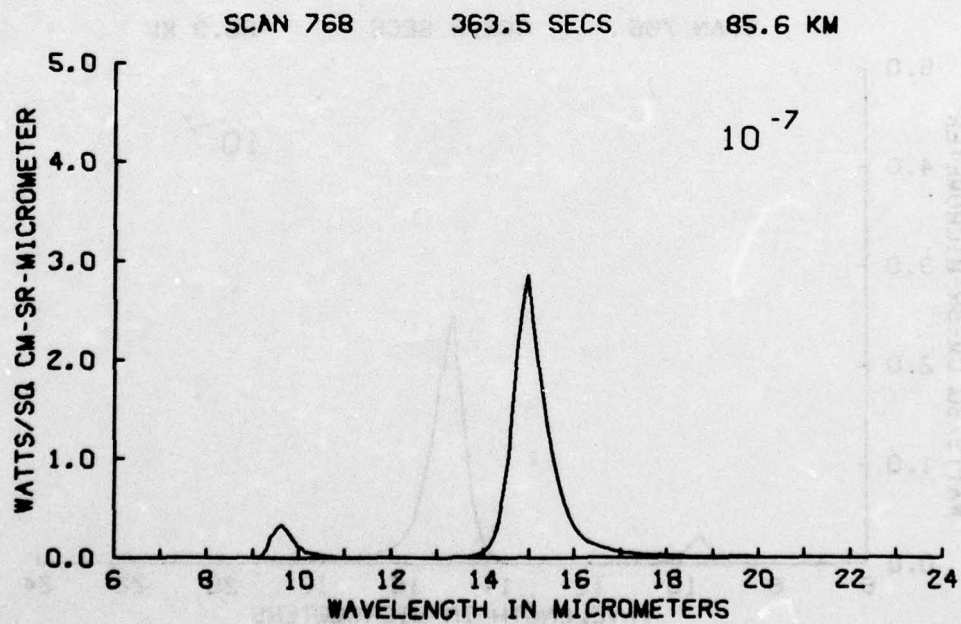


Figure A102

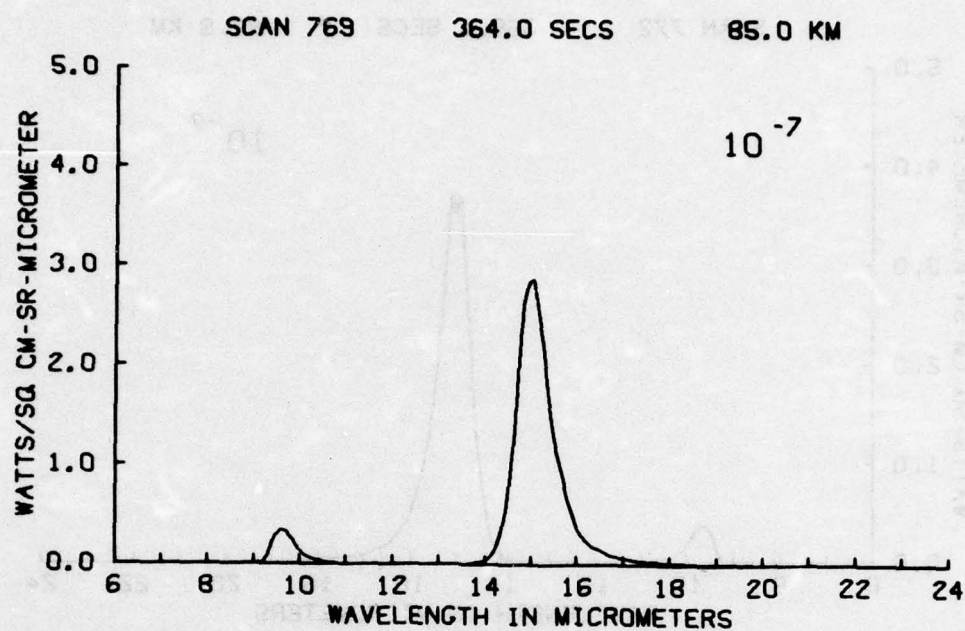


Figure A103

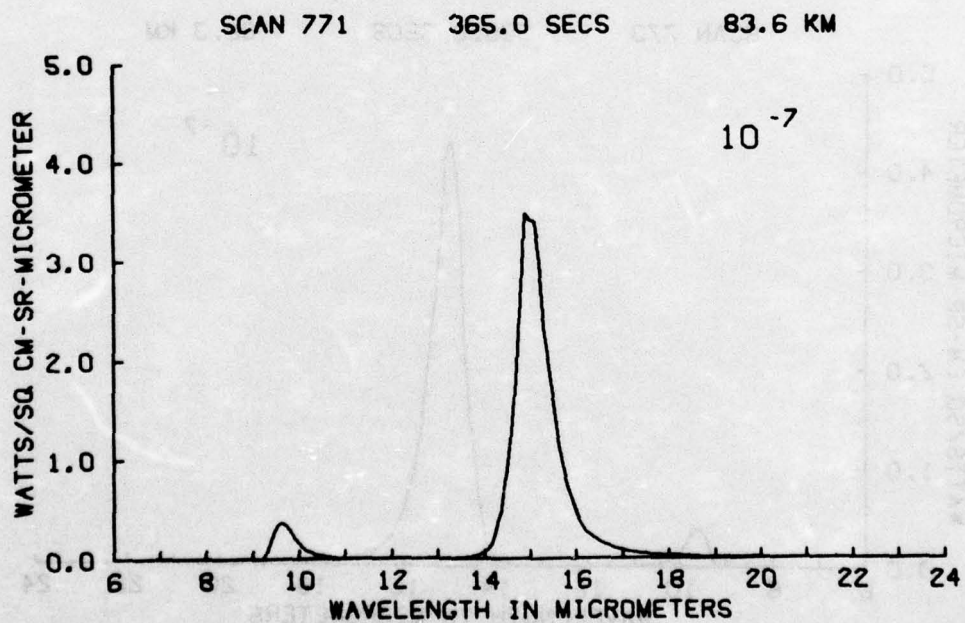


Figure A104

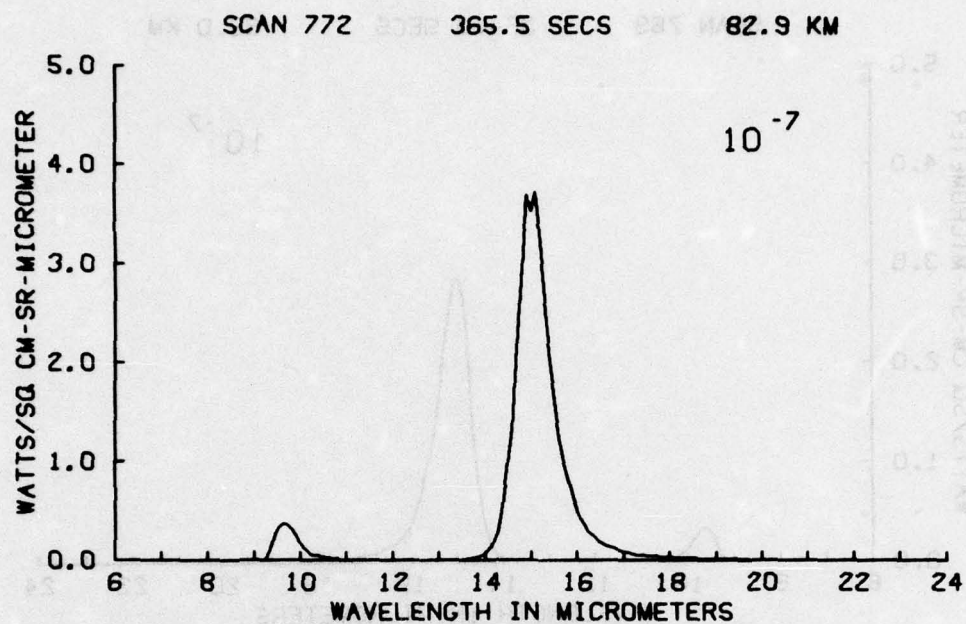


Figure A105

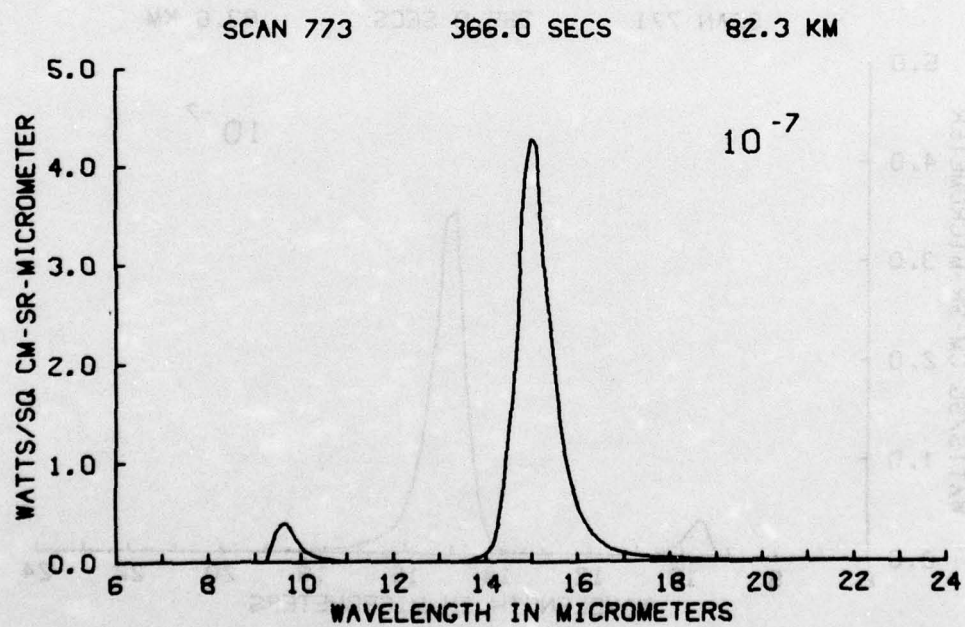


Figure A106

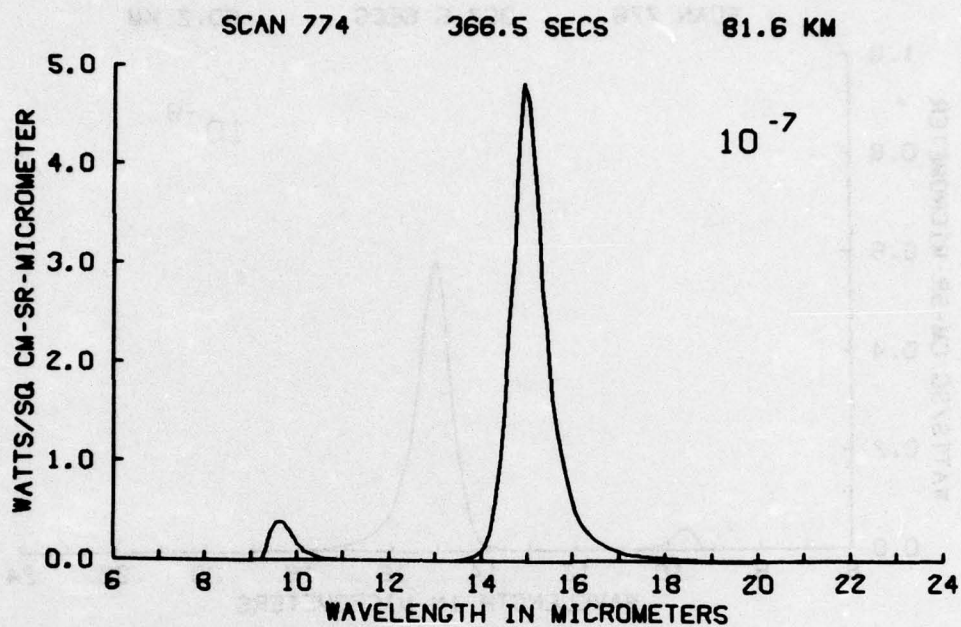


Figure A107

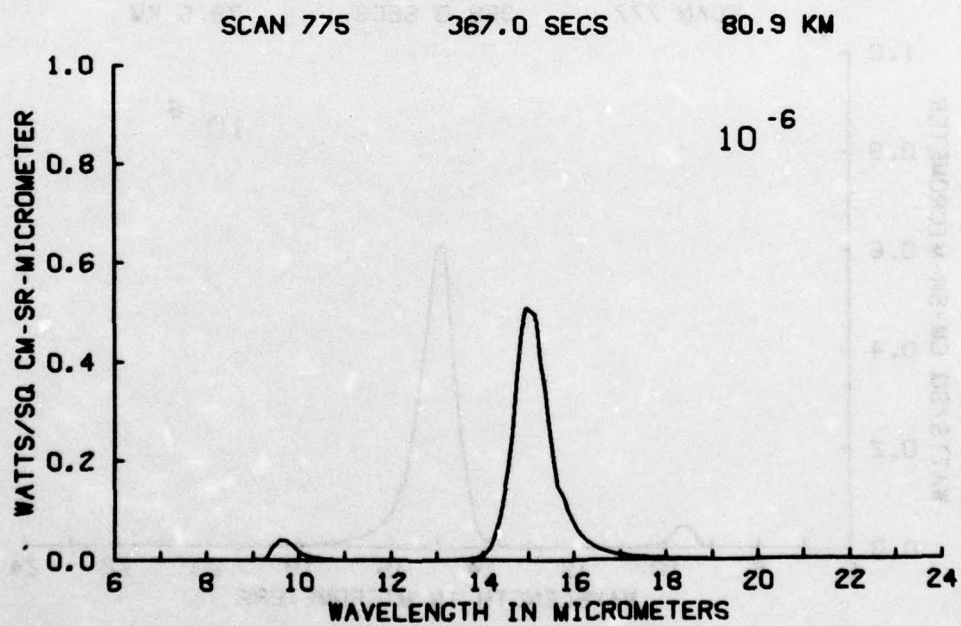


Figure A108

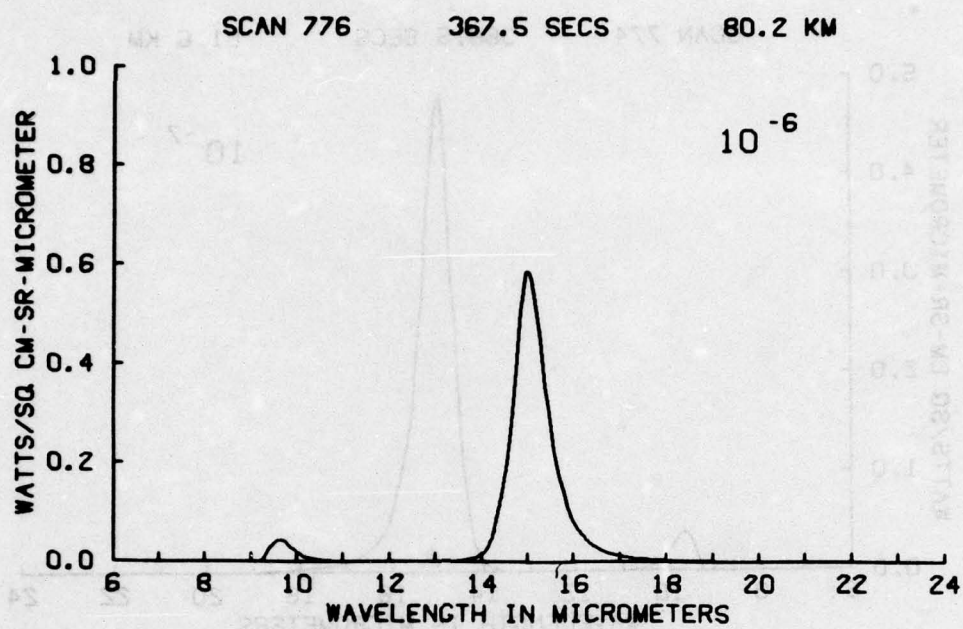


Figure A109

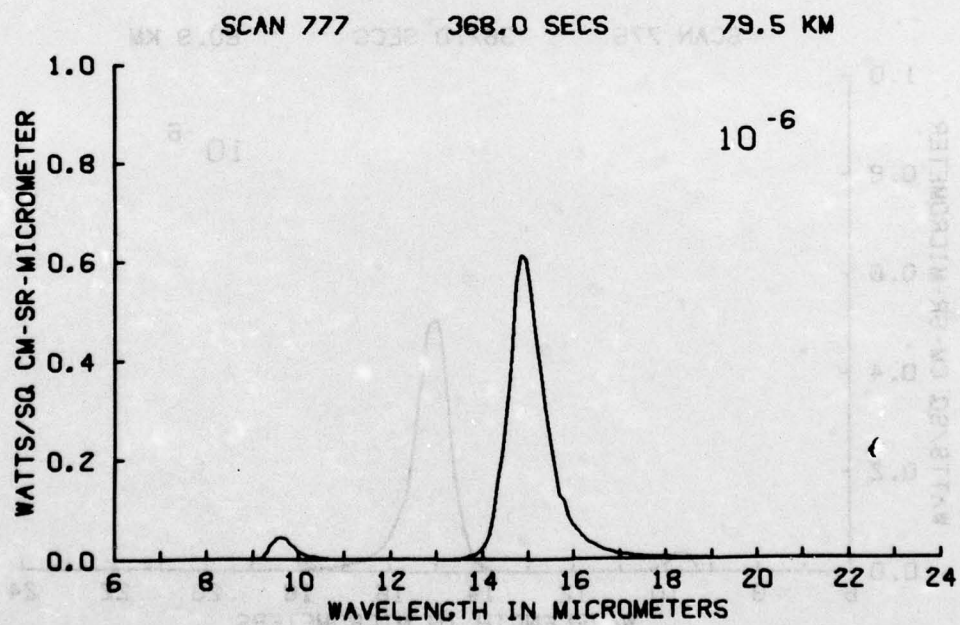


Figure A110

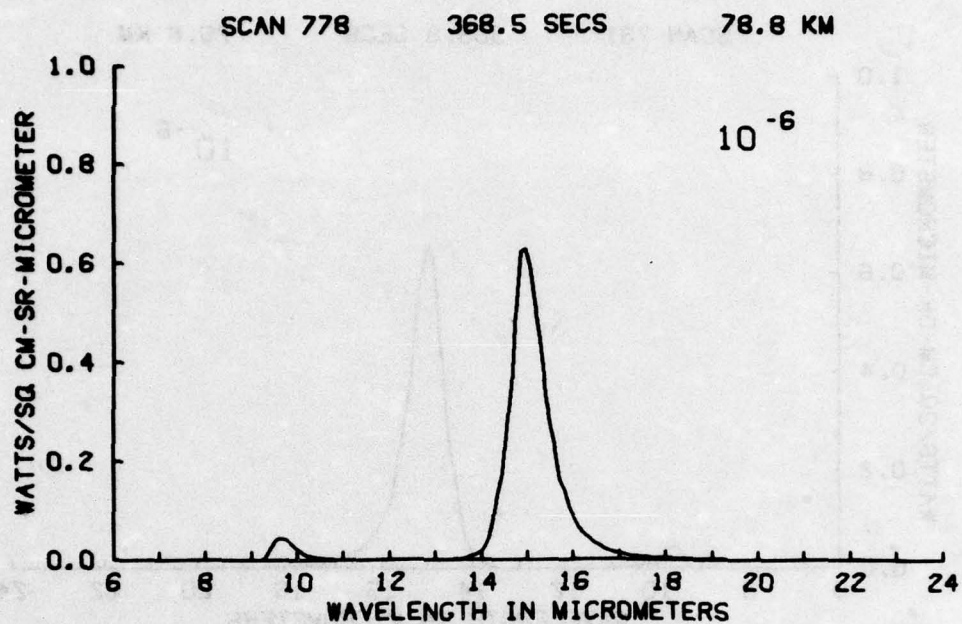


Figure A111

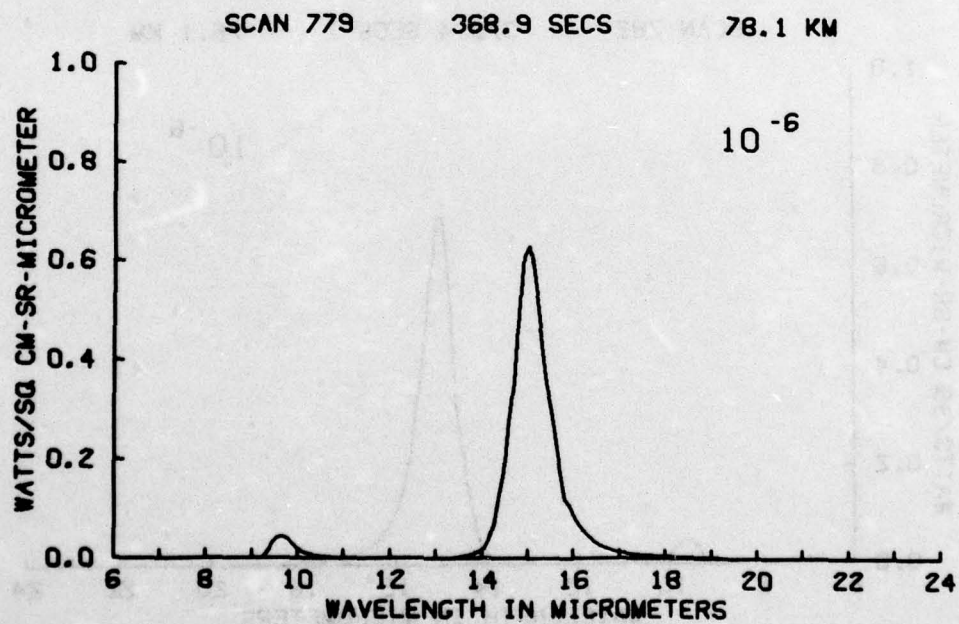


Figure A112

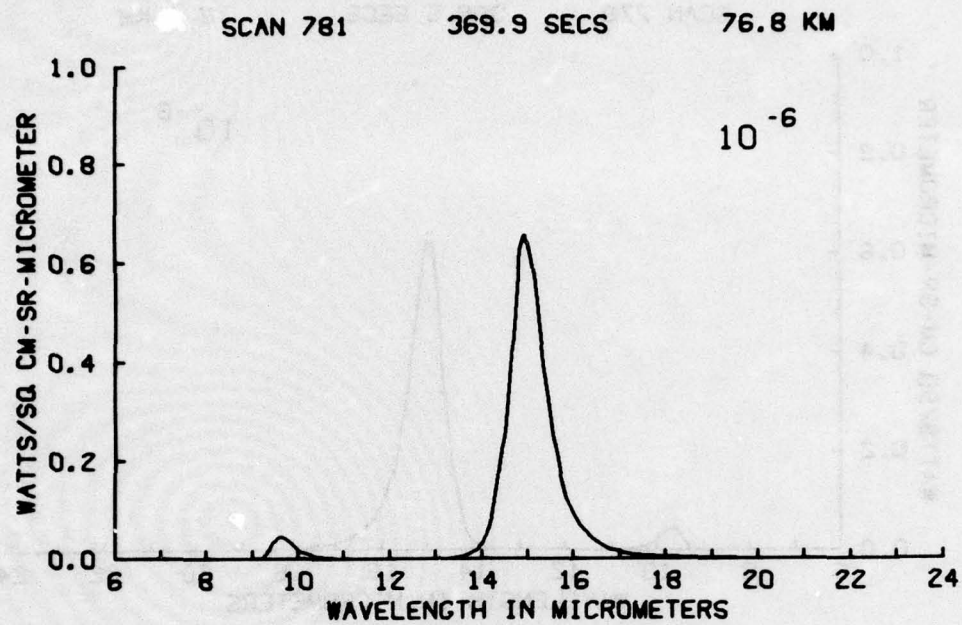


Figure A113

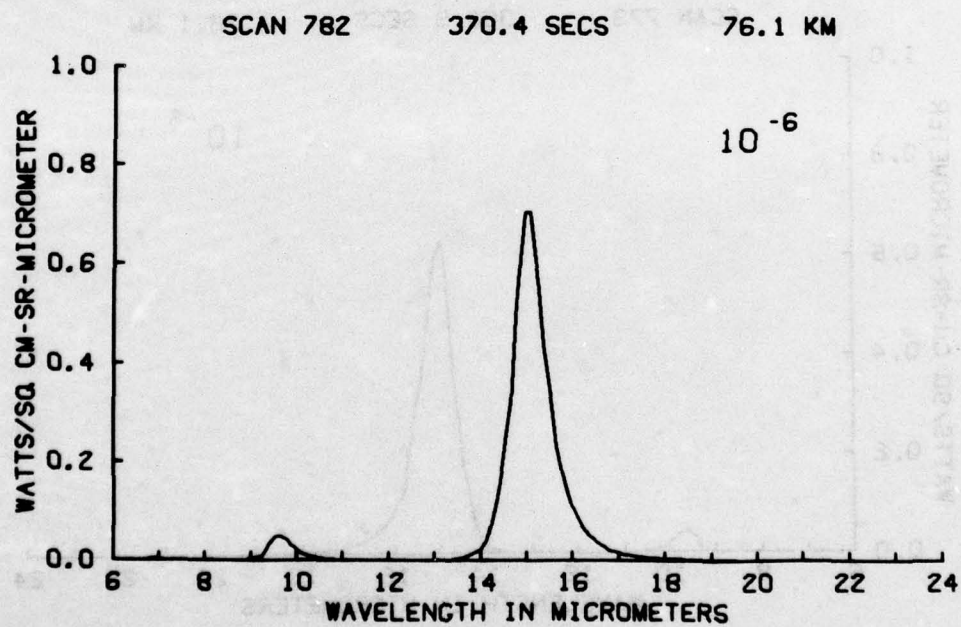


Figure A114

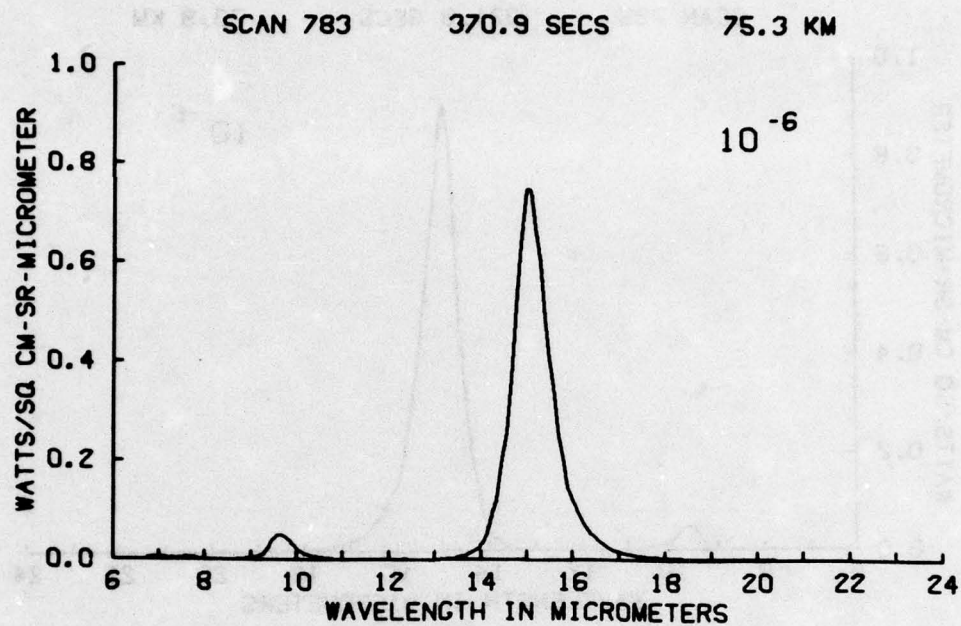


Figure A115

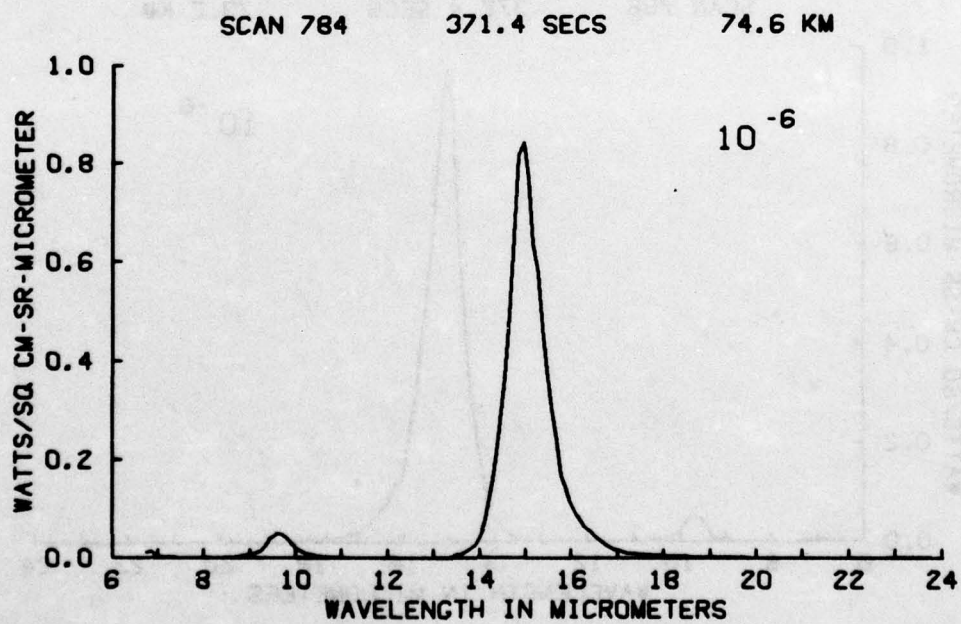


Figure A116

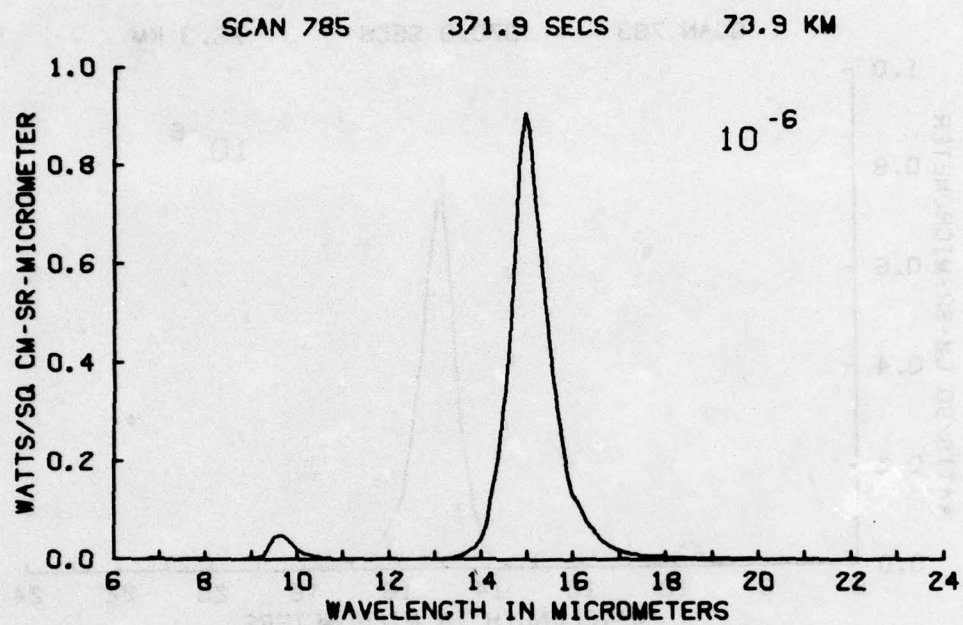


Figure A117

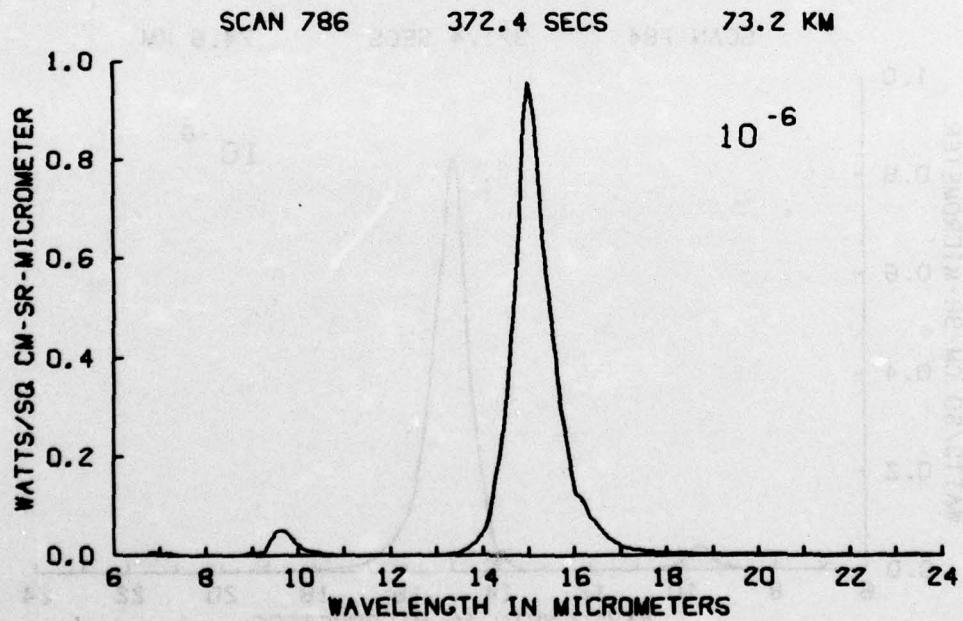


Figure A118

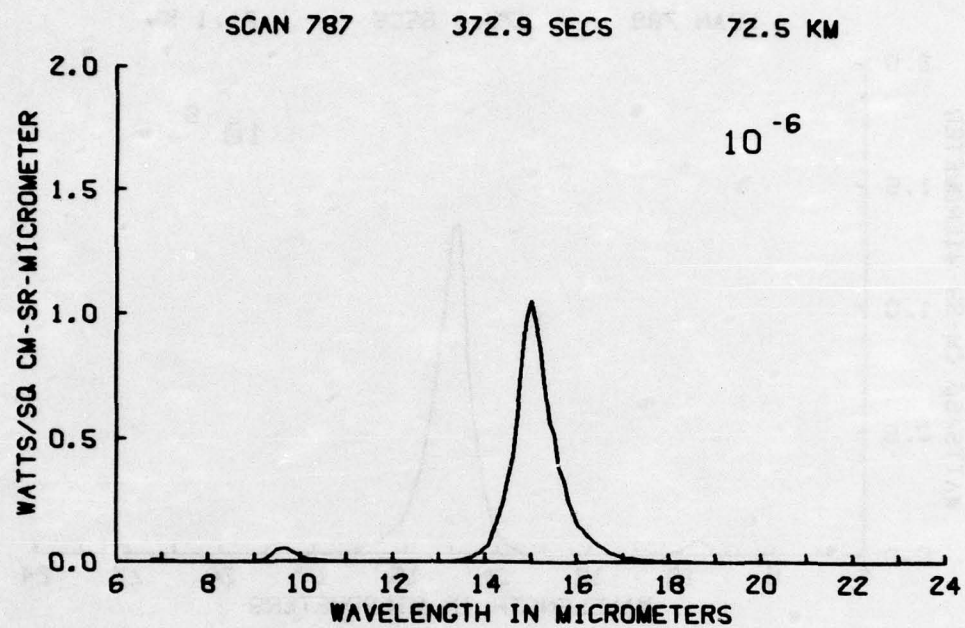


Figure A119

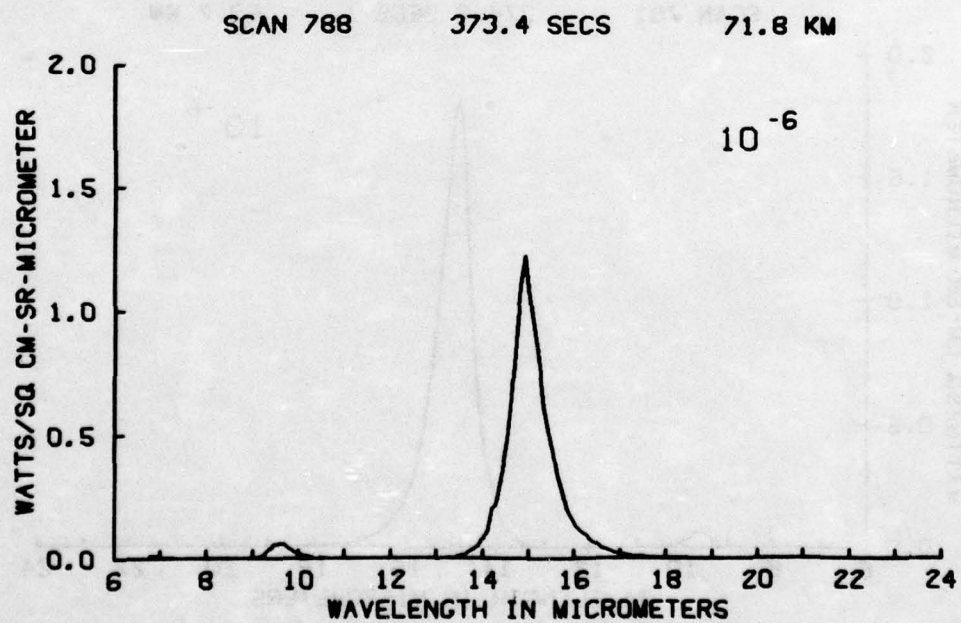


Figure A120

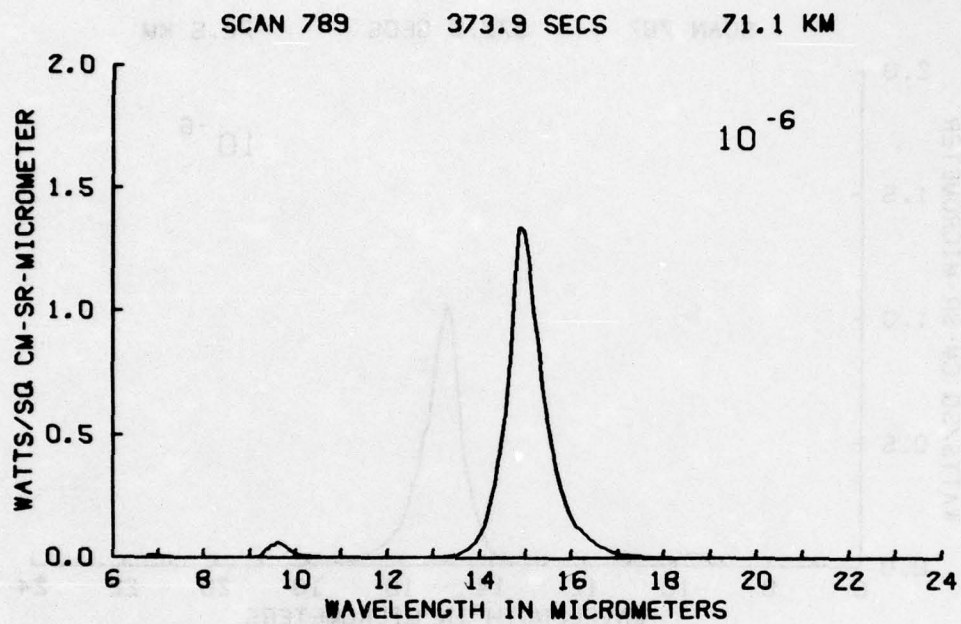


Figure A121

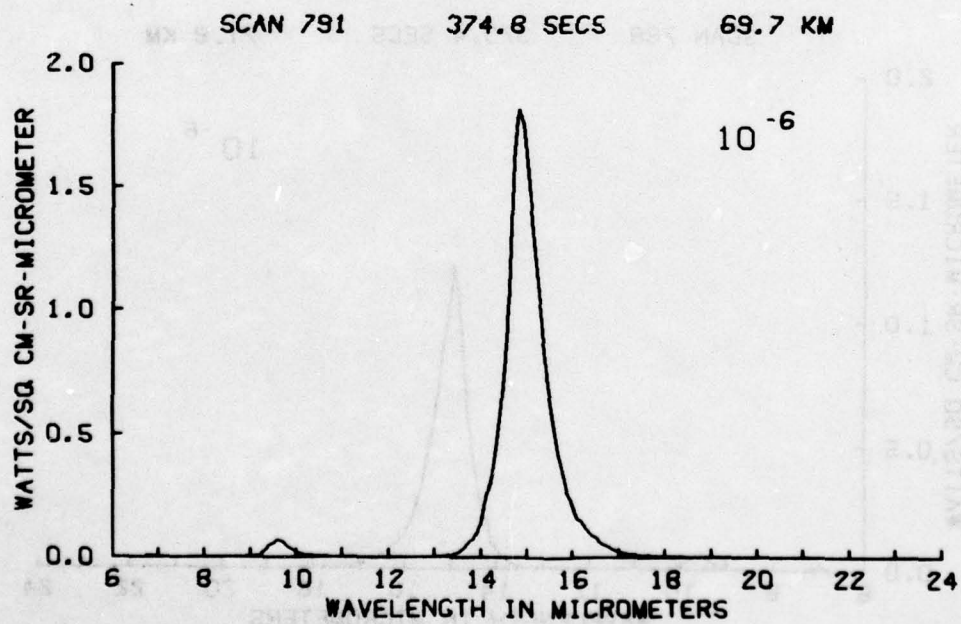


Figure A122

AD-A038 239

AIR FORCE GEOPHYSICS LAB HANSCOM AFB MASS
LWIR (7-24 MICROMETER) MEASUREMENTS FROM THE LAUNCH OF A ROCKET--ETC(U)
NOV 76 J W ROGERS, A T STAIR, N B WHEELER
AFGL-TR-76-0274

F/G 4/1

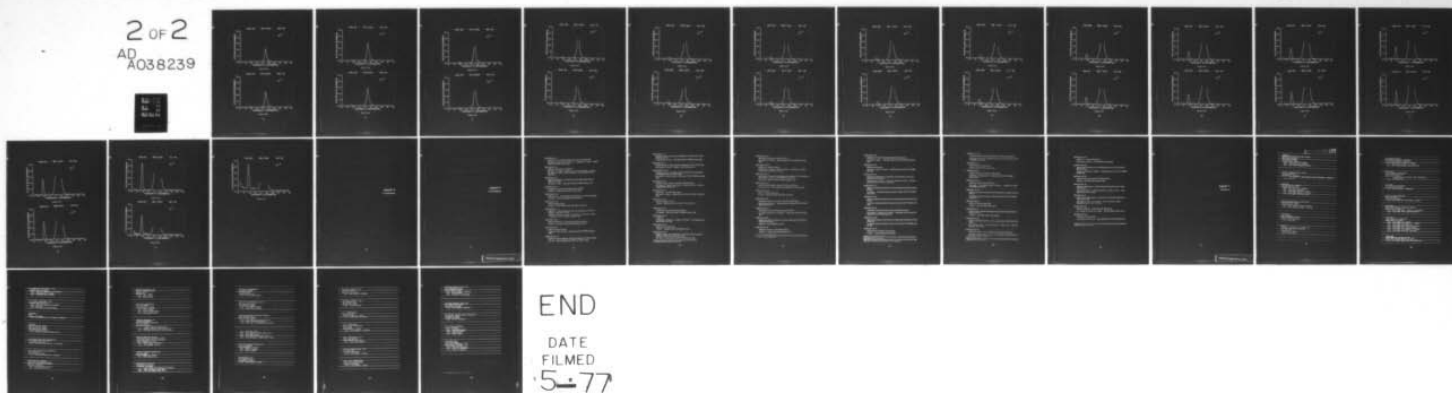
UNCLASSIFIED

DNA-HAES-51

NL

2 OF 2

AD
A038239



END

DATE
FILMED
5-77

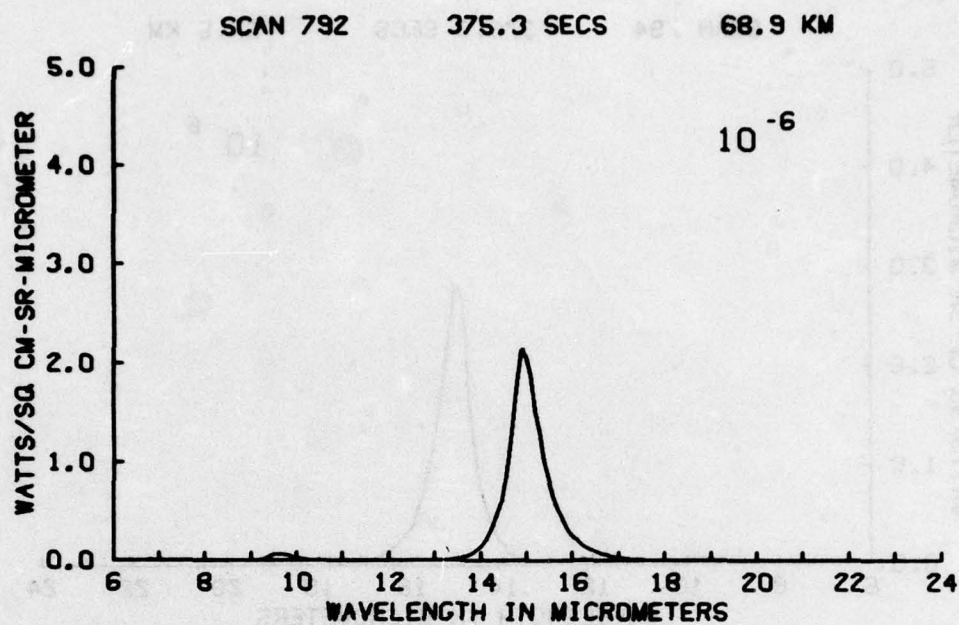


Figure A123

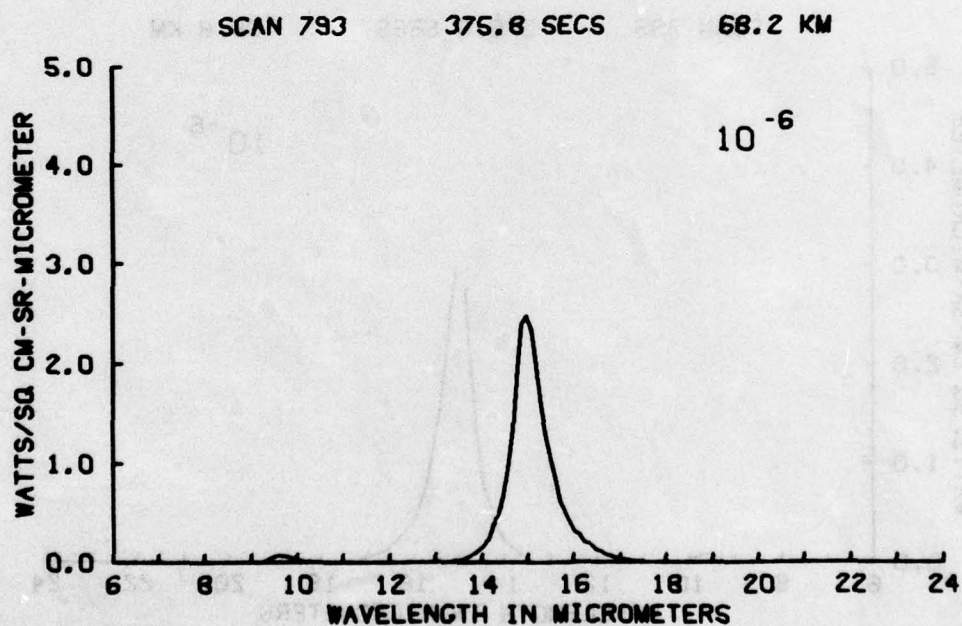


Figure A124

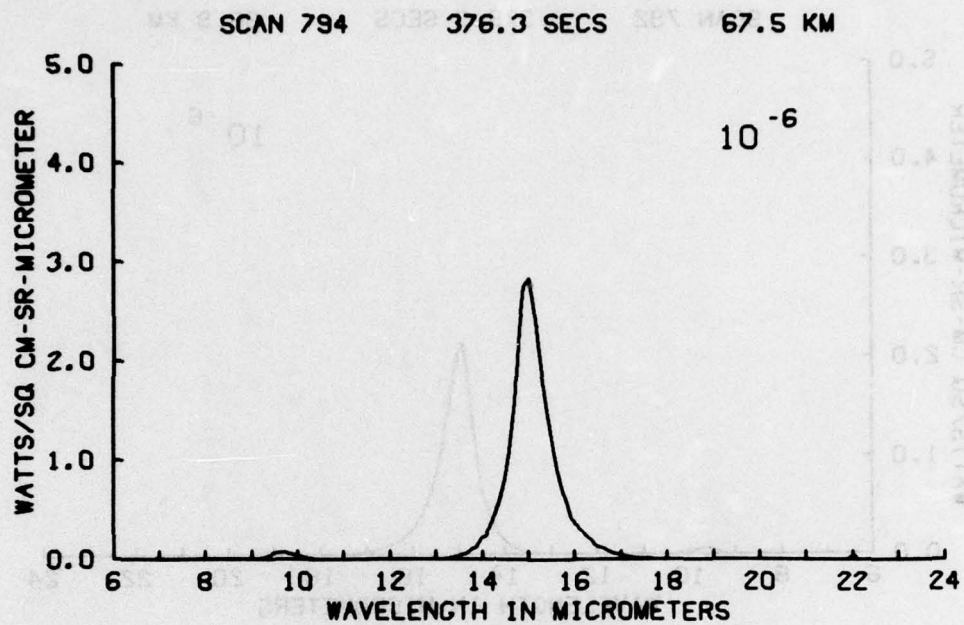


Figure A125

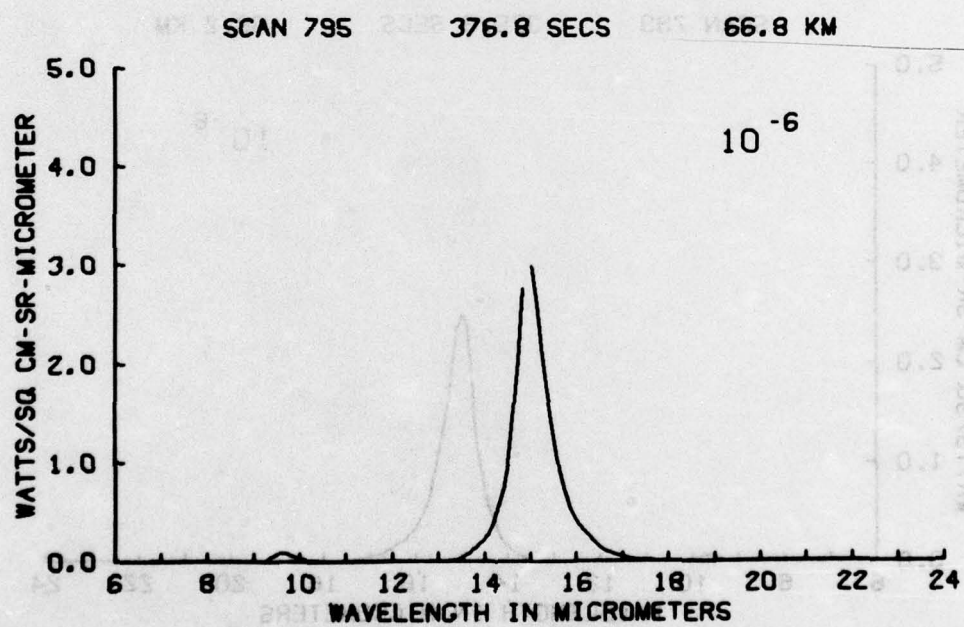


Figure A126

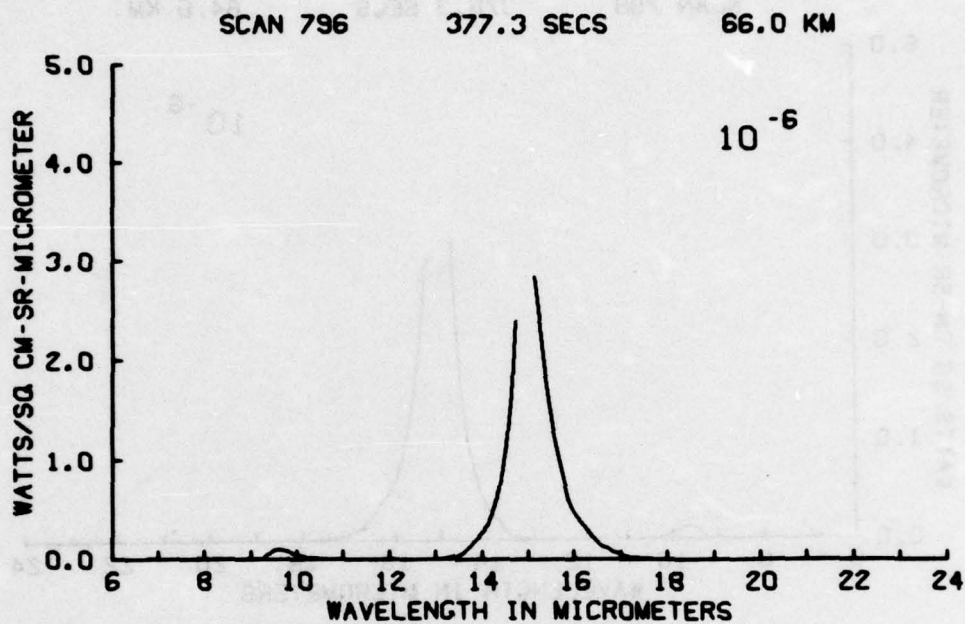


Figure A127

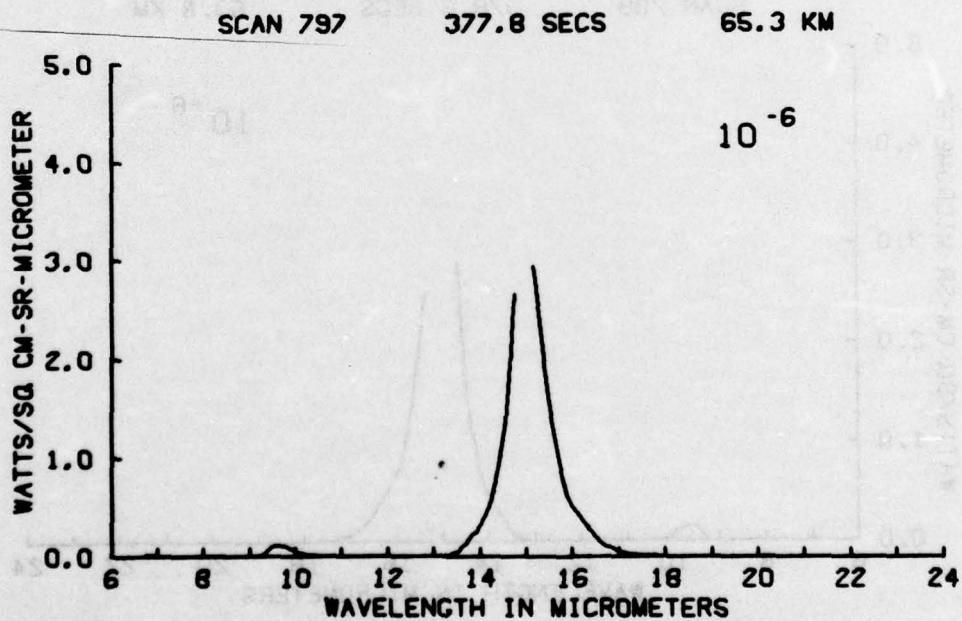


Figure A128

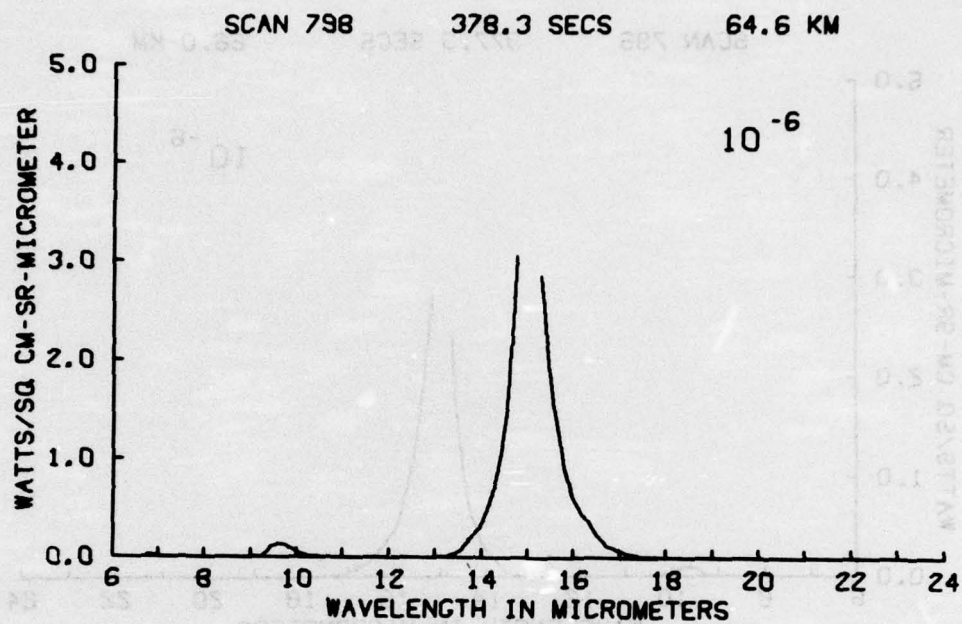


Figure A129

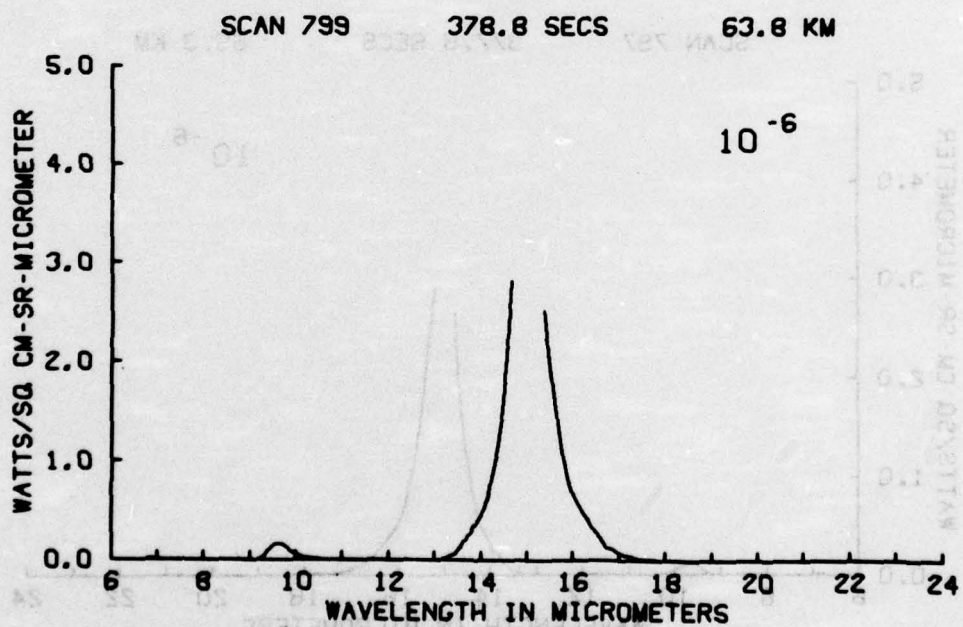


Figure A130

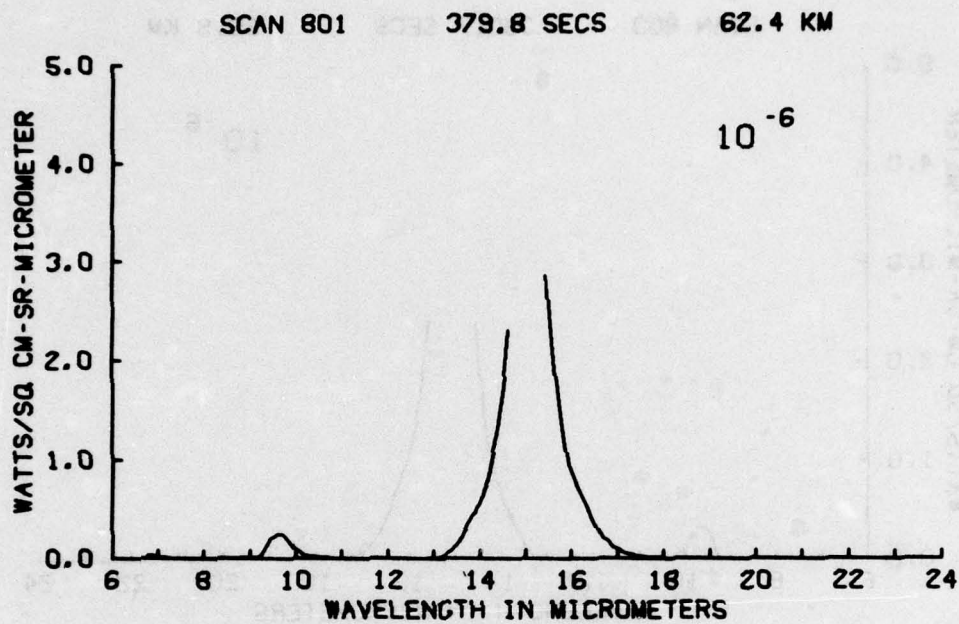


Figure A131

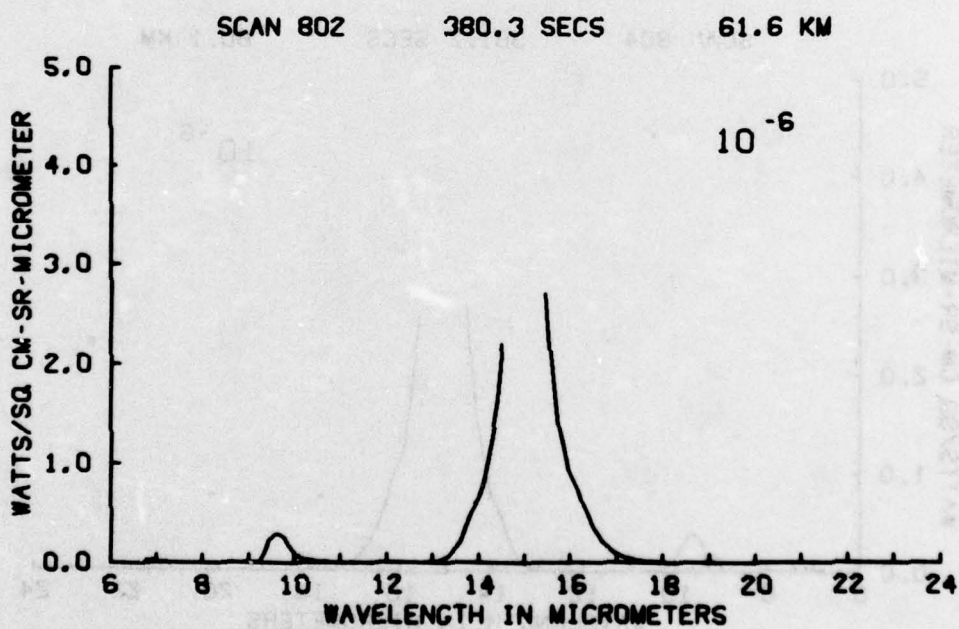


Figure A132

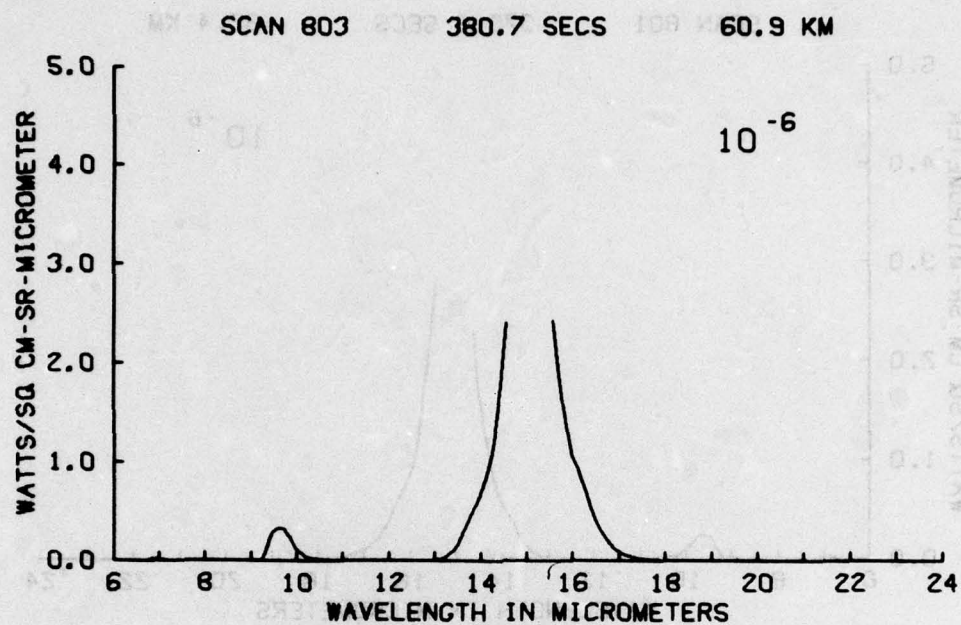


Figure A133

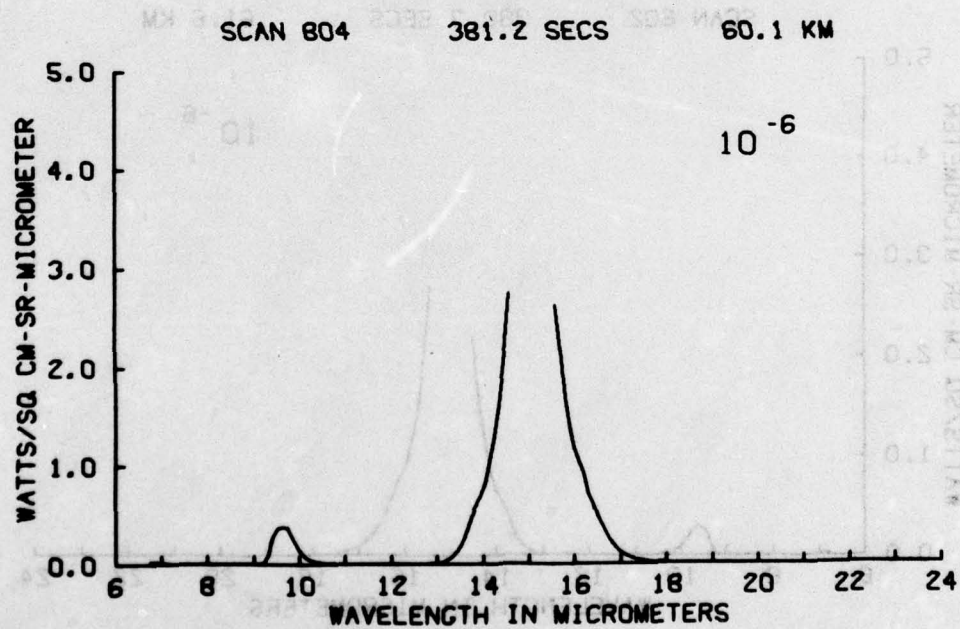


Figure A134

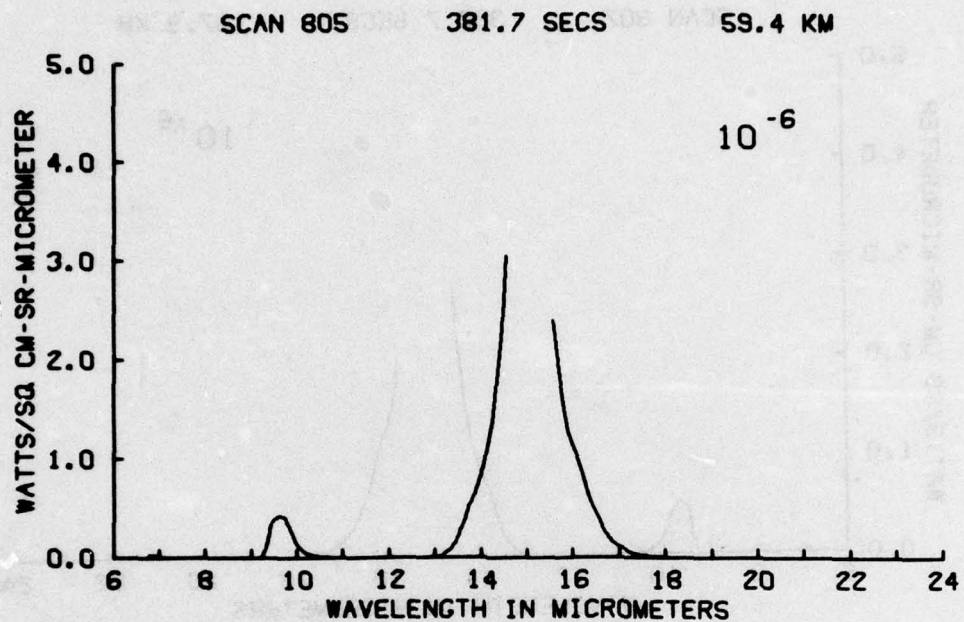


Figure A135

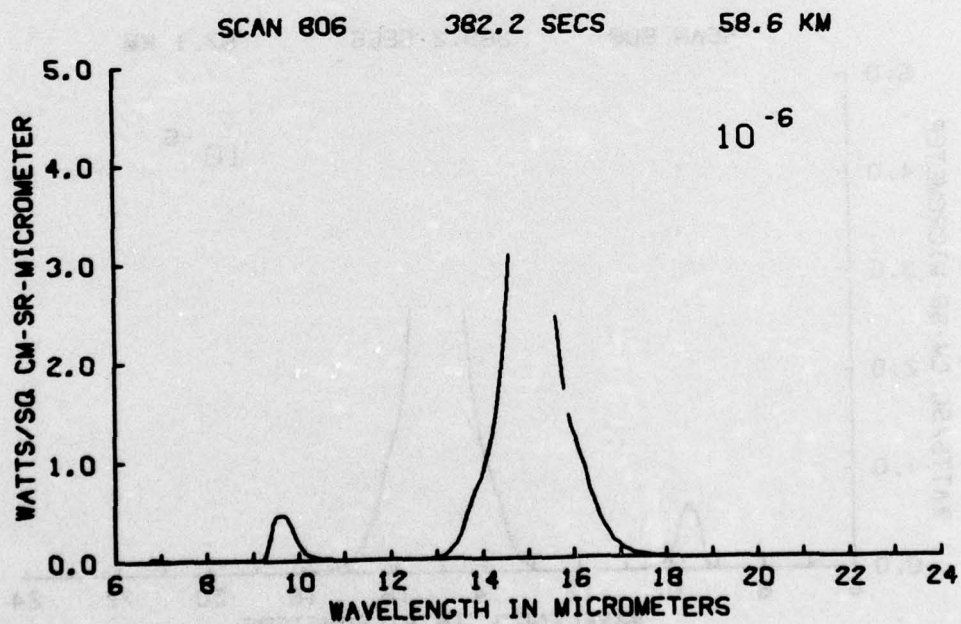


Figure A136

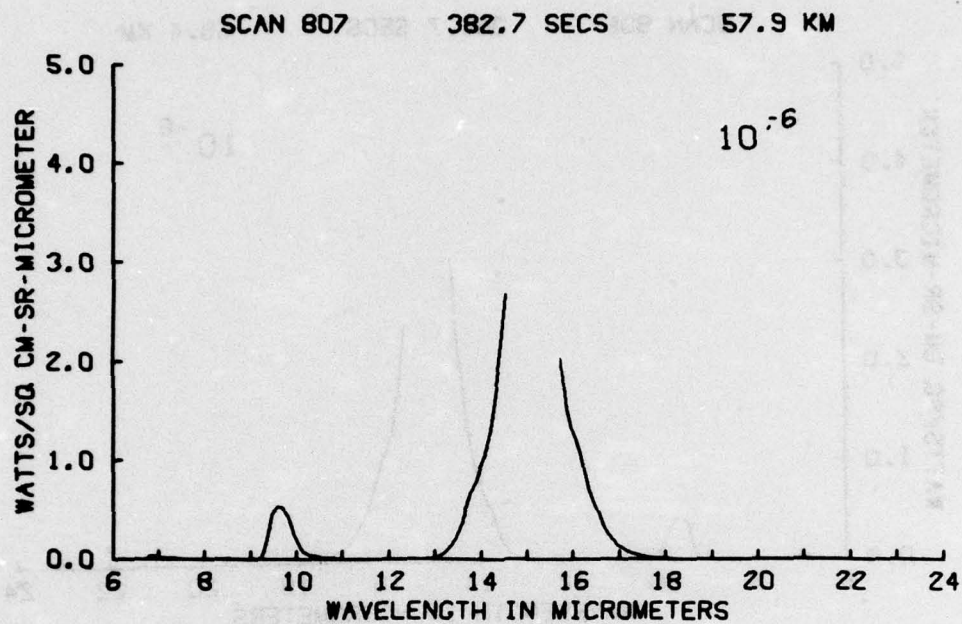


Figure A137

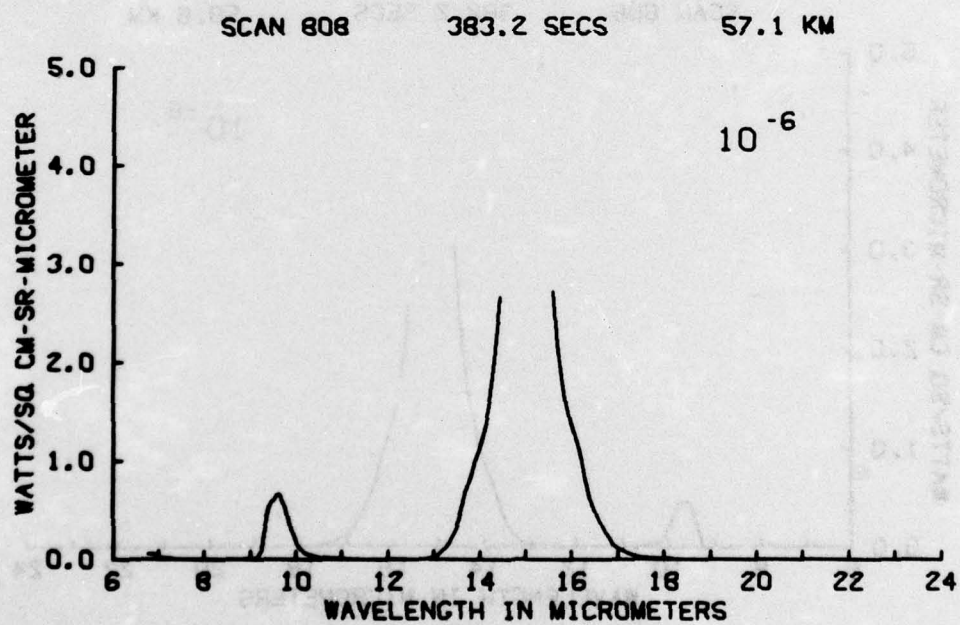


Figure A138

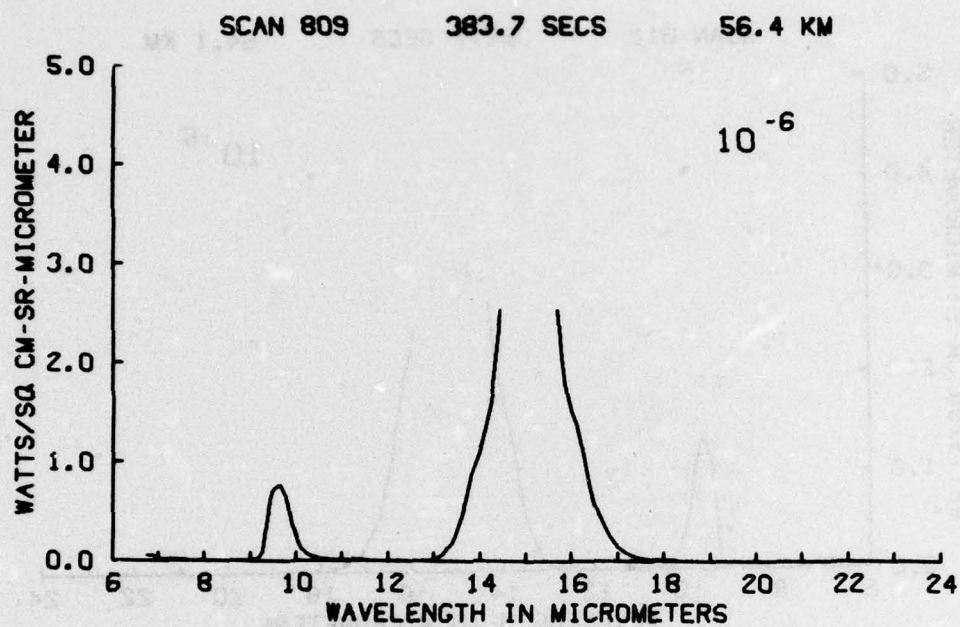


Figure A139

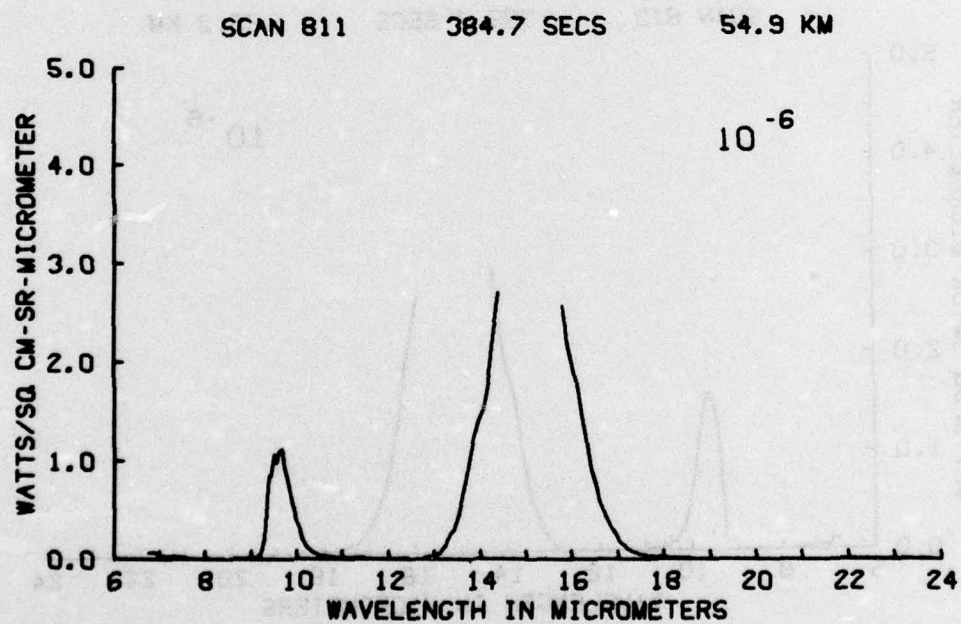


Figure A140

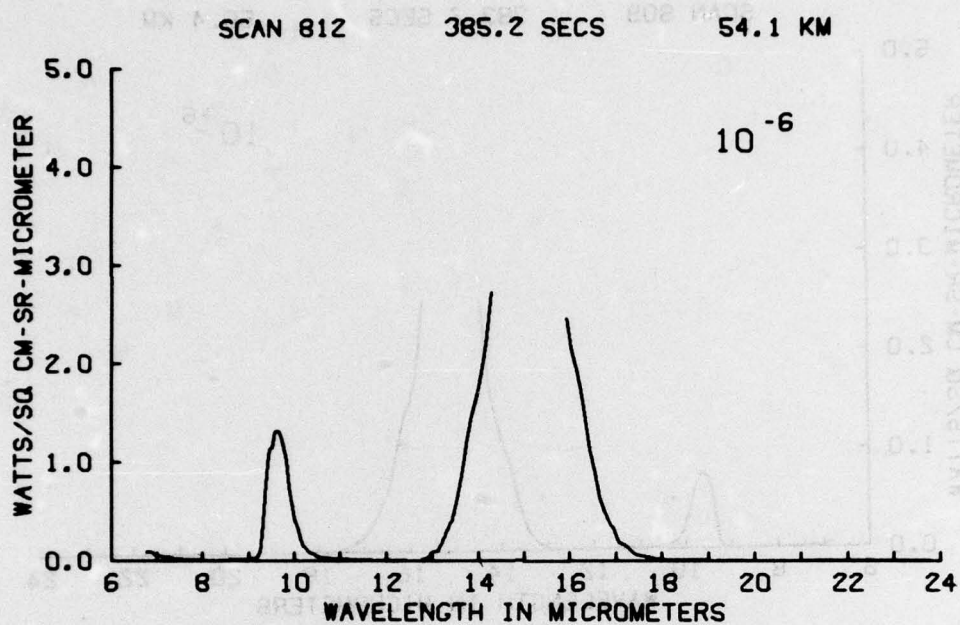


Figure A141

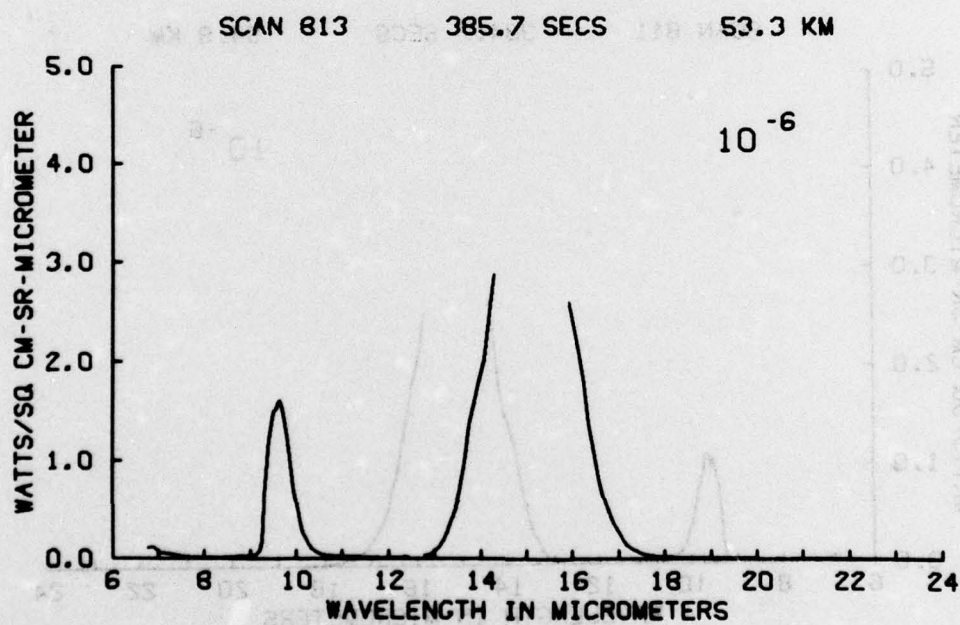


Figure A142

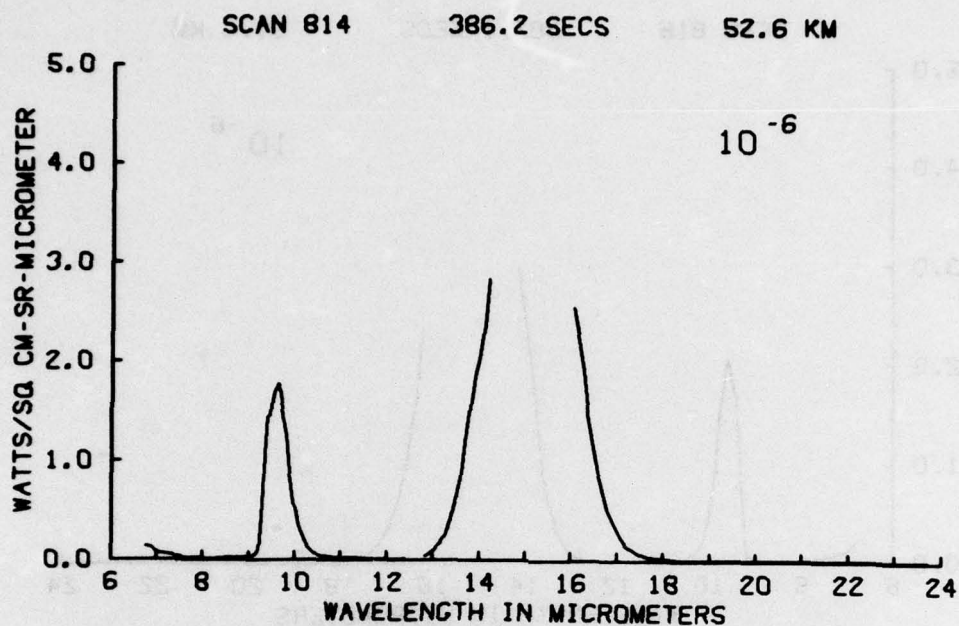


Figure A143

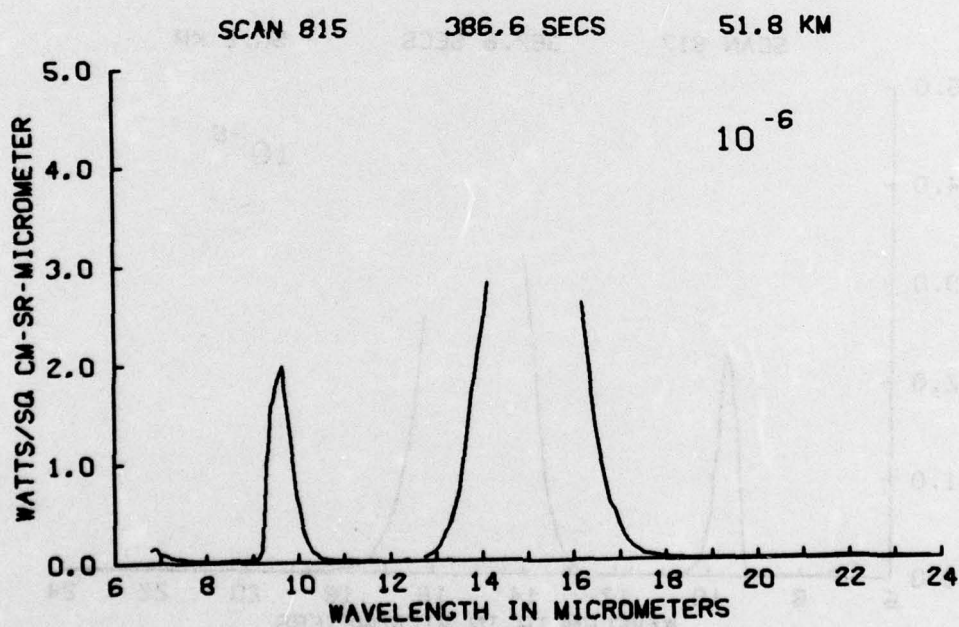


Figure A144

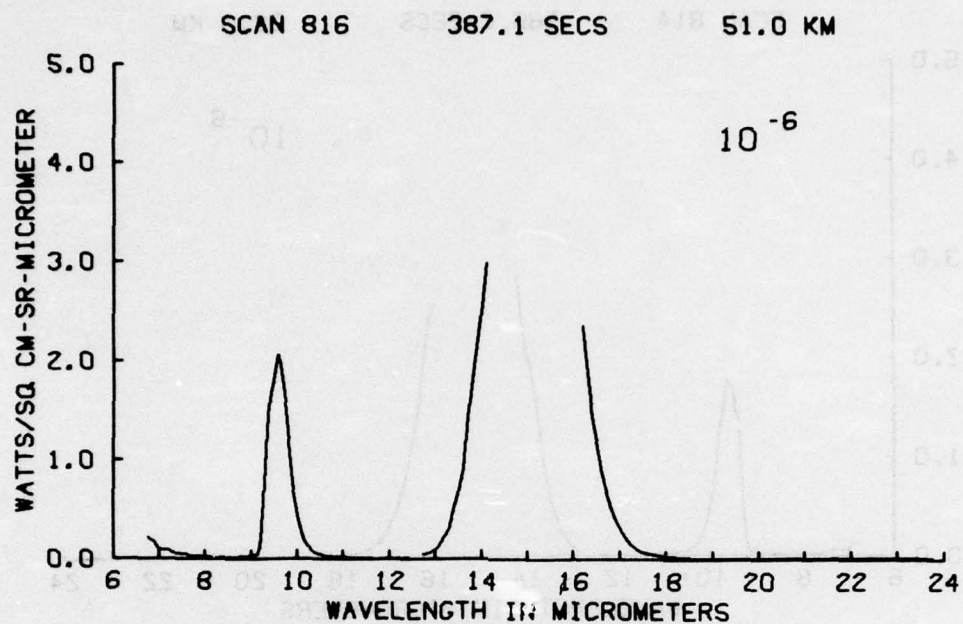


Figure A145

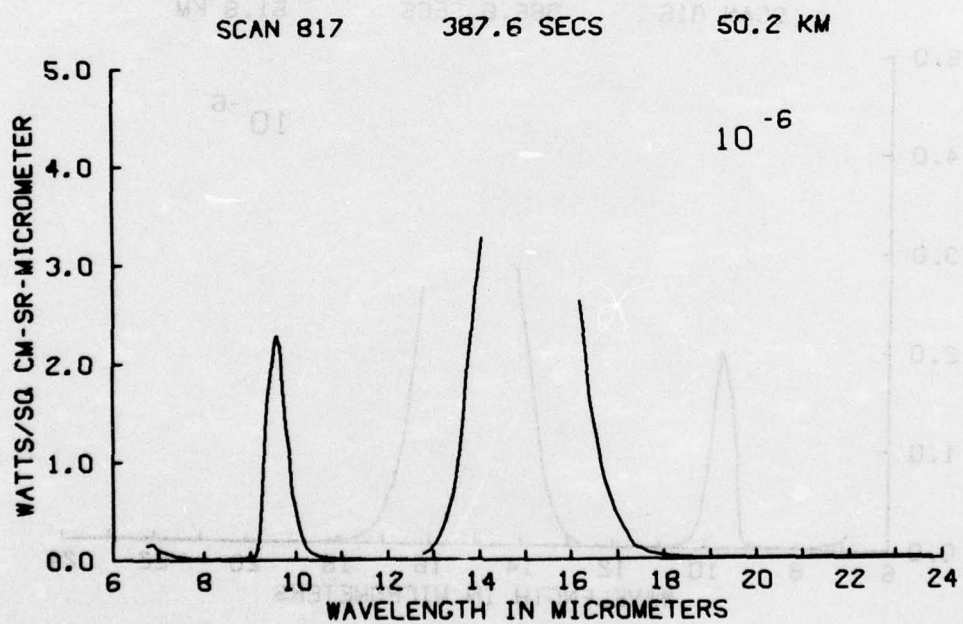


Figure A146

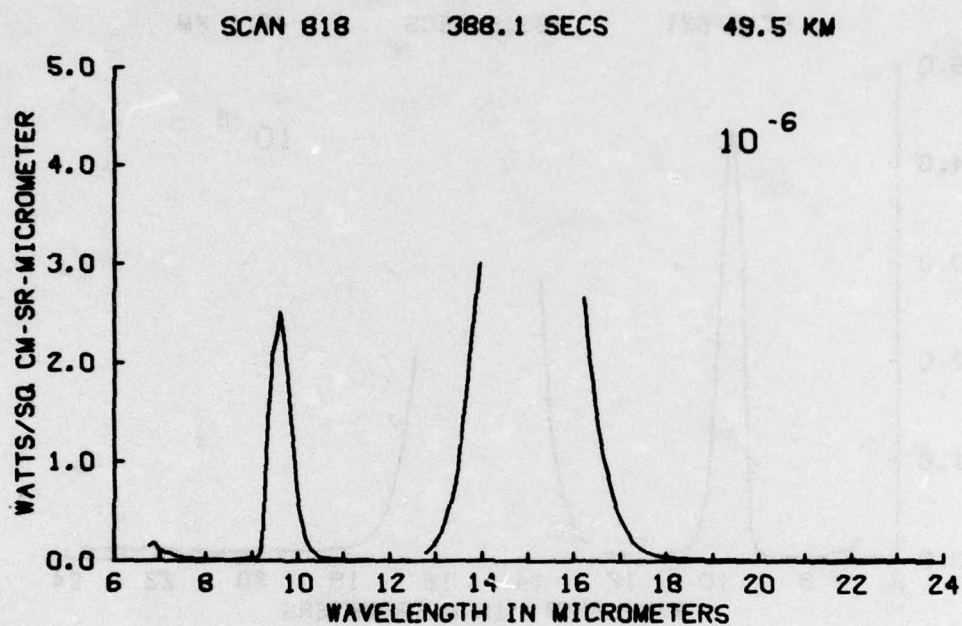


Figure A147

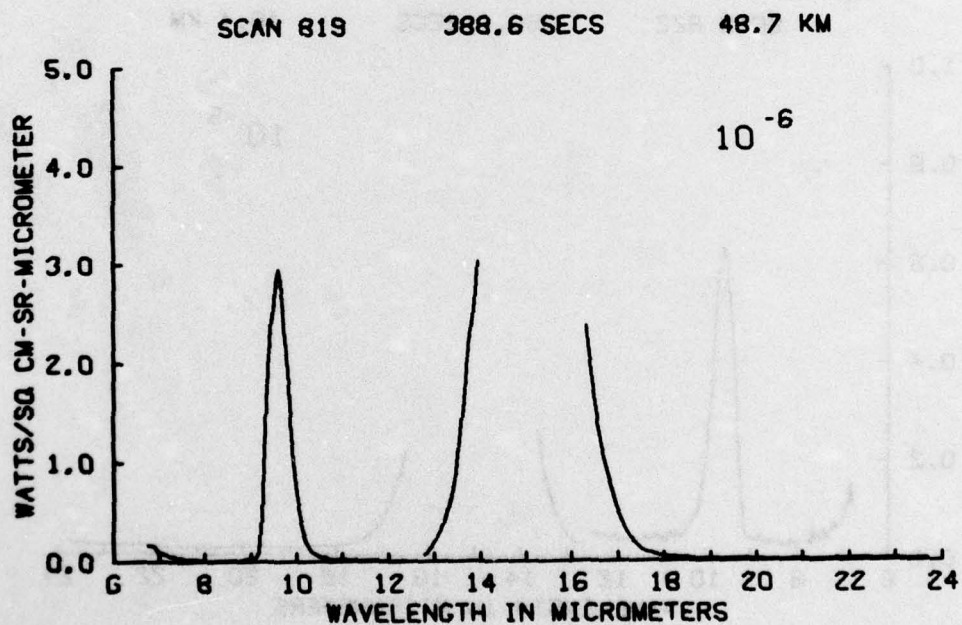


Figure A148

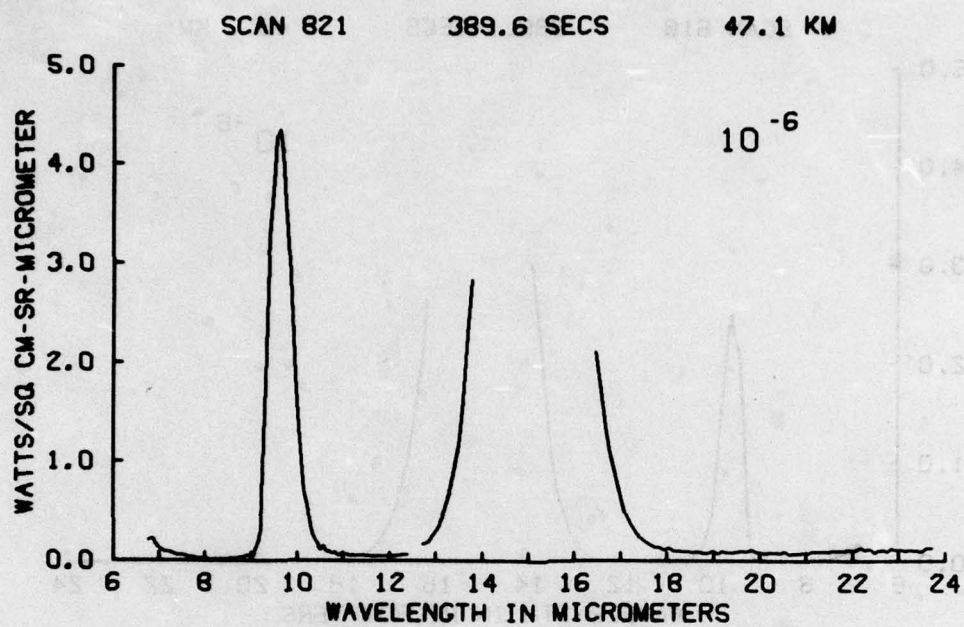


Figure A149

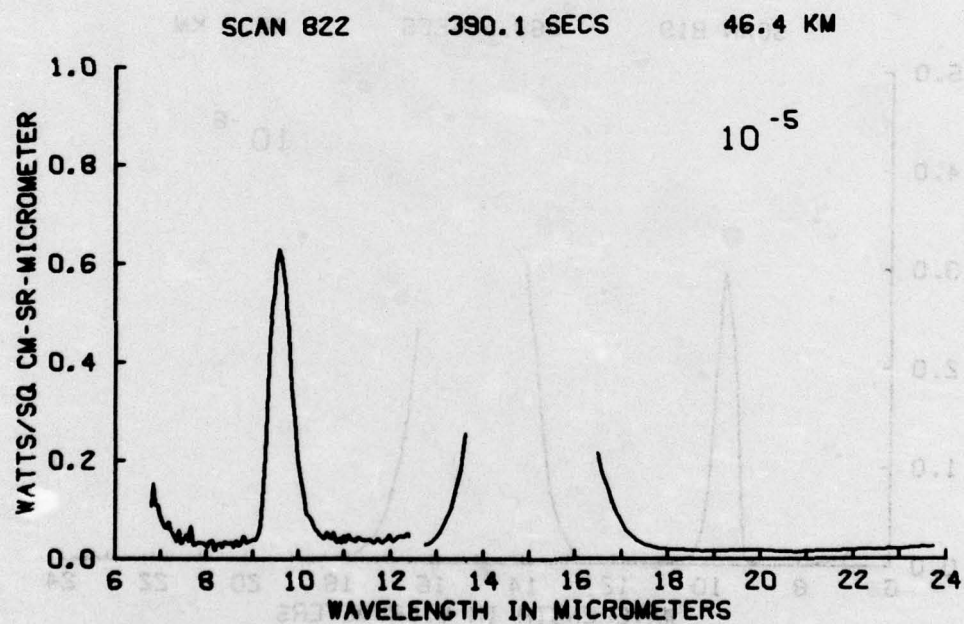


Figure A150

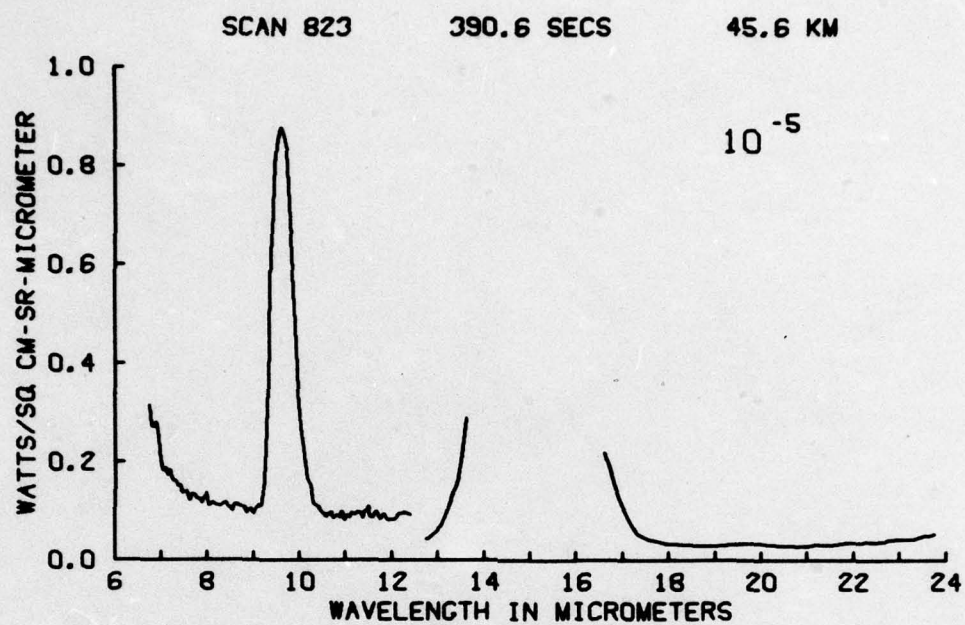


Figure A151

Appendix B

List of HAES Reports

Appendix B

List of HAES Reports

HAES Report No. 1

Rocket Launch of a SWIR Spectrometer into an Aurora (ICECAP 72)

D.J. Baker, C.L. Wyatt, W.R. Pendelton, Jr. - Utah State, J.C. Ulwick - AFCRL;
AFCRL-TR-74-0077, February 1974.

HAES Report No. 2

Analysis of HAES Results: ICECAP 72

W.P. Reidy, T.C. Degges, O.P. Manley, H.J. Smith, J.W. Carpenter - Visidyne,
A.T. Stair, J.C. Ulwick - AFCRL, D.J. Baker - Utah State; DNA 3247F,
April 1974.

HAES Report No. 3

*Rocket Instrumentation for ICECAP 73A, Auroral Measurements Program -
Black Brant 18.205-1*

D.A. Burt, C.S. Davis - Utah State; AFCRL-TR-74-0195, February 1974.

HAES Report No. 4

Data Reduction and Auroral Characterization for ICECAP

I. Kofsky -- Photometrics; DNA 3511F, January 1975.

HAES Report No. 5

ICECAP Analysis: Energy Deposition and Transport in the Auroral Ionosphere

R.D. Sears - Lockheed; DNA 3566F, November 1974

HAES Report No. 6

Auroral Simulation Studies

D. Archer - Mission Research Corp; DNA 3567T, April 1975.

HAES Report No. 7

*ICECAP 72 - Rocket Measurement Program for Investigation of Auroral IR
Emissions - Black Brant 17.110-3.*

D.A. Burt, G.D. Allred, J.C. Kemp, L.C. Howlett, E.F. Pound, G.K. LeBaron
- Utah State; AFCRL-TR-75-0001, September 1974.

HAES Report No. 8

Design and Calibration of a Rocket-Borne Electron Spectrometer

P.C. Neal - Utah State; AFCRL-TR-74-0629, December 1974.

HAES Report No. 9

Near Infrared Auroral Spectra

D. Baker, A. Steed, R. Huppi - Utah State; AFCRL-TR-75-0010, December
1974.

HAES Report No. 10

Arctic Code Electron Deposition Theory with Application to Project EXCEDE

P.W. Tarr - Mission Research Corp; MRC-R-173, February 1975.

HAES Report No. 11

Rocketborne Instrumentation for the Measurement of Electric Fields - Paiute Tomahawk 10.312-3

L. Carl Howlett, R.J. Bell - Utah State; AFCRL-TR-75-0023, January 1975.

HAES Report No. 12

Auroral Chemistry and Energy Deposition Calculations with the OPTAUR Code

H.J.P. Smith, O.P. Manley - Visidyne; VI 266, February 1975.

HAES REPORT No. 13*

Theoretical Evaluation of Vertically Viewing and Earth-Limb Scanning Modes for Rocketborne Earth-Limb Measurements

C.L. Wyatt, R.Y. Han, D.J. Baker - Utah State; AFCRL-TR-75-0072, September 1974.

HAES Report No. 14

Ionospheric Effects Induced by Precipitating Auroral Electrons

J.D. Cladis, G.T. Davidson, W.E. Francis, L.L. Newkirk, M. Walt - Lockheed; LMSC/D454890, February 1975.

HAES Report No. 15

ICECAP 73A - Chatanika Radar Results

M.J. Baron, N.J. Chang - Stanford Research Institute; DNA 3531T, September 1974.

HAES Report No. 16

Numerical Modeling of Aurora

T. Coffey - Naval Research Labs; NRL-MR-3120, October 1975.

HAES Report No. 17

TMA Payload Field Services and Data Reduction

J.F. Bedinger - GCA Corp; AFCRL-TR-75-0009, February 1975.

HAES Report No. 18

Auroral NO

E. Hyman, D.J. Strickland, P.S. Julienne, D.F. Strobel - Naval Research Labs; NRL-MR-3070, July 1975.

HAES Report No. 19

Analysis of 4.3μ ICECAP Data

J. Kumer - Lockheed; AFCRL-TR-74-0334, July 1974.

HAES Report No. 20

Cylindrical Langmuir Probe Measurements from Rocket Flights Covering the Period 31 January 1961 through 3 April 1974

R.C. Wilson - Boston College; AFCRL-TR-75-0265, April 1975.

*HAES number omitted from this report. If you are a recipient of this report, please add the appropriate HAES report number to the front cover.

HAES Report No. 21

Data System Developed for Project ICECAP 74

D.E. Delorey, P.N. Pruneau — Boston College; AFCRL-TR-75-0303, December 1974.

HAES Report No. 22

Rocket-Borne Accelerator Module

D. Shephard, J. Carpenter, W. Reidy, W. Sheean, T. Zehnpfennig — Visidyne; VI-289, AFCRL-TR-75-0379, July 1975.

HAES Report No. 23

Instrumentation Analysis and Data Processing for Rocketborne LWIR Spectrometers (with Application to Rocket A18.006-2 of 22 March 1973)

J.W. Rogers — AFCRL; AFCRL-TR-75-0535, December 1975.

HAES Report No. 24

Auroral Simulation Studies in Support of ICECAP and EXCEDE

D. Archer, P. Tarr — Mission Research Corp; MRC-R-211, September 1975.

HAES Report No. 25*

Studies of Disturbed Ionospheres

K. Baker — Utah State; AFCRL-TR-75-0342, June 1975.

HAES Report No. 26*

Sky Radiance Calculations in the 0.5 μm - 5.0 μm Wavelength Range

W.G.M. Blättner, M.B. Wells — Radiation Research Associates; AFCRL-TR-75-0317, RRA-T7501, May 1975.

HAES Report No. 27

Data Reduction and Auroral Characterizations for ICECAP II

I.L. Kofsky, R.B. Sluder, C.A. Trowbridge — Photometrics; PhM 05-76, October 1975.

HAES Report No. 28*

Effective Recombination Coefficient of the Polar D Region Under Conditions of Intense Ionizing Radiation

T.M. Watt — SRI; DNA 3663T, July 1975.

HAES Report No. 29

Ionospheric Irregularities: HAES Program Support

R.D. Sears — Lockheed; DNA 3782F, September 1975.

*HAES number omitted from this report. If you are a recipient of this report, please add the appropriate HAES report number to the front cover.

HAES Report No. 30*

Development of a Liquid-Helium Cooled Rocketborne Spectrometer

C.L. Wyatt, D.J. Baker — Utah State University; AFCRL-TR-75-0164, February 1975.

HAES Report No. 31*

SIMS Interferometer Study

R.W. Esplin, D.J. Baker, R.J. Huppi — Utah State University; AFCRL-TR-75-0500, July 1975.

HAES Report No. 32

Rocket Spectral Measurement of Atmospheric Infrared Emission During a Quiet Condition in the Auroral Zone

N.B. Wheeler and A.T. Stair, Jr. — AFGL; G. Frodsham and D.J. Baker — Utah State University; AFGL-TR-76-0252, October 1976.

HAES Report No. 33*

Report on the Geophysical Description and the Available Data Associated with Rocket PF-BB-53

G.J. Romick — Geophysical Institute, University of Alaska; AFCRL-TR-75-0040, January 1975.

HAES Report No. 34*

Report on the Geophysical Description and the Available Data Associated with Rocket PF-CI-97

G.J. Romick, Geophysical Institute, University of Alaska; AFCRL-TR-75-0327, May 1975.

HAES Report No. 35

A Correlation of Discrete and Diffuse Aurora With Particle Precipitation

R.S. Caverly, G.J. Romick, and R.D. Sharp — Geophysical Institute, University of Alaska; AFCRL-TR-75-0508, August 1975.

HAES Report No. 36*

Report on the Geophysical Description and the Available Data Associated with Rocket PF-HJ-NJ-90

G.J. Romick, Geophysical Institute, University of Alaska; AFCRL-TR-75-0362, December 1975.

HAES Report No. 37†

ICECAP 73A Partial Reflection Sounder Results

G. Falcon — ITS; DNA 3943F, November 1975.

*HAES number omitted from this report. If you are a recipient of this report, please add the appropriate HAES report number to the front cover.

†DNA 3943F was erroneously issued as HAES Report No. 17 when in actuality it should have read "HAES Report No. 37." Holders of this report are urged to correct their copies.

HAES Report No. 38

Rocket Measurement of OH Emission Profiles in the 1.56 and 1.99 μ m Bands

W.F. Grieder, K.D. Baker — Utah State University and A.T. Stair, AFCRL; AFCRL-TR-76-0057, January 1976.

HAES Report No. 39

ICECAP 74 Chatanika Radar Results

M. Baron, SRI; DNA 3871T, October 1975.

HAES Report No. 40

Analyses of High-Altitude Effects Simulation (HAES)

W.P. Reidy, T.C. Degges, W. Neal — Visidyne; VI-311, AFGL-TR-76-0039, February 1976.

HAES Report No. 41

Geometrical Aspects of Rocket Photometry

W.F. Grieder — Utah State University, L.A. Whelan — Logicon Corp.; AFCRL-TR-76-0046, February 1976.

HAES Report No. 42*

Report on the Geophysical Description and Available Data Associated with Rocket PF-PT-81

G.J. Romick, Geophysical Institute, University of Alaska; AFCRL-TR-74-0540, October 1974.

HAES Report No. 43

ICECAP '75 Chatanika Radar Results

T.M. Watt — SRI; DNA 4086F, August 1976.

HAES Report No. 44

Results of Lower Ionospheric Measurements using the Partial Reflection Sounder During ICECAP '74

G. Falcon — ITS; Report number not yet assigned.

HAES Report No. 45*

EXCEDE: SWIR EXPERIMENT — Quick Look Data Report of 28 February 1976 Launch

R.R. O'Neil, A.T. Stair, Jr., J.C. Ulwick, R. Narcisi — AFGL; D. Burt — Utah State University; 3 March 1976.

HAES Report No. 46*

HIRIS EXPERIMENT — Quick Look Data Report of 1 April 1976 Launch

A.T. Stair, Jr. and J.W. Rogers — AFGL; W.R. Williamson-Honeywell Radiation Center; AFGL-OP-TM-02, July 1976.

*HAES number omitted from this report. If you are a recipient of this report, please add the appropriate HAES report number to the front cover.

HAES Report No. 47*

ICECAP '74 - Chatanika Radar Results

P.D. Perreault, M.J. Baron - SRI; DNA 3871T, October 1975.

HAES Report No. 48*

***Bias and Signal Processing Circuits for a Mass Spectrometer in the Project EXCEDE:
SWIR Experiment***

R. Sukys, J.S. Rochefort, S. Goldberg - Northeastern University; AFGL-TR-76-0060,
October 1975.

HAES Report No. 49

Chatanika Radar Results during the EXCEDE Experiment

T.M. Watt - SRI; DNA 4123T, September 1976.

HAES Report No. 50

***Rocketborne Measurements of Infrared Enhancements Associated with a Bright
Auroral Breakup***

K.D. Baker, D.J. Baker - Utah State University, J.C. Ulwick, A.T. Stair - AFGL.
Report number not yet assigned.

HAES Report No. 51

***LWIR (7-24 μ m) Measurements from the Launch of a Rocketborne Spectrometer
into an Aurora (1973)***

J.W. Rogers, A.T. Stair, Jr., N.B. Wheeler - AFGL; C.L. Wyatt, D.J. Baker -
Utah State University. AFGL - TR - 76 - 0274.

HAES Report No. 52*

DNA Project 609 Radar: Auroral Backscatter Measurements

R.T. Tsunoda, R.I. Presnell, T.N.C. Wang - SRI; DNA 3929F, February 1976.

HAES Report No. 53*

ICECAP Data Processing System

D.E. Delorey and P.N. Pruneau -- Boston College; AFGL-TR-76-0138, May 1976.

*HAES number omitted from this report. If you are a recipient of this report, please add the appropriate
HAES report number to the front cover.

BEST AVAILABLE COPY

DIRECTOR
DEFENSE ADVANCED RSCH PROJ AGENCY
ARCHITECT BUILDING
1400 WILSON BLVD.
ARLINGTON, VA 22209
OICY ATTN LTC W A WHITAKER
OICY ATTN STO CAPT J JUSTICE
OICY ATTN MAJOR GREGORY CANAVAN

DEFENSE DOCUMENTATION CENTER
CAMERON STATION
ALEXANDRIA, VA 22314
(12 COPIES IF OPEN PUBLICATION, OTHERWISE 2 COPIES)
12CY ATTN TC

DIRECTOR
DEFENSE NUCLEAR AGENCY
WASHINGTON, DC 20305
OICY ATTN STYL TECH LIBRARY
OICY ATTN STST ARCHIVES
OICY ATTN RAAF CHARLES A BLANK
OICY ATTN RAAF HAROLD C FITZ JR
OICY ATTN RAAF MAJ JOHN CLARK

DIR OF DEFENSE RSCH & ENGINEERING
DEPARTMENT OF DEFENSE
WASHINGTON DC 20301
OICY ATTN DD/S&SS DANIEL BROCKWAY
OICY ATTN DD/S&SS RICHARD S RUFFINE

COMMANDER
FIELD COMMAND
DEFENSE NUCLEAR AGENCY
KIRTLAND AFB, NM 87115
OICY ATTN FCPR

CHIEF
LIVERMORE DIVISION FLD COMMAND DNA
LAWRENCE LIVERMORE LABORATORY
P.O. BOX 808
LIVERMORE, CA 94550
OICY ATTN FCPR

COMMANDER/DIRECTOR
ATMOSPHERIC SCIENCES LABORATORY
U S ARMY ELECTRONICS COMMAND
WHITE SANDS MISSILE RANGE, NM 88002
OICY ATTN DRSEL-RL-SY-S F F NILES
OICY ATTN E BUTTERFIELD DRSEL-RL-SY-R

COMMANDER
HARRY DIAMOND LABORATORIES
2800 POWDER MILL ROAD
ADELPHI MD 20783
(COMM-TINNER ENVELOPE: ATTN: DRXDD-RRH)
OICY ATTN DRXDD-NP

COMMANDER
U S ARMY NUCLEAR AGENCY
FORT BLISS, TX 79916
OICY ATTN ATCA-NAW J RFRBRET

CHIEF OF NAVAL RESEARCH
NAVY DEPARTMENT
ARLINGTON, VA 22217
OICY ATTN CODE 427 CDR RONALD J ORERLE

COMMANDER
NAVAL ELECTRONICS LABORATORY CENTER
SAN DIEGO, CA 92152
OICY ATTN CODE 2200 1 VERNE E HILDERRAND
OICY ATTN CODE 2200 ILAN ROTHMULLER

DIRECTOR
NAVAL RESEARCH LABORATORY
WASHINGTON, DC 20375
OICY ATTN DOUGLAS P MCNUTT
OICY ATTN CODE 7127 CHARLES Y JOHNSON
OICY ATTN CODE 2027 TECH LIA
OICY ATTN CODE 7700 TIMOTHY P COFFEY
OICY ATTN CODE 7701 JACK D BROWN
OICY ATTN CODE 7750 DARRELL F STRUBEL
OICY ATTN CODE 7750 PAUL JULIENNE

COMMANDER
NAVAL SURFACE WEAPONS CENTER
WHITE OAK, SILVER SPRING, MD 20910
OICY ATTN CODE W4501 NAVY NUC PRGMS OFF

AF GEOPHYSICS LABORATORY, AFSC

HANSCOM AFB, MA 01731

OICY ATTN LRB RENNEETH S W CHAMPYHN

OICY ATTN OP JOHN S GARING

OICY ATTN OPR ALVA T SYAIR

AF WEAPONS LABORATORY, AFSC

KIRTLAND AFB, NM 87117

OICY ATTN DYT CAPT DAVID W GOFYZ

OICY ATTN SUL

OICY ATTN DYT LTC DON MITCHELL

COMMANDER

ASH

WPAFB, OH 45433

OICY ATTN ASD-YH-FX LTC ROBERTY LEVERETT

SAMSO/SZ

POST OFFICE BOX 92960

WORLDWAY POSTAL CENTER

LOS ANGELES, CA 90009

(SPACE DEFENSE SYSTEMS)

OICY ATTN SZJ MAJOR LAWRENCE D HAN

DIVISION OF MILITARY APPLICATION

U S ENERGY RESEARCH & DEV ADMIN

WASHINGTON, DC 20545

OICY ATTN DDC CON FOR MAJ D A HAYCOCK

LOS ALAMOS SCIENTIFIC LABORATORY

P.O. BOX 1663

LOS ALAMOS, NM 87545

OICY ATTN DDC CON FOR R A JEFFRIES

DEPARTMENT OF COMMERCE

OFFICE OF TELECOMMUNICATIONS

INSTITUTE FOR TELECOM SCIENCE

BOULDER, CO 80302

OICY ATTN WILLYAM F UTLAUT

OICY ATTN GLENN FALCON

AERODYNE RESEARCH, INC.
BEDFORD RESEARCH PARK
CROSBY DRIVE
BEDFORD, MA 01730
OICY ATTN F BLEN
OICY ATTN M CAMAC

AEROSPACE CORPORATION
P.O. BOX 92957
LOS ANGELES, CA 90009
OICY ATTN T TAYLOR
OICY ATTN R GROVE
OICY ATTN R D RAWCLIFFE
OICY ATTN HARRIS MAYER

DENVER UNIVERSITY OF
COLORADO SEMINARY
DENVER RESEARCH INSTITUTE
P.O. BOX 10127
DENVER, CO 80210
(ONLY 1 COPY OF CLASS RPTS)
OICY ATTN SEC OFFICER FOR MR VAN ZYL
OICY ATTN SEC OFFICER FOR DAVID MURCRAE

GENERAL ELECTRIC COMPANY
TEMP-CENTER FOR ADVANCED STUDIES
818 STATE STREET (P.O. DRAWN 80)
SANTA BARBARA, CA 93102
OICY ATTN DASTAC ART PERRY
OICY ATTN WARREN S KNAPP

GENERAL RESEARCH CORPORATION
P.O. BOX 3507
SANTA BARBARA, CA 93105
OICY ATTN JOHN ISF JR

GEOPHYSICAL INSTITUTE
UNIVERSITY OF ALASKA
FAIRBANKS, AK 99701
(ALL CLASS ATTN: SECURITY OFFICER)
OICY ATTN T M DAVIS (UNCL ONLY)
OICY ATTN NEAL BROWN (UNCL ONLY)

HONEYWELL INCORPORATED
RADIATION CENTER
2 FURBER ROAD
LEXINGTON, MA 02173
OICV ATTN W WILLIAMSON

INSTITUTE FOR DEFENSE ANALYSES
400 ARMY-NAVY DRIVE
ARLINGTON, VA 22202
OICV ATTN ERNEST RAUER
OICV ATTN HANS WOLFHARD

LOCKHEED MISSILES AND SPACE COMPANY
3251 HANOVER STREET
PALM ALTO, CA 94304
OICV ATTN JOHN R CLADIS DEPT 52-12
OICV ATTN J R REAGAN DEPT 52-12
OICV ATTN RILLY M MCCORMAC DEPT 52-54

OICV ATTN TOM JAMES
OICV ATTN ROBERT D SEARS DEPT 52-14
OICV ATTN JOHN KUMER
OICV ATTN MARTIN WALT DEPT 52-10
OICV ATTN RICHARD G JOHNSON DEPT 52-12

MISSION RESEARCH CORPORATION
735 STATE STREET
SANTA BARBARA, CA 93101
OICV ATTN P FISCHER
OICV ATTN D ARCHER

PHOTOMETRICS, INC.
442 WARRETT ROAD
LEXINGTON, MA 02173
OICV ATTN TRYING L KOFKY

PHYSICAL DYNAMICS INC.
P.O. BOX 1069
BERKELEY, CA 94701
OICY ATTN JOSEPH R WORKMAN

PHYSICAL SCIENCES, INC.
30 COMMERCE WAY
WOBURN, MA 01801
OICY ATTN KURT WRAY

R & D ASSOCIATES
P.O. BOX 9695
MARINA DEL REY CA 90291
OICY ATTN FURWFEST GILMORE

R & D ASSOCIATES
1815 N. FT. MYER DRIVE
11TH FLOOR
ARLINGTON, VA 22209
OICY ATTN HERBERT J MITCHELL

HAND CORPORATION, THE
1700 MAIN STREET
SANTA MONICA, CA 90406
OICY ATTN JAMES OAKLEY

SCIENCE APPLICATIONS, INC.
P.O. BOX 2351
LA JOLLA, CA 92038
OICY ATTN DANIEL A HAMLIN

SPACE DATA CORPORATION
1331 SOUTH 26TH STREET
PHOENIX, AZ 85034
OICY ATTN EDWARD F ALLEN

STANFORD RESEARCH INSTITUTE
333 RAVENSWOOD AVENUE
MENLO PARK, CA 94025
OICV ATTN WALTER G CHESTNUT
OICV ATTN W HARRIS
OICV ATTN RAY L LEAHARRAND

STANFORD RESEARCH INSTITUTE
1611 NORTH RENT STREET
ARLINGTON, VA 22209
OICV ATTN WARREN W BERNING

TECHNOLOGY INTERNATIONAL CORPORATION
75 WIGGINS AVENUE
BEDFORD, MA 01730
OICV ATTN W P BROUJIST

UTAH STATE UNIVERSITY
LOGAN, UT 84321
OICV ATTN DORAN BAKER
OICV ATTN KAY HARPER
OICV ATTN D BURT
OICV ATTN C WYATT

VISIOTNE, INC.
19 THIRD AVENUE
NORTH WEST INDUSTRIAL PARK
HURLINGTON, MA 01903
OICV ATTN WILLIAM REIDY
OICV ATTN J W CARPENTER
OICV ATTN T C DEGGES